2023-09-22

# Optimality, Objectives, and Trade-Offs in Motor Control under Uncertainty

Ryu, Hansol

UNIVERSITY OF CALGARY

# Optimality, Objectives, and Trade-Offs in Motor Control under Uncertainty

by

Hansol Ryu

A THESIS

SUBMITTED TO THE FACULTY OF GRADUATE STUDIES

IN PARTIAL FULFILMENT OF THE REQUIREMENTS FOR THE

DEGREE OF DOCTOR OF PHILOSOPHY

GRADUATE PROGRAM IN BIOMEDICAL ENGINEERING

CALGARY, ALBERTA

SEPTEMBER, 2023

# Abstract

Biological motor control involves multiple objectives and constraints. In this thesis, I investigated the influence of uncertainty on biological sensorimotor control and decision-making, considering various objectives.

In the first study, I used a simple biped walking model simulation to study the control of a rhythmic movement under uncertainty. Uncertainty necessitates a more sophisticated form of motor control involving internal model and sensing, and their effective integration. The optimality of the neural pattern generator incorporating sensory information was shown to be dependent on the relative amount of physical disturbance and sensor noise. When the controller was optimized for state estimation, other objectives of improved energy efficiency, reduced variability, and reduced number of falls were also satisfied.

In the second study, human participants performed regression and classification tasks on visually presented scatterplot data. The tasks involved a trade-off between acting on small but prevalent errors and acting on big but scarce errors. We used inverse optimization to characterize the loss function used by humans in these regression and classification tasks, and found that these loss functions change systematically as the data sparsity changed. Despite being highly variable, there were overall shifts towards

compensating for prevalent small errors more when the sparsity of the visual data decreased.

In the third study, I extended the pattern recognition tasks to include visually mediated force tracking. When participants tracked force targets with visual noise, we observed a slight yet consistent force tracking bias. This bias, which increased with noise, was not explained by commonly hypothesized objectives such as a tendency to reduce effort while regulating error. Additional experiments revealed that a model balancing error reduction and transition reduction tendencies effectively explained and predicted experimental data. Transition reduction tendency was further separated into recency bias and central tendency bias. Notably, this bias disappeared when the task became purely visual, suggesting that such biases could be task-dependent.

These findings across the three studies provide useful insights into understanding how uncertainty changes objectives and their trade-offs in biological motor control, and in turn, results in a different control strategy and behaviors.

# Preface

**Chapter 2** of this thesis has been published as Hansol X. Ryu and Arthur D. Kuo, "An optimality principle for locomotor central pattern generators." *Scientific Reports* 11.1 (2021): 13140 under the terms of the Creative Commons CC BY license. The second author of the paper, Dr. Artrhur D. Kuo, was the student's PhD supervisor when this research was conducted and published.

**Chapter 3** of this thesis has been posted on a preprint server, *BioRxiv* as Hansol X. Ryu and Manoj Srinivasan, "What loss functions do humans optimize when they perform regression and classification", https://doi.org/10.1101/2023.09.19.558376, under a CC-BY-NC 4.0 International license.

**Chapter 4** of this thesis has been posted on a preprint server, *BioRxiv* as Hansol X. Ryu and Manoj Srinivasan, "Human force control may trade-off force error with central tendency and recency biases", https://doi.org/10.1101/2023.09.19.558388, under a CC-BY-NC 4.0 International license.

The format of the manuscripts has been changed to match the University of Calgary thesis guidelines.

# Acknowledgments

I would like to express my deepest gratitude to my supervisors, Dr. John E. A. Bertram and Dr. Manoj Srinivasan, for their unwavering support and guidance. I'm honored to have had you as my mentors.

I extend heartfelt gratitude to my thesis committee, Drs. Patrick Whelan, Dagmar Sternad, and Jackson Cone, for their valuable insights and feedback. I warmly appreciate my mentors at KAIST, Drs. Sukyung Park, Jennifer H. Shin, and Jung Kim, and Dr. Max Donelan at SFU. Support from friends and colleagues, whom I met at KAIST, U of C, OSU, and various points in my journey, was indispensable to my accomplishments.

I am profoundly thankful to BME department and many university staff, including counselors Alex Klassen and Kaitlin van Geel, student ombuds Jeff Stransky, and sexual and gender-based violence support coordinator Carla Bertsch. With your support, I navigated challenging times and grew from those experiences.

My sincere thanks are to my parents, who are here with me in Canada as I write this acknowledgment, and my brother. My curiosity, courage, resilience, and love for the world, must have all come from you.

This thesis would not have been possible without many people's help and support. I appreciate all of you for being a part of my journey.

# Contents

# List of Figures

# Chapter 1

# Introduction

> All animals, however insignificant, have a mission to perform—a destiny to fulfil; and their manner of doing it cannot be a matter of indifference (...) it is but natural we should take an interest in the movements of our fellow-travellers.
>
> James Bell Pettigrew. *Animal Locomotion: Or, Walking, Swimming, and Flying, with a Dissertation on Aëronautics.*

## 1.1 Background and motivation

Understanding principles of biological motor control could contribute to expanding our knowledge of the world and ourselves (Haldane, 1949; Elftman, 1966), helping people and animals with motor disorders (Abbruzzese and Berardelli, 2003; Piek and Dyck, 2004), and improving technologies that are related to biological movements (Ackermann and Van den Bogert, 2010; Zhang et al., 2017). One of the challenges in studying goal-directed motor control is that it often involves multiple objectives and constraints, which could be competing or in alignment with each other. Even seemingly

mundane movements, such as scratching our own body, require precise control over the force and trajectory of our extremities: it requires a fine balance between feeling good and damaging the skin, executed within the capacities and limitations of our physical bodies.

One way to model the movement control is to view it as an optimal solution among other feasible solutions when it is evaluated with some measurable criteria (Baron and Kleinman, 1969; Kleinman et al., 1970). For example, human and animal movement controls seem to be energetically optimal in many cases, especially during movements that they repetitively perform throughout their lives. One common example is locomotion. It has been reported that humans and animals choose a gait that minimizes metabolic energy consumption (Alexander, 1989). People tend to choose a step length at a given speed that minimizes metabolic energy expenditure, which means, increasing or decreasing the natural step length results in increased metabolic energy expenditure (Atzler and Herbst, 1927; Bertram and Ruina, 2001). When speed is not constrained, people seem to choose an optimal walking speed that minimizes metabolic energy expenditure per distance travelled (Margaria, 1968). People and animals seem to select a mode of gait that minimizes metabolic cost at a given speed (Hoyt and Taylor, 1981), and people switch between walking and running and the switch is roughly associated with metabolic cost minimization albeit with some small hysteresis (Long III and Srinivasan, 2013; Diedrich and Warren Jr, 1995).

However, there also are abundant examples showing that human and animal behaviors seem to be suboptimal in terms of a particular measure. That is, some criterion that was regarded as a control objective sometimes

turned out to be not a good descriptor of the behaviors to various degrees (Alexander, 1958; Zamparo et al., 1995). This suboptimality with respect to one criterion could mean that humans and animals are optimal in a different way, but sometimes there might not be a simple alternative explanation to their behaviors. For example, while non-pathological gaits seem to be energetically optimal, pathological gaits could be sometimes better explained by minimizing apparent abnormality or minimizing pain, rather than minimizing metabolic energy consumption (Winter et al., 1990; Tesio et al., 1991). On the other hand, sometimes people and animal behaviors seem to be simply irrational (Ellis, 1975; Arkes and Ayton, 1999), let alone the absurdity of the concept of living (Nagel, 1971).

Despite these complications, because motor behaviors are usually not totally random but are goal-directed at least on a macroscopic level, it is reasonable to look for useful tools to describe them. This thesis aims to improve our current knowledge of how uncertainty shapes control and decision-making strategies. Here, uncertainty includes unexpected disturbances from the environment, noise in neural information, imperfect execution of motor commands in muscles, or even vagueness in the task itself. The effects of such uncertainty could sometimes be eliminated if the system properly reacts to it, may introduce variability to the final result without significantly altering overall behavior, or could drastically change the result. Some studies on biological motor control do not take uncertainty into account and still provide useful insights. However, when uncertainty adds more than mere variability to the system, its omission may lead to misleading results. A strategy that works great only if everything is perfect might not be a good strategy in most cases in life.

## 1.2 Summary of chapters

In the research projects presented in the following chapters, I will discuss the principles of motor control under uncertainty in the context of agreeing or competing objectives. Two main approaches I used were: 1) performing optimization on movement simulation models and 2) applying inverse optimization analysis to experimental data collected from human participants performing sensorimotor or decision-making tasks. Optimization is the process of seeking the best decision parameters given certain criteria, or in other words, the objective function. Optimization of a biped walking model will be presented in Chapter 2, demonstrating both optimal and suboptimal behaviors in terms of multiple performance criteria. Inverse optimization is the process of searching for a formulation of an optimization problem whose result best describes the observations. I applied inverse optimization analysis to characterize how human participants performed pattern recognition tasks and force tracking tasks, as discussed in Chapters 3 and 4. In the three studies presented here, I investigated a range of tasks, including rhythmic tasks (such as walking), discrete or episodic tasks involving pattern recognition, and tasks that fall in between, which involve tracking continuously changing forces (Hogan and Sternad, 2007).

In Chapter 2, I will discuss how multiple control objectives can be satisfied through an optimal combination of signals that come from sensors and from a central pattern generator (CPG) for locomotion control in the presence of noise. We used a simplified biped locomotion model simulation to demonstrate the trade-off between sensor information and CPG signal, and how this combination could be optimized for certain objectives. Here, the

CPG is a neural circuit that is capable of generating rhythmic patterns even without any sensor inputs, which is observed in animal studies. However, further investigation is needed to understand its structure and integration with sensors. We modeled this circuit as a forward predictor that uses an internal model of the movements — forward prediction of the body dynamics is obtained by combining current body configurations with muscle actions, and its performance is affected by motor disturbances. The advantage of this perspective is that sensor information can be systematically integrated, since the measurement using sensors is another source of information on the configurations of the body. Sensor performance is affected by sensor noise, thus there is an optimal balance between sensor information and forward predictions depending on the relative strength of sensor noise and motor disturbance. We predicted the optimal CPG based on an even more simplified model of the walking model using classical control theory, and then applied it to a more complicated model. The CPG controller that minimized the estimation error of a simplified model also minimized the estimation error of the more complicated nonlinear model which undergoes collision with the ground. For the model considered, this combination yielded the best walking performance that had minimum energetic cost, step length variability, and least frequent fallings.

In Chapter 3, I will discuss how humans perceive visually presented noisy data in the context of simple 'machine learning' or 'statistical inference' tasks. Motor control involves error regulations — for example, deviation from the posture one tried to hold, or deviation from the motion trajectory one wanted to perform, need to be reduced for a better execution of the task. As a particularly simplified special case, we studied how humans perceive

and perceptually penalize errors when they perform simple regression and classification tasks. Specifically, we presented scattered dots to participants and asked them to draw a line that best describes the dots (regression). We also showed scattered dots of two colors and asked participants to draw a line that best separated dots into two groups (classification). Our aim was to capture the trade-off people made while performing the task: some lines capture the majority of data well but make a huge error on a few exceptional dots, while some lines reduce this exceptionally big error on a few dots at the cost of making slightly more errors on many dots. We used inverse optimization approach to quantitatively characterize how humans performed the task. That is, we modeled people's responses as a solution of an optimization problem, and investigated which optimization objective function would produce the results closest to what humans did. Despite being largely variable, we could explain average behavior using inverse optimization method. There was a systematic shift in the behavior and the inferred loss function when subjects were presented with less sparse data.

In Chapter 4, I will discuss how humans execute a sensorimotor task, specifically a force-exertion task, which involves the perception of noisy visually presented data similar to what we used in Chapter 3. We asked human subjects to produce force following the loosely defined visual targets that changed force requirements every few seconds. Our aim was to characterize the trade-off between performance-enhancing tendency and energy-saving tendency during force tacking tasks. This form of optimization is commonly used in human behavior modeling, robot motion planning, and biomechanical simulations. We found shifts towards producing less force when the force requirement increased and when the vagueness of the target in-

creased. However, unexpectedly, we also found that subjects consistently made an error in a way that seemed like they wasted energy in some cases. We investigated how different models of force tracking error may or may not capture the observations, by conducting additional prospective experiments that were designed to distinguish different models. We could explain the observations using a model of force production bias, which seems to be a previously overlooked phenomenon. Similar biases were reported in visual perception studies, but we did not observe a significant bias when we made the task almost fully visual, suggesting that these biases may be task-dependent.

**Statement of contribution.** In Chapter 2, I implemented and performed simulations, analyzed results, produced figures, contributed to the conceptualization of the project, and prepared the manuscripts and publication process. In Chapters 3 and 4, I contributed to the conceptualization of the idea, development of the experimental protocols, data collection and analysis, and preparation of figures and manuscripts.

# Chapter 2

# An optimality principle for locomotor central pattern generators

## 2.1 Abstract

Two types of neural circuits contribute to legged locomotion: central pattern generators (CPGs) that produce rhythmic motor commands (even in the absence of feedback, termed “fictive locomotion”), and reflex circuits driven by sensory feedback. Each circuit alone serves a clear purpose, and the two together are understood to cooperate during normal locomotion. The difficulty is in explaining their relative balance objectively within a control model, as there are infinite combinations that could produce the same nominal motor pattern. Here we propose that optimization in the presence of uncertainty can explain how the circuits should best be combined for locomotion. The key is to re-interpret the CPG in the context of

state estimator-based control: an internal model of the limbs that predicts their state, using sensory feedback to optimally balance competing effects of environmental and sensory uncertainties. We demonstrate use of optimally predicted state to drive a simple model of bipedal, dynamic walking, which thus yields minimal energetic cost of transport and best stability. The internal model may be implemented with neural circuitry compatible with classic CPG models, except with neural parameters determined by optimal estimation principles. Fictive locomotion also emerges, but as a side effect of estimator dynamics rather than an explicit internal rhythm. Uncertainty could be key to shaping CPG behavior and governing optimal use of feedback.

## 2.2 Introduction

A combination of two types of neural circuitry appears responsible for the basic locomotory motor pattern. One type is the central pattern generator (CPG; Fig. 2.1A), which generates pre-programmed, rhythmically timed, motor commands (Brown, 1914; Wilson, 1961; Wilson and Wyman, 1965). The other is the reflex circuit, which produces motor patterns triggered by sensory feedback (Fig. 2.1C). Although they normally work together, each is also capable of independent action. The intrinsic CPG rhythm patterns can be sustained with no sensory feedback and only a tonic, descending input, as demonstrated by observations of fictive locomotion (Grillner, 1975; Feldman and Orlovsky, 1975). Reflex loops alone also appear capable of controlling locomotion1, particularly with a hierarchy of loops integrating multiple sensory modalities for complex behaviors such as stepping and standing

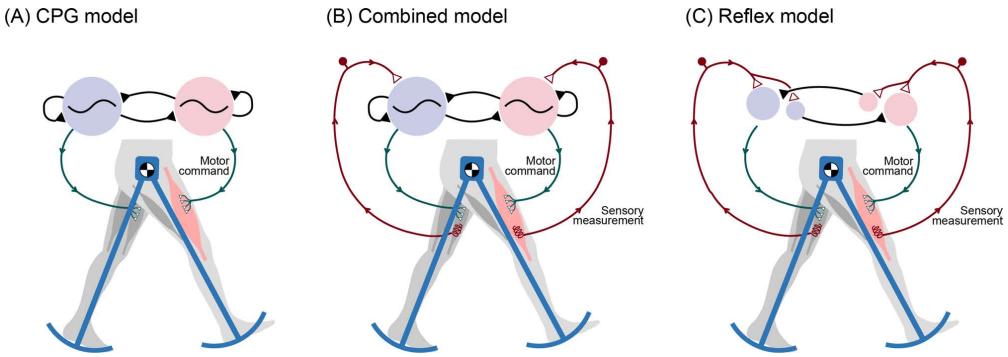


Figure 2.1: **Three ways to control bipedal walking.** (A) The central pattern generator (CPG) comprises neural oscillators that can produce rhythmic motor commands, even in the absence of sensory feedback. Rhythm can be produced by mutually inhibiting neural half-center oscillators (shaded circles). (B) In normal animal locomotion, the CPG is thought to combine an intrinsic rhythm with sensory feedback, so that the periphery can influence the motor rhythm. (C) In principle, sensory feedback can also control and stabilize locomotion through reflexes, without need for neural oscillators. The extreme of (A) CPG control without feedback is referred to here as pure feedforward control, and the opposite extreme (C) with no oscillators as pure feedback control. Any of these schemes could potentially produce the same nominal locomotion pattern, but some (B) combination of feedforward and feedback appears advantageous.

control (Sherrington, 1910; Pringle, 1940). We refer to the independent extremes as pure feedforward control and pure feedback control. Of course, within the intact animal, both types of circuitry work together for normal locomotion (Fig. 2.1B) (Büschges, 2005). However, this cooperation also presents a dilemma, of how authority should optimally be shared between the two (Bässler and Büschges, 1998).

The combination of central pattern generators with sensory feedback has been explored in computational models. For example, some models have added feedback (Liu et al., 2012; Habib et al., 2009; Auddy et al., 2019; Cristiano et al., 2015) to biologically-inspired neural oscillators (e.g., Matsuoka (1987)), which employ networks of mutually inhibiting neurons to

intrinsically produce alternating bursts of activity. Sensory input to the neurons can change network behavior based on system state, such as foot contact and limb or body orientation, to help respond to disturbances. The gain or weight of sensory input determines whether it slowly entrains the CPG (Iwasaki and Zheng, 2006), or whether it resets the phase entirely (Nassour et al., 2014; Tsuchiya et al., 2003). Controllers of this type have demonstrated legged locomotion in bipedal(Morimoto et al., 2006) and quadrupedal robots (Kimura et al., 2007; Righetti and Ijspeert, 2008), and even swimming and other behaviors (Bliss et al., 2012). A general observation is that feedback improves robustness such as against uneven terrain (Endo et al., 2004). And the addition of feedforward into feedback-based control has been used to vary walking speed (Dzeladini et al., 2014), adjust interlimb coordination(Owaki and Ishiguro, 2017), or enhance stability (Daley et al., 2007). However, a disadvantage is that the means of combining CPG and feedback is often designed ad hoc. This makes it challenging to extend the findings from one CPG model to another or to other gaits or movement tasks.

Optimization principles offer a means for a model to be uniquely defined by quantitative and objective performance measures (Alexander, 1996). Indeed, CPG models have long used optimization to determine parameter values (Dzeladini et al., 2014; Kimura et al., 1993; Taylor et al., 2000). However, the most robust and capable models to date have tended not to use CPGs or intrinsic timing rhythms. For example, human-like optimization models can traverse highly uneven terrain (Geyer and Herr, 2010; Heess et al., 2017; Peng et al., 2017) using only state-based control, where the control command is a function of system state (e.g., positions and velocities

of limbs). In fact, reinforcement learning and other robust optimization approaches (e.g., dynamic programming (Bellman, 1954; Bryson, 1975)) are typically expressed solely in terms of state, and do not even have provision for time as an explicit input. They have no need for, nor even benefit from, an internally generated rhythm. But feedforward is clearly important in biological CPGs, suggesting that some insight is missing from these optimal control models.

There may be a principled reason for a biological controller not to rely on state, as measured, alone. Realistically, a system's state can only be known imperfectly, due to noisy and imperfect sensors. The solution is state estimation (Bryson, 1975), in which an internal model of the body is used to predict the expected state and sensory information, and feedback from actual sensors is used to correct the state estimate. The sensory feedback gains may be optimized for minimum estimation error separate from control. The separation principle(Bryson, 1975) of control systems shows that state-based control may be optimized for control performance without regard to noisy sensors, and nevertheless combine well with state estimation(Bryson, 1975). In practice, actual robots (e.g., bipedal Atlas(Kuindersma et al., 2016) and quadrupedal BigDog(Wooden et al., 2010)) gain high performance and robustness through such a combination of state estimation driving state-(estimator)-based control. In fact, state-estimator control may be optimized for a noisy environment(Bryson, 1975), and has been proposed as a model for biological systems (Kuo, 2005, 1995; Todorov, 2005). The internal model for state estimation is not usually regarded as relevant to the biological CPG's feedforward, internal rhythm, but we have proposed that it can potentially produce a CPG-like rhythm under conditions simulating fictive

locomotion(Kuo, 2002b). Here the rhythmic output is interpreted not as the motor command per se, but as a state estimate that drives the motor command. We demonstrated this concept with a simple model of rhythmic leg motions(Kuo, 2002b) and a preliminary walking model(O'Connor, 2009). This suggests that a walking model designed objectively with state estimator-based control might produce CPG-like rhythms that objectively contribute to locomotion performance.

The purpose of the present study was to test an estimator-based CPG controller with a dynamic walking model. We devised a simple state-based control scheme to produce a stable and economical nominal gait, producing stance and swing leg torques as a function of the leg states. Assuming a noisy system and environment, we devised a state estimator for leg states. A departure from other CPG models is that we optimize sensory feedback and associated gains not for walking performance, but for accurate state estimation. The combination of control and estimation define our interpretation of a CPG controller that incorporates sensory feedback in a noisy environment. Moreover, this same controller may be realized in the form of a biologically-inspired half center oscillator (Matsuoka, 1987), with neuron-like dynamics. Because the control scheme depends on accurate state information for its stability and economy, we expected that minimizing state estimation error (and not explicitly walking performance) would nonetheless allow this model to achieve better walking performance. Scaling the sensory feedback either higher or lower than theoretically optimal would be expected to yield poorer performance. Such a model may conceptually explain how CPGs could optimally incorporate sensory feedback.

## 2.3 Results

### Central pattern generator controls a dynamic walking model

The CPG controller produced a periodic gait with a model of human-like dynamic walking (Fig. 2.2A). The model was inspired by the mechanics and energetics of humans(Kuo et al., 2005), whose legs have pendulum-like passive dynamics(Alexander, 1995) (the swing leg as a pendulum, the stance leg as inverted pendulum), modulated by active control. Model parameters such as mass distribution and foot curvature, and the resultant walking speed and step length were similar to human walking. The nominal step length for a given walking speed also minimized the model's energy expenditure, as also observed in humans (Kuo, 2001). Acting on the legs were torque commands ($T_1$ and $T_2$, Fig. 2.2B) from the CPG, designed to yield a periodic gait (Fig. 2.2C), by restoring energy dissipated with each step's ground contact collision (Donelan et al., 2002; Kuo, 2002a). The leg angles and the ground contact condition ("GC", 1 for contact, 0 otherwise; Fig. 2.2C) were treated as measurements to be fed back to the CPG. Each leg's states ($\boldsymbol{x_i} \triangleq [\theta_i, \dot{\theta}_i]^T$) described a periodic orbit or limit cycle (Fig. 2.2D), which was locally stable for zero or mild disturbances, but could easily be perturbed enough to make it fall (Fig. 2.2E).

The resulting nominal (undisturbed) gait had approximately human-like walking speed and step length. The nominal walking speed was equivalent to 1.25 m/s with step length 0.55 m (or normalized 0.4 $(gl)^0.5$ and $0.55l$, respectively; $g$ is gravitational constant, $l$ is leg length). The corresponding

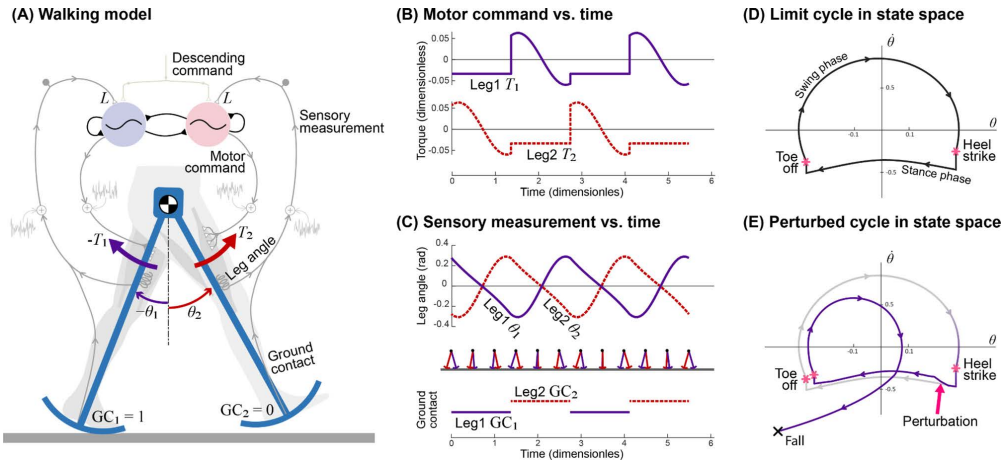


Figure 2.2: **Dynamic walking model controlled by CPG controller with feedback.** (A) Pendulum-like legs are controlled by motor commands for hip torques $T_1$ and $T_2$, with sensory feedback of leg angle and ground contact "GC" relayed back to controller. (B) Controller produces alternating motor commands versus time, which drive (C) leg movement $\theta$. Sensory measurements of leg angle and ground contact in turn drive the CPG. (D) Resulting motion is a nominal periodic gait (termed a "limit cycle") plotted in state space $\dot{\theta}$ versus $\theta$. (E) Discrete perturbation to the limit cycle can cause model to fall.

mechanical cost of transport was 0.053, comparable to other passive and active dynamic walking models (e.g., Kuo (2001); McGeer (1990); Collins et al. (2005)).

This controller had four important features for the analyses that follow. First, the gait had dynamic, pendulum-like leg behavior similar to humans(Kuo et al., 2005; Alexander, 1995). Second, the controller stabilized walking, meaning ability to withstand minor perturbations due to its state-based control. Third, the information driving control was produced by the controller including CPG, whose entire dynamics and feedback gains were objectively designed by optimal estimation principles, with no ad hoc design. And fourth, the overall amount of feedback could be varied continuously between either extreme of pure feedforward and pure feedback

(sensory feedback gain $\boldsymbol{L}$ ranging zero to infinity), while always producing the same nominal gait under noiseless conditions. This was to facilitate study of how parametric variation of sensory feedback affects performance, particularly under noisy conditions.

## Pure feedforward and pure feedback are both susceptible to noise

The critical importance of sensory feedback was demonstrated with a disturbance acting on the legs (Fig. 2.3A). Termed process noise, it represents not only disturbances but also any uncertainty in the environment or internal model. For this demonstration, the disturbance consisted of a single impulsive swing leg angular acceleration (amplitude 5 $(g/l)$ at 15% of nominal stride time). The pure feedforward controller failed to recover (Fig. 2.3A left), and would fall within about two steps. Its perturbed leg and ground contact states became mismatched to the nominal rhythm, which in pure feedforward does not respond to state deviations. In contrast, the feedback controller could recover from the same perturbation (Fig. 2.3A right) and return to the nominal gait. Feedback control is driven by system state, and therefore automatically alters the motor command in response to perturbations. Our expectation is that even if a feedforward control is stable under nominal conditions (with zero or mild disturbances), a feedback controller could generally be designed to be more robust.

We also applied an analogous demonstration with sensor noise (Fig. 2.3B). Adding continuous sensor noise (standard deviation of 0.1 for each independent leg) to sensory measurements had no effect on pure feedfor-

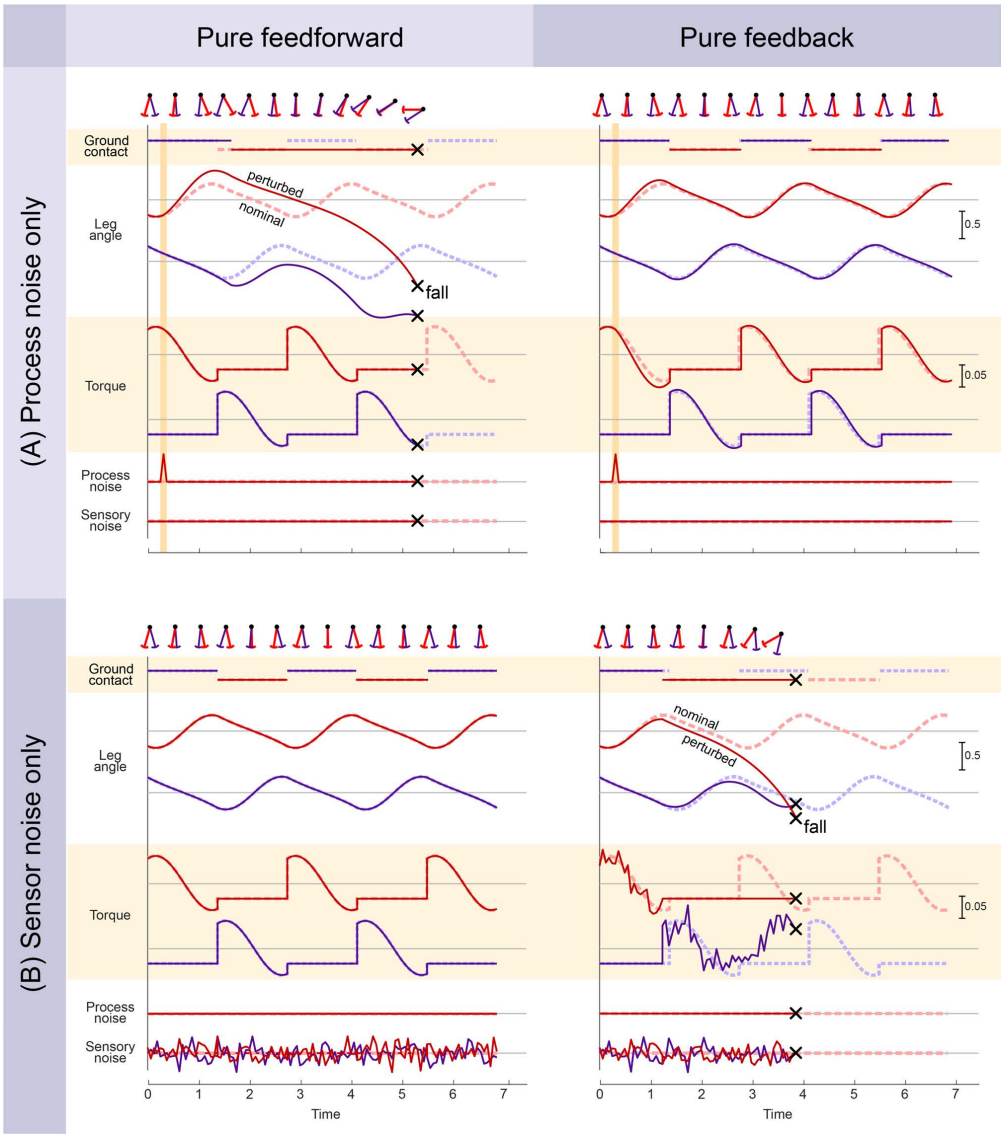


Figure 2.3: **Demonstration of pure feedforward and pure feedback.** Pure feedforward and pure feedback (left and right columns, respectively) are adversely affected by (A) process and (B) sensor noise. Process noise refers to disturbances from the environment or imperfect actuation, and sensor noise refers to imperfect sensing. Plots show ground contact condition, leg angles, commanded leg torques, and noise levels versus time, including both the nominal condition without noise (dashed lines), and the perturbed condition with noise (solid lines). With an impulsive, process noise disturbance, pure feedforward control tended to fall, whereas pure feedback was quite stable. With sensor noise alone, pure feedforward was unaffected, but pure feedback tended to fall.

ward control (Fig. 2.3B left), which ignores sensory signals entirely. But pure feedback was found to be sensitive to noise-corrupted measurements, and would fall within a few steps (Fig. 2.3B right). This is because erroneous feedback would trigger erroneous motor commands not in accordance with actual limb state. The combined result was that both pure feedforward and pure feedback control had complementary weaknesses. They performed identically without noise, but each was unable to compensate for its particular weakness, either process noise or sensor noise. Feedback control can be robust, but it needs accurate state information.

## Neural half-center oscillators are re-interpreted as state estimator

We determined two apparently different representations for the same CPG model. This first was a biologically inspired, neural oscillator (Fig. 2.4A) representation, intended to resemble previous CPG models (Liu et al., 2012; Habib et al., 2009; Auddy et al., 2019; Cristiano et al., 2015) demonstrating incorporation of sensory feedback. As with such models, the intrinsic rhythm was produced with two mutually inhibiting half-center oscillators, one driving each leg ($i = 1$ for left leg, $i = 2$ for right leg). Each half-center had a total of three neurons, one a primary neuron with standard second-order dynamics (states $\boldsymbol{u}$ and $\boldsymbol{v}$). Its output drove the second neuron ($\boldsymbol{\alpha}$) producing the motor command to the ipsilateral leg. The third neuron was responsible for relaying ground contact ("$\boldsymbol{c}$") sensory information, to both excite the ipsilateral primary neuron and inhibit the contralateral one. Although this architecture is superficially similar to previous ad hoc models, the present

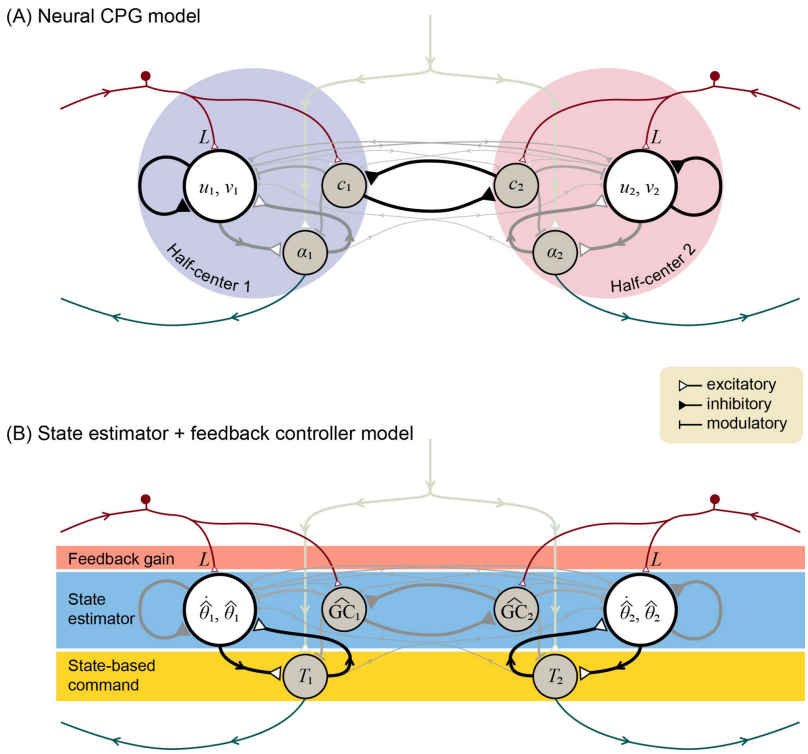


Figure 2.4: **Locomotion control circuit interpreted in two representations.** Representation in (A) Neural central pattern generator with mutually inhibiting half-center oscillators, and as (B) state estimator with feedback control. Each half-center has a primary neuron with two states ($u$ and $v$, respectively), an auxiliary neuron $c$ for registering ground contact, and an alpha motoneuron $\alpha$ driving leg torque commands. Inputs include a tonic descending drive, and afferent sensory data with gain $L$. State estimator acts as second-order internal model of leg dynamics to estimate leg states $\hat{\theta}$ (hat symbol denotes estimate) and ground contact $\hat{\text{GC}}$, which drive state-based command $T$. The estimator dynamics and estimator parameters including sensory feedback $L$, and thus the corresponding neural connections and weights, are designed for minimum mean-square estimation error. Leg dynamics have nonlinear terms (see "Methods" section) of small magnitude (thin grayed lines).

CPG rhythmic dynamics were determined objectively by optimal estimation principles.

The same CPG architecture was then re-interpreted in a second, control systems and estimation framework (Fig. 2.4B), while changing none of the

neural circuitry. Here, the structure was not treated as half-center oscillators, but rather as three neural stages from afferent to efferent. The first stage receiving sensory feedback signal was interpreted as a feedback gain $\boldsymbol{L}$ (upper rectangular block, Fig. 2.4B), modulating the behavior of the second stage, interpreted as a state estimator (middle rectangular block, Fig. 2.4B) acting as an internal model of leg dynamics. Its output was interpreted as the state estimate, which was fed into the third, state-based motor command stage (lower rectangular block, Fig. 2.4B). In this interpretation, the three stages correspond with a standard control systems architecture for a state estimator driving state feedback control. In fact, the neural connections and weights of the half-center oscillators were determined by, and are therefore specifically equivalent to, a state estimator driving motor commands to the legs.

The two representations provide complementary insights. The half-center model shows how sensory information can be incorporated into and modulate a CPG rhythm. Half-center models have previously been designed ad hoc and tuned for a desired behavior, and have generally lacked an objective and unique means to determine the architecture (e.g., number of neurons and interconnections) and neural weights. The state estimator-based model offers a means to determine the architecture, neural weights, and parameters for the best performance. This half-center model with feedback could thus be regarded as optimal, for producing accurate state estimates despite the presence of noise.

## Optimized sensory feedback gain L yields accurate state estimates

We next examined walking performance in the presence of both process and sensor noise, while varying sensory feedback gain $\boldsymbol{L}$ above and below optimal (Fig. 2.5; result from 20 simulation trials per condition, 100 steps per trial). We intentionally applied a substantial amount of noise (with fixed covariances), sufficient to topple the model. This was to demonstrate how walking performance can be improved with appropriate sensory feedback gain $\boldsymbol{L}$, unlike the noiseless case where the model always walks perfectly.

As expected of optimal estimation, best estimation performance was achieved for the gain $\boldsymbol{L}$ equal to theoretically predicted optimum $\boldsymbol{L}^*_{\mathbf{lqe}}$ (Fig. 2.5, normalized sensory feedback gain of 1). We had designed $\boldsymbol{L}^*_{\mathbf{lqe}}$ with linear quadratic estimation (LQE) based on the covariances of process and sensor noise. Applying that gain in nonlinear simulation with added noise resulted in minimum estimation error (Fig. 2.5, bottom). This suggests that a linear gain was sufficient to yield a good state estimate despite system nonlinearities.

The optimal sensory feedback gain also yielded best walking performance. Even though the same state-based motor command function ($\boldsymbol{\alpha}$ in Fig. 2.4) was applied in all conditions, that function was dependent on accurate state information. As a result, the optimal gain $\boldsymbol{L}^*_{\mathbf{lqe}}$ yielded greater economy, less step length variability, and fewer falls (Fig. 2.5). This was actually a side-effect of optimal state estimation, because our state-based motor command was not explicitly designed to optimize any of these performance measures. The minimal mechanical cost of transport was 0.077 under noisy

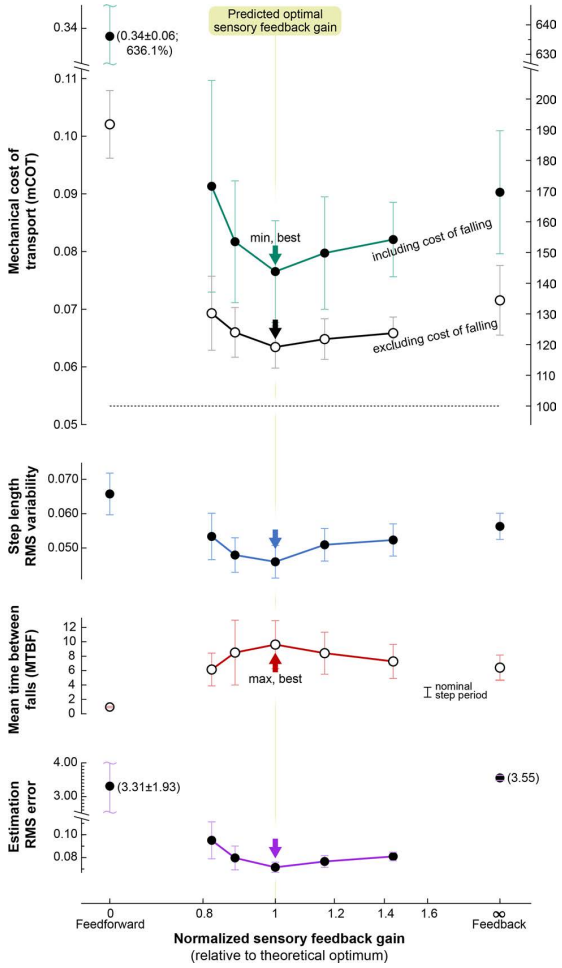


Figure 2.5: **State estimation accuracy and walking performance under noisy conditions, as a function of sensory feedback gain.** The theoretically optimal sensory feedback gain (normalized gain of 1) yielded best performance, in terms of mechanical cost of transport (mCOT), step length variability, mean time between falls (MBTF), and state estimator error. Normalized sensory feedback gain varies between extremes of pure feedforward (to the left) and pure feedback (to the right), with 1 corresponding to theoretically predicted optimum $L^*_{\text{lqe}}$. Formally, normalized gain is defined as $|L|/|L^*_{\text{lqe}}|$ where $|\cdot|$ denotes matrix norm. Vertical arrow indicates best performance (minimum for all measures except maximum for MTBF). For all gains, model was simulated with a fixed combination of process and sensor noise as input to multiple trials, yielding ensemble average measures. Each data point is an average of 20 trials of 100 steps each, and errorbar indicates standard deviation of the trials. Mechanical cost of transport (mCOT) was defined as positive work divided by body weight and distance travelled, and step variability as root-mean-square (RMS) variability of step length. Falling takes time and dissipates mechanical energy, and so mCOT was computed both including and excluding losses from falls (work, time, distance).

conditions, somewhat higher than the nominal 0.053 without noise. Step length variability was 0.046 $l$, and the model experienced occasional falls, with MTBF (mean time between falls) of about 9.61 $g^{-0.5}l^{0.5}$) (or about 7.1 steps). This optimal case served as a basis for comparisons with other values for gain $\boldsymbol{L}$.

## Accurate state estimates yield good walking performance

Applying sensory feedback gains either lower or higher than theoretically predicted optimum generally resulted in poorer walking performance (Fig. 2.5). We expected that any state-based motor command would be adversely affected by poorer state estimates. The effect of reducing sensory feedback gain (normalized gain less than 1) was to make the system (and particularly its state estimate) more reliant on its feedforward rhythm, and less responsive to external perturbations. The effect of increasing sensory feedback gain was to make the system more reliant and responsive to noisy feedback. Indeed, the direct effect of selecting either too low or too high a sensory feedback gain was an increased error in state estimate. The consequences of control based on less accurate state information were more falls, more step length variability, and greater cost of transport. Over the range of gains examined (normalized sensory feedback gain $|\boldsymbol{L}|/|\boldsymbol{L}^*_{\mathbf{lqe}}|$ ranging 0.82–1.44), the performance measures worsened on the order of about 10% (Fig. 2.5). This suggests that, in a noisy environment, a combination of feedforward and feedback is important for achieving precise and economical walking, and for avoiding falls. Moreover, the optimal combination can be designed using control and estimation principles. This testing condition was referred

as “reference condition” for the following demonstration.

## Amount of noise determines optimal sensory feedback gain L

We next evaluated how walking performance and feedback gain would change with different amounts of noise. The theoretically calculated optimum sensory feedback gain $\boldsymbol{L}$ depends on the ratio of process noise to sensor noise covariances(Kailath, 1980). Relatively more process noise favors higher sensory feedback gain, and relatively more sensor noise favors a lower sensory feedback gain and thus greater reliance on the feedforward internal model. We demonstrated this by applying different amounts of process noise (low, medium, and high) with a fixed amount of sensor noise, evaluating the optimal sensory feedback gain, and performing walking simulations with gains varied about the optimum. Noise covariances were set to multiples of the reference conditions (Fig. 2.5), of 0.36, 1.15, and 2.06 respectively for low, medium, high process noise; sensor noise was 1.15 of reference condition. The ratio of process to sensor noise covariance was thus smaller (low), the same (medium), and larger (high) compared to the reference condition, as was the theoretically optimal gain obtained using linear quadratic estimation (LQE) equation (Fig. 2.6).

With varying noise, good performance was still achieved with the corresponding, theoretically optimal gain (Fig. 2.6). The theoretically predicted optimal gain increased with greater process noise, and simulation trials yielded minimum state estimation error at that gain (Fig. 2.6, Estimation RMS error). Accurate state estimation also contributed to walking perfor-

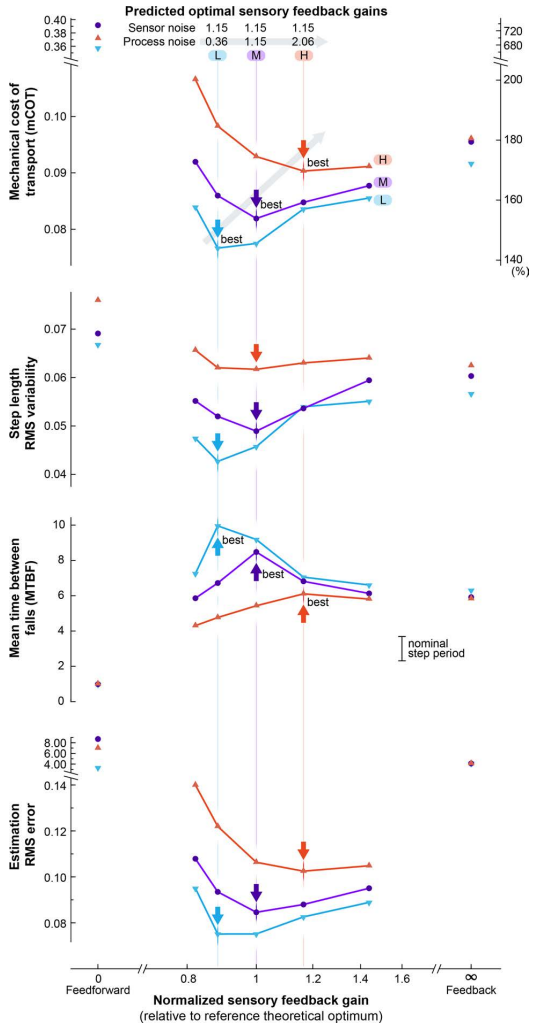


Figure 2.6: **Theoretically optimal sensory feedback gains increase with greater process noise.** Effect of three conditions of increasing process noise (L low, M medium, H high) on walking performance as a function of sensory feedback gain. The theoretically optimal gains (vertical lines) led to best performance, as quantified by mechanical cost of transport (mCOT, including falls), step length variability, mean time between falls (MBTF), and state estimator error. (An exception was step length variability, which had a broad and indistinct minimum.) The predicted optimal sensory feedback gains for each noise condition are indicated with vertical lines. Arrows indicate best performance for each measure for each noise condition. Performance is plotted with normalized sensory feedback gain ranging between extremes of pure feedforward (to the left) and pure feedback (to the right), with 1 corresponding to theoretical optimum $L^*_{\text{lqe}}$ of the previous testing condition (Fig. 2.5). The process noise covariance was set to multiples of the previous reference values: 0.36 for L, 1.15 for M, and 2.06 for H. Sensor noise covariance was set to 1.15 of previous value.

mance, with a trend of minimum cost of transport and step variability, and maximum time between falls at the corresponding theoretical optimum. An exception was step length variability in the high process noise condition, which had a broad minimum, with simulation optimum at a slightly lower gain than theoretically predicted. Overall, the linear state estimator predicted the best performing gain well, in terms of state estimation error, energy economy, and robustness to falls. These results are consistent with the expectation that accurate state estimation contributes to improved control.

## Removal of sensory feedback causes emergence of fictive locomotion

Although the CPG model normally interacts with the body, it was also found to produce fictive locomotion with peripheral feedback removed (Fig. 2.7). Here we considered two types of biological sensors, referred to as "error feedback" and "measurement feedback" sensors. Error feedback refers to sensors that can distinguish unexpected perturbations from intended movements(Dimitriou and Edin, 2010). For example, some muscle spindles and fish lateral lines(Straka et al., 2018) receive corollary efferent signals (e.g. gamma motor neurons in mammals, alpha in invertebrates(Delcomyn, 1998)) that signify intended movements, and could be interpreted as effectively computing an error signal within the sensor itself(Straka et al., 2018). Measurement feedback sensors refers to those without efferent inputs (e.g., nociceptors, golgi tendon organs, cutaneous skin receptors, and other muscle spindles(Iggo, 1973)), that provide information more directly related

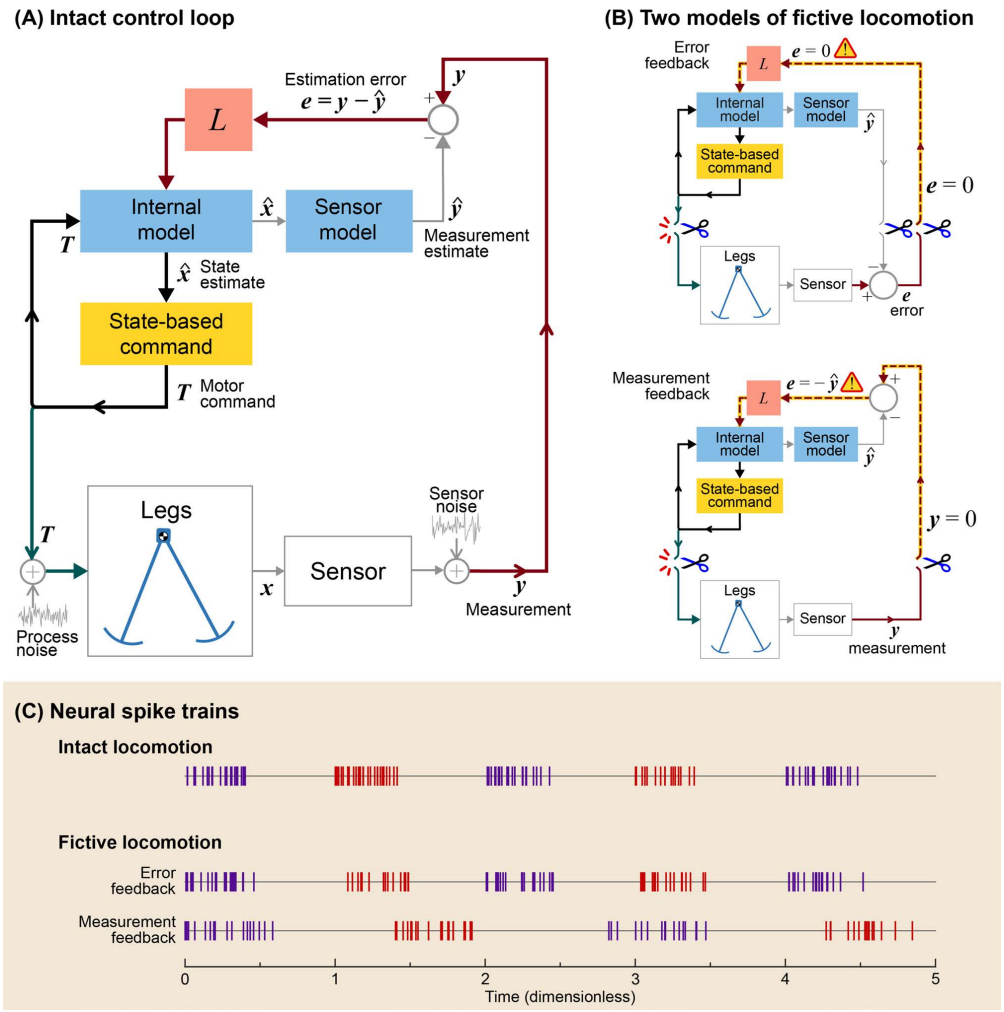


Figure 2.7: **Emergence of fictive locomotion from CPG model.** (A) Block diagram of intact control loop, where sensory measurements $y$ and estimation error $e$ are fed into internal model. Motor command $T$ drives the legs and (through efference copy) the internal model of legs. (B) Two models of fictive locomotion, starting with the intact system but with sensory feedback removed in two ways. Error feedback refers to sensors that receive efferent copy as inhibitory drive (e.g., some muscle spindles). Removal of error (dashed line) results in sustained fictive rhythm, due to feedback between internal model and state-based command. Measurement feedback refers to other, more direct sensors of limb state $\boldsymbol{x}$. Removal of such feedback can also produce sustained rhythm from internal model of legs and sensors, interacting with state-based command. (C) Simulated motor spike trains show how fictive locomotion can resemble intact. Measurement feedback case produces slower and weaker rhythm than error feedback.

to body movement. Both types of sensors are considered important for locomotion, and so we examined the consequences of removing either type.

These cases were modeled by disconnecting the periphery in two different ways. This is best illustrated by redrawing the CPG (Fig. 2.4) more explicitly as a traditional state estimator block diagram (Fig. 2.7A). The state estimator block diagram could be rearranged into two equivalent forms (Fig. 2.7B) by relocating the point where the error signal is calculated. In the Error feedback model (Fig. 2.7B, top), the error is treated as a peripheral comparison associated with the sensor, and in the Measurement feedback model (Fig. 2.7B, bottom), as a more central comparison. The two block diagrams are logically equivalent when intact, but they differ in behavior with the periphery disconnected.

The case of fictive locomotion with Error feedback sensors (Fig. 2.7B, top) was modeled by disconnecting error signal $\boldsymbol{e}$, so that the estimator would run in an open-loop fashion, as if the state estimate were always correct. Despite this disconnection, there remained an internal loop between the estimator internal model and the state-based command generator, that could potentially sustain rhythmic oscillations. The case of fictive locomotion with measurement feedback sensors (Fig. 2.7C Measurement feedback) was modeled by disconnecting afferent signal $\boldsymbol{y}$, and reducing estimator gain by about half, as a crude representation of highly disturbed conditions. There remained an internal loop, also potentially capable of sustained oscillations. We tested whether either case would yield a sustained fictive rhythm, illustrated by transforming the motor command $\boldsymbol{T}$ into neural firing rates using a Poisson process.

We found that removal of both types of sensors still yielded sustained

neural oscillations (Fig. 2.7C), equivalent to fictive locomotion. In the case of Error feedback (Fig. 2.7B), the motor commands from the isolated CPG were equivalent to the intact case without noise in terms of frequency and amplitude. In the case of Measurement feedback (Fig. 2.7B), the state estimator tended to drive estimate $\hat{\boldsymbol{\theta}}$ toward zero, and simulations still produced periodic oscillations, albeit with slower frequency and reduced amplitude compared to intact. This is not unlike observations of fictive locomotion in animals(Wallén and Williams, 1984), although our model's response depends on manner of disconnection. Here, with both types of disconnection, the resulting fictive locomotion should not be interpreted as evidence of an intrinsic rhythm, but rather a side effect of incorrect state estimation.

## 2.4 Discussion

We have examined how central pattern generators could optimally integrate sensory information to control locomotion. Our CPG model offers an adjustable gain on sensory feedback, to allow for continuous adjustment between pure feedback control to pure feedforward control, all with the same nominal gait under perfect conditions. The model is compatible with previous neural oscillator models, while also being designed through optimal state estimation principles. Simulations reveal how sensory feedback becomes critical under noisy conditions, although not to the exclusion of intrinsic, neural dynamics. In fact, a combination of feedforward and feedback is generally favorable, and the optimal combination can be designed through standard estimation principles. Estimation principles apply quite

broadly, and could be readily applied to other models, including ones far more complex than examined here. The state estimation approach also suggests new interpretations for the role of CPGs in animal or robot locomotion.

## Feedforward and feedback may be combined optimally for state estimation

One of our most basic findings was that the extremes of pure feedforward or pure feedback control each performed relatively poorly in the presence of noise (Fig. 2.3). Pure feedforward control, driven solely by an open-loop rhythm, was highly susceptible to falling as a result of process noise. The general problem with a feedforward or time-based rhythm is that a noisy environment can disturb the legs from their nominal motion, so that the nominal command pattern is mismatched for the perturbed state. Under noisy conditions, it is better to trigger motor commands based on feedback of actual limb state, rather than time. But feedback also has its weaknesses, in that noisy sensory information can lead to noisy commands.

Better than these extremes is to combine both feedforward and feedback together, modulated by sensory feedback gain $\boldsymbol{L}$. The relative trade-off between process and measurement noise, described by the ratio of their covariances, determines the theoretically optimal gain. That gain was found to yield the least estimation error in simulation (normalized sensory feedback gain = 1 in Fig. 2.5). Moreover, variations in covariance produced predictable shifts in the theoretical optimum, which again yielded least estimation error in simulation (Fig. 2.6). We demonstrated this using relatively simple, but

rigorously defined(Bryson, 1975) linear estimator dynamics, which worked well despite nonlinearities in the motor command and walking dynamics. Still better performance would be expected with nonlinear estimation techniques such as extended Kalman filters and particle filters(Barfoot, 2017).

## State estimation may be separated from state-based control

A unique aspect of our approach is the separation of sensory processing from control. We treat sensory information as inherently noisy, and treat the CPG as the optimal filter of noisy sensory information yielding the best state estimate. The control is then driven by that estimate, and may be designed independently of sensors and for arbitrary objectives. In fact, the present state-based motor command (Eq. 2.6) was designed ad hoc for reasonable performance, without explicitly optimizing any performance measures. Nevertheless, measures such as cost of transport and robustness against falls showed best performance with the theoretically optimal sensory feedback gain $\boldsymbol{L}$ (Figs. 2.5, 2.6).

There are several advantages to this combination of control and estimation. First, accurate state estimation contributes to good state-based control, and poor estimation to poor control. For example, imprecise visual information can induce variability in foot placement(O'Connor and Kuo, 2009). Increased variability in walking has been associated with poorer walking economy(O'Connor et al., 2012) and increased fall risk(Hausdorff et al., 2001). Second, this is manifested more rigorously as "the separation principle" of control systems design, where state-based control and state estimation may be optimized separately and then combined for good per-

formance(Bryson, 1975; Kailath, 1980). Third, the same state estimator (and therefore most of the CPG) can be paired with a variety of different state-based motor control schemes, such as commands for different gaits, for non-rhythmic movements including gait transitions, or to achieve different objectives such as balance and agility. This differs from ad hoc approaches, where different tasks are generally expected to require re-design of the entire CPG.

## Central pattern generators may be re-interpreted as state estimators

Our model also explains how neural oscillators can be interpreted as state estimators (Fig. 2.4). Previous CPG oscillator models have incorporated sensory feedback for locomotion(Iwasaki and Zheng, 2006; Nassour et al., 2014; Tsuchiya et al., 2003; Morimoto et al., 2006; Righetti and Ijspeert, 2008; Bliss et al., 2012; Endo et al., 2004; Kimura et al., 2007), but have not generally defined an optimal feedback gain based on mechanistic control principles. We have re-interpreted neural oscillator circuits in terms of state estimation (Fig. 2.4), and shown how the gain can be determined in a principled manner, to minimize estimation error (Fig. 2.5) in the presence of noise. Here, the entire optimal state estimator architecture is defined objectively by the dynamics of the body and environment (including noise parameters), with no ad hoc parameters or architecture. This makes it possible to predict how feedback gains should be altered for different disturbance characteristics (Fig. 2.6). The nervous system has long been interpreted in terms of internal models, for example in central motor planning and

control(Hwang and Shadmehr, 2005; Kawato, 1999; Uno et al., 1989) and in peripheral sensors(Dimitriou and Edin, 2010). Here we apply internal model concepts to CPGs, for better locomotion performance.

This interpretation also explains fictive locomotion as an emergent behavior. We observed persistent CPG activity despite removal of sensors (and either error or measurement feedback; Fig. 2.7), but this was not because the CPG was in any way intended to produce rhythmic timing. Rather, fictive locomotion was a side effect of a state-based motor command, in an internal feedback loop with a state estimator, resulting in an apparently time-based rhythm (Fig. 2.7B). Others have cautioned that CPGs should not be interpreted as generating decisive timing cues(Bässler, 1986; Cruse, 2002; Pearson, 1987), especially given the critical role of peripheral feedback in timing(Bässler and Büschges, 1998; Donelan and Pearson, 2004; Pearson, 1995). In normal locomotion, central circuits and periphery act together in a feedback loop, and so neither can be assigned primacy. The present model operationalizes this interaction, demonstrates its optimality for performance, and shows how it can yield both normal and fictive locomotion.

## Optimal control principles may be compatible with neural control

This study argues that it is better to control with state rather than time. The kinematics and muscle forces of locomotion might appear to be time-based trajectories driven by an internal clock. But another view is that the body and legs comprise a dynamical system dependent on state (described e.g.

by phase-plane diagrams, Fig. 2.2), such that the motor command should also be a function of state. That control could be continuous as examined here, or include discrete transitions between circuits (e.g., Büschges (2005)), and could be optimized or adapted through a variety of approaches, such as optimal control(Bryson, 1975), dynamic programming(Bellman, 1954), iterative linear quadratic regulators(Li and Todorov, 2004), and deep reinforcement learning(Peng et al., 2017)). Such state-based control is capable of quite complex tasks, including learning different gaits and their transitions, avoiding or climbing over obstacles, and kicking balls(Peng et al., 2017; Heess et al., 2017). But with noisy sensors(Kuindersma et al., 2016; Wooden et al., 2010), state-based control typically also requires state estimation(Kuindersma et al., 2016; Barfoot, 2017), which introduces intrinsic dynamics and the possibility of sustained internal oscillations. We therefore suggest that models should be controlled by state-based control (e.g. deep reinforcement learning) coupled with state estimation for noisy environments to achieve advanced capability and performance. The resulting combination of state-driven control and estimation might also exhibit CPG-like fictive behavior, despite having no explicit time-dependent controls.

State estimation may also be applicable to movements other than locomotion. The same circuitry employed here (Fig. 2.4) could easily contribute a state estimate $\hat{\boldsymbol{x}}$ for any state-dependent movements. For example, a different rhythmic(Kuo, 2002b) movement might be produced with a different state-based motor command; a non-rhythmic postural stabilization might employ a reflex-like (proportional-derivative) control; and a point-to-point movement might be produced by a descending command, supplemented by local stabilization. All of these would be equivalent to substituting differ-

ent gains and interconnections to the state-based motor command ($\boldsymbol{\alpha}$ or $\boldsymbol{T}$ in Fig. 2.4), while still relying on all of the remaining circuitry (of Fig. 2.4). In our view, persistent oscillations could be the outcome of state estimation with an appropriate state-based command for the $\boldsymbol{\alpha}$ motoneuron (see "Methods" section). But the same half-center circuitry could be active and contribute to other movements that use non-locomotory, state-based commands. It is certainly possible that biological CPGs are indeed specialized purely for locomotion alone, but the state estimation interpretation suggests the possibility of a more general, and perhaps previously unrecognized, role in other movements.

The present optimization approach may offer insight on neural adaptation. Although we have explicitly designed a state estimator here, we would also expect a generic neural network, given an appropriate objective function, to be able to learn the equivalent of state estimation. The learning objective could be to minimize error of predicted sensory information, or simply locomotion performance such as cost of transport. Moreover, our results suggest that the eventual performance and control behavior should ultimately depend on body dynamics and noise. A neural system adapting to relatively low process noise (and high sensor noise) would be expected to learn and rely heavily on an internal model. Conversely, relatively high process noise (and low sensor noise) would rely more heavily on sensory feedback. A limitation of our model is that it places few constraints on neural representation, because there are many ways (or "state realizations"(Kailath, 1980)) to achieve the same input–output function for estimation. But the importance and effects of noise on adaptation are hypotheses that might be testable with artificial neural networks or animal preparations.

## Limitations of the study

There are, however, cases where state estimation is less applicable. State estimation applies best to systems with inertial dynamics or momentum. Examples include inverted pendulum gaits with limited inherent (or passive dynamic(McGeer, 1990)) stability and pendulum-like leg motions(Kuo, 2002b). The perturbation sensitivity of such dynamics makes state estimation more critical. But other organisms and models may have well-damped limb dynamics and inherently stable body postures, and thus benefit less from state estimation. Others have proposed that intrinsic CPG rhythms may have greater importance in lower than higher vertebrates, potentially because of differences in inherent stability(Ryczko et al., 2020). There may also be task requirements that call for fast reactions with short synaptic delays, or organismal, energetic, or developmental considerations that limit the complexity of neural circuitry. Such concerns might call for reduced-order internal models(Kailath, 1980), or even their elimination altogether, in favor of faster and simpler pure feedforward or feedback. At the same time, actual neural circuitry is considerably more complex than the half-center model depicted here, and animals have far more degrees of freedom than considered here. There are some aspects of animal CPGs that could be simpler than full state estimation, and others that encompass very complex dynamics. A more holistic view would balance the principled benefits of internal models and state estimation against the practicality, complexity, and organismal costs.

There are a number of other limitations to this study. The "Anthropomorphic" walking model does not capture three-dimensional motion and

multiple degrees of freedom in real animals. We used such a simple model because it is unlikely to have hidden features that could produce the same results for unexpected reasons. We also modeled extremely simple sensors, without representing the complexities of actual biological sensors. The estimator also used a constant, linear gain, and could be improved with nonlinear estimator variants. However, more complex body dynamics could be incorporated quite readily, because the state estimator (Fig. 2.4) consists of an internal model of body dynamics (Eq. 2.7) and a feedback loop with appropriate gain ($\boldsymbol{L}$ designed by estimation principles), and no ad hoc parameters. Nonlinearities might also be accommodated by methods of Bayesian estimation(Rieke et al., 1999), of which optimal state estimation or Kalman filtering is a special case.

Another limitation is that we used a particularly simple, state-based command law, which was designed more for robustness than for economy. Better economy could be achieved by powering gait with precisely-triggered, trailing-leg push-off(Kuo, 2002b), rather than the simple hip torque applied here. However, the timing is so critical that feedforward conditions (low sensory feedback gains, Fig. 2.5) would fall too frequently to yield meaningful economy or step variability measures. We therefore elected for more robust control to allow a range of feedforward through feedback to be compared (Fig. 2.5). But even with more economical control or other control objectives, we would still expect best performance to correspond with optimal sensory gain, due to the advantages of accurate state information. We also used a relatively simple model of walking dynamics, for which more complex models could readily be substituted (Eq. 2.7) to yield an appropriate estimator. But more complex dynamics also imply more complex state-based locomotion

control, for which there are few principled approaches. The present study interprets the CPG as a means to produce an accurate state estimate, which could be considered helpful for state-based control of any complexity.

## 2.5 Conclusion

Our principal contribution has been to reconcile optimal control and estimation with biological CPGs. Evidence of fictive locomotion has long shown that neural oscillators produce timing and amplitude cues. But pre-determined timing is also problematic for optimal control in unpredictable situations(Cruse, 2002), leading some to question why CPG oscillators should dictate timing(Bässler, 1986; Pearson, 1987). To our knowledge, previous CPG models have not included process or sensor noise in control design. Such noise is simply a reality of non-uniform environments and imperfect sensors. But it also yields an objective criterion for uniquely defining control and estimation parameters. The resulting neural circuits resemble previous oscillator models and can produce and explain nominal, noisy, or fictive locomotion. In our interpretation, there is no issue of primacy between CPG oscillators and sensory feedback, because they interact optimally to deal with a noisy world.

## 2.6 Method

Details of the model and testing are as follows. The CPG model is first described in terms of neural, half-center circuitry, which is then paired with a walking model with pendulum-like leg dynamics. The walking gait is

produced by a state-based command generator, which governs how state information is used to drive motor neurons. The model is subjected to process and sensor noise, which tend to cause the gait to be imprecise and subject to falling. The CPG is then re-interpreted as an optimal state estimator, for which sensory feedback gain and internal model parameters may be designed, as a function of noise characteristics. The model is then simulated over multiple trials to computationally evaluate its walking performance as a function of sensory feedback gain. It is also simulated without sensory feedback, to test whether it produces fictive locomotion.

## CPG architecture based on Matsuoka oscillator

The CPG consists of two, mutually-inhibiting half-center oscillators, receiving a tonic descending input (Fig. 2.4A). Each half-center has second-order dynamics, described by states $u_i$ and $v_i$. This is equivalent to a primary Matsuoka neuron with states for a membrane potential and adaptation or fatigue (Matsuoka, 1987). Locomotion requires relatively longer time constants than is realistic for a single biological neuron, and so each model neuron here should be regarded as shorthand for a network of biological neurons with adaptable time constants and synaptic weights, that in aggregate produce first- or second-order dynamics of appropriate time scale. The state $u_i$ produces an output $q_i$ that can be fed to other neurons. In addition, we included two types of auxiliary neurons (for a total of three neurons per half-center): one for accepting the ground contact input ($c_i$, with value 1 when in ground contact and 0 otherwise for leg $i$), and the other to act as an alpha ($\alpha_i$) motoneuron to drive the leg. We used a single motoneuron to

generate both positive and negative (extensor and flexor) hip torques, as a simplifying alternative to including separate rectifying motoneurons.

Each half-center receives a descending command and two types of sensory feedback. The descending command is a tonic input $s$, which determines the walking speed. Sensory input from the corresponding leg includes continuous and discrete information. The continuous feedback contains information about leg angle from muscle spindles and other proprioceptors (Proske and Gandevia, 2012), which could be modeled as leg angle $y_i$ for measurement feedback, or error $e_i$ for error feedback sensors. The discrete information is about ground contact $c_i$ sent from cutaneous afferents (Trulsson, 2001).

The primary neuron's second-order dynamics are described by two states. The state $u_i$ is mainly affected by its own adaptation, a mutually inhibiting connection from other neurons, sensory input, and efference copy of the motor commands. The second state $v_i$ has a decay term, and is driven by the same neuron's $u_i$ as well as sensory input. This is described by the following equations, inspired by Matsuoka (1987) and previous robot controllers designed for rhythmic arm movements (e.g.,(Williamson, 1998) and walking(Endo et al., 2004)):

$$\dot{u}_i + a_i u_i = -b_i v_i + \sum_{j=1}^{2} -w_{ij} q_j + \sum_{j=1}^{2} h_{ij} e_j + \sum_{j=1}^{2} r_{ij} \alpha_j(s, v_j, c_j) + f_i(\boldsymbol{u}, \boldsymbol{v}, \boldsymbol{c}) \tag{2.1}$$

$$q_i = g(u_i) \tag{2.2}$$

$$\dot{v}_i + a'_i v_i = q_i + \sum_{j=1}^{2} h'_{ij} e_j \tag{2.3}$$

where there are several synaptic weightings: decays $a_i$ and $a'_i$, adaptation gain $b_i$, mutual inhibition strength $w_{ij}$ (weighting of neuron $i$'s input from neuron $j$'s output, where $w_{ii} = 0$), an output function $g(u_i)$ (set to identity here), sensory input gains $h_{ij}$ and $h'_{ij}$, and efference copy strength $r_{ij}$. The neuron also receives efference copy of its associated motor command $\alpha_j(s, v_j, c_j)$, which depends on neuron state, descending drive and ground contact. There are also secondary, higher-order influences summarized by the function $f_i(\boldsymbol{u}, \boldsymbol{v}, \boldsymbol{c})$, which have a relatively small effect on neural dynamics but are part of the state estimator as described below (see "Theoretical equivalence" section). The network parameters for such CPG oscillators are traditionally set through a combination of design rules of thumb and hand-tuning, but here nearly all of the parameters will be determined from an optimal state estimator, as described below.

## Walking model with pendulum dynamics

The system being controlled is a simple bipedal model walking in the sagittal plane (Fig. 2.2A). The model features pendulum-like leg dynamics(McGeer, 1990) with 16% of body mass at each leg (of length $l$) and 68% to pelvis/torso, which is modeled as a point mass. The leg's center of mass was located at $0.645l$ from the feet, radius of gyration of $0.326l$, and curved foot with radius $0.3l$. The legs are also actively actuated by added torque inputs (the "Anthropomorphic Model"(Kuo, 2001)), and energy is dissipated mainly with the collision of leg with ground in the step-to-step transition. The dissipation determines the amount of positive work required each step. In humans, muscles perform much of that work, which in turn accounts for

much of the energetic cost of walking(Donelan et al., 2002).

The walking model is described mathematically as follows. The equations of motion may be written in terms of vector $\boldsymbol{\theta} \triangleq [\theta_1, \theta_2]^T$ as

$$\mathrm{M}(\boldsymbol{\theta}, \mathbf{GC})\ddot{\boldsymbol{\theta}} + \mathrm{C}(\boldsymbol{\theta}, \dot{\boldsymbol{\theta}}, \mathbf{GC})\dot{\boldsymbol{\theta}} + \mathrm{G}(\boldsymbol{\theta}, \mathbf{GC}) = \mathrm{T}(s, \boldsymbol{\theta}, \mathbf{GC}) \tag{2.4}$$

where M is the mass matrix, C describes centripetal and Coriolis effects, G contains position-dependent moments such as from gravity, $\mathbf{GC} \triangleq [\mathrm{GC}_1, \mathrm{GC}_2]^T$ contains ground contact, and $\mathbf{T} \triangleq [T_1, T_2]^T$ contains hip torques exerted on the legs (State-based control, below). The equations of motion depend on ground contact because each leg alternates between stance and swing leg behaviors, inverted pendulum and hanging pendulum, respectively. We define each matrix to switch the order of elements at heel-strikes, so that equation of motion can be expressed in the same form.

At heelstrike, the model experiences a collision with ground affecting the angular velocities. This is modeled as a perfectly inelastic collision. Using impulse-momentum, the effect may be summarized as the linear transformation

$$\begin{bmatrix} \dot{\theta}_1^{\,+} \\ \dot{\theta}_2^{\,+} \\ \mathrm{GC}_1^{+} \\ \mathrm{GC}_2^{+} \end{bmatrix} = \mathrm{S}(\boldsymbol{\theta}, \mathbf{GC}) \cdot \begin{bmatrix} \dot{\theta}_1^{\,-} \\ \dot{\theta}_2^{\,-} \\ \mathrm{GC}_1^{-} \\ \mathrm{GC}_2^{-} \end{bmatrix} \tag{2.5}$$

where the plus and minus signs ('+' and '-') denote just after and before impact, respectively. The ground contact states are switched such that the previous stance leg becomes the swing leg, and vice versa. The simulation

avoided inadvertent ground contact of the swing legs by ignoring collisions until the stance leg reached a threshold (set as 10% of nominal stance leg angle at heel strike), as is common in simple 2D walking models with rigid legs(McGeer, 1990).

The resulting gait has several characteristics relevant to the CPG. First, the legs have pendulum-like inertial dynamics, which allow much of the gait to occur passively. For example, each leg swings passively, and its collision with ground automatically induces the next step of a periodic cycle(McGeer, 1990). Second, inertial dynamics integrate forces over time, such that disturbances can disrupt timing and cause falls. This sensitivity could be reduced with overdamped joints and low-level control, but humans are thought to have significant inertial dynamics(Alexander, 1995). And third, inertial dynamics are retained in most alternative models with more degrees of freedom and more complexity (e.g.,Geyer and Herr (2010); Peng et al. (2017)). We believe most other dynamical models would also benefit from feedback control similar in concept to presented here.

## State-based motor command generator

The model produces state-dependent hip torque commands to the legs. Of the many ways to power a dynamic walking model (e.g., Kuo (2001); Srinivasan and Ruina (2006); Westervelt et al. (2003); Spong (1999)), we apply a constant extensor hip torque against the stance leg, for its parametric simplicity and robustness to perturbations. The torque normally performs positive work (Fig. 2.2B) to make up for collision losses, and could be produced in reaction to a torso leaned forward (not modeled explicitly here; McGeer

(1990)). The swing leg experiences a hip torque proportional to swing leg angle (Fig. 2.2B,C), with the effect of tuning the swing frequency(Kuo, 2002b). This control scheme is actually suboptimal for economy, and is selected for its robustness. Optimal economy actually requires perfectly-timed, impulsive forces from the legs(Kuo, 2002a), and has poor robustness to the noisy conditions examined here. The present non-impulsive control is much more robust, and can still have its performance optimized by appropriate state estimation.

The overall torque command $T_i$ for leg $i$ is used as the motor command $\alpha_i$, and may be summarized as

$$T_i(s, \theta_i, \mathrm{GC}_i) = -(k_{st} + \mu_{st} s) \cdot \mathrm{GC}_i - (k_{sw} \theta_i) \cdot (1 - \mathrm{GC}_i) \qquad (2.6)$$

where the stance phase torque is increased from the initial value $k_{st}$ by the amount proportional to the descending command $s$ with gain $\mu_{st}$. The swing phase torque has gain $k_{sw}$ for the proportionality to leg angle $\theta_i$.

There are also two higher level types of control acting on the system. One is to regulate walking speed, by slowly modulating the tonic, descending command $s$ (Eq. 2.6). An integral control is applied on $s$, so keep attain the same average walking speed despite noise, which would otherwise reduce average speed. The second type of high-level control is to restart the simulation after falling. When falling is detected (as a horizontal stance leg angle), the walking model is reset to its nominal initial condition, except advanced one nominal step length forward from the previous footfall location. No penalty is assessed for this re-set process, other than additional energy and time wasted in the fall itself. We quantify the susceptibility to falling with a mean time between falls (MTBF), and report overall energetic cost in two

ways, including and excluding failed steps. The wasted energy of failed steps is ignored in the latter case, resulting in lower reported energy cost.

## Noise model with process and sensor noise

The walking dynamics are subject to two types of disturbances, process and sensor noise (Fig. 2.3). Both are modeled as zero-mean, Gaussian white noise. Process noise $n_x$ (with covariance $N_x$) acts as an unpredictable disturbance to the states, due to external perturbations or noisy motor commands. Sensor or measurement noise $n_y$ (with covariance $N_y$) models imperfect sensors, and acts additively to the sensory measurements $y$. The errors induced by both types of noise are unknown to the central nervous system controller, and so both tend to reduce performance.

The noise covariances were set so that the model would be significantly affected by both types of noise. We sought levels sufficient to cause significant risk of falling, so that good control would be necessary to avoid falling while also achieving good economy. Process noise was described by covariance matrix $N_x$, with diagonals filled with variances of noisy angular accelerations, which had standard deviations of $0.015(g/l)$ for stance leg, $0.16(g/l)$ for swing leg for the reference testing condition. Sensor noise covariance $N_y$ was also set as a diagonal matrix with both entries of standard deviation 0.1 for the reference testing condition. For the later demonstrations to test the effect of the different amount of noise, we multiplied 1.15 to the sensor noise covariance, and 0.36, 1.15, 2.06 to the process noise covariance. Noise was implemented as a spline interpolation of discrete white noise sampled at frequency of $16(g/l)^{0.5}$ (well above pendulum bandwidth)

and truncated to no more than ±3 standard deviations.

## State estimator with internal model of dynamics

A state estimator is formed from an internal model of the leg dynamics being controlled (see block diagram in Fig. 2.4), to produce a prediction of the expected state $\hat{x}$ and sensory measurements $\hat{y}$ (with the hat symbol '$\hat{}$' denoting an internal model estimate). Although the actual state is unknown, the actual sensory feedback $y$ is known, and the expectation error $e = y - \hat{y}$ may be fed back to the internal model with negative feedback (gain $L$) to correct the state estimate. Estimation theory shows that regulating error $e$ toward zero also tends to drive the state estimate towards actual state (assuming system observability, as is the case here; e.g.,(Kailath, 1980)). This may be formulated as an optimization problem, where gain $L$ is selected to minimize the mean-square estimation error. Here we interpret the half-center oscillator network as such an optimal state estimator, the design of which will determine the network parameters.

The estimator equations may be described in state space. The estimator states are governed by the same equations of motion as the walking model (Eqs. 2.4, 2.5), with the addition of the feedback correction. Again using hat notation for state estimates, the nonlinear state estimate equations are

$$\begin{bmatrix} \dot{\hat{\boldsymbol{\theta}}} \\ \ddot{\hat{\boldsymbol{\theta}}} \end{bmatrix} = \begin{bmatrix} \dot{\hat{\boldsymbol{\theta}}} \\ \mathrm{M}^{-1}(-\mathrm{C}\dot{\hat{\boldsymbol{\theta}}} - \mathrm{G} + \mathrm{T}) \end{bmatrix} + \mathrm{L}(\boldsymbol{\theta} - \hat{\boldsymbol{\theta}}) \tag{2.7}$$

We used standard state estimator equations to determine a constant sensory feedback gain $L$. This was done by linearizing the dynamics about

a nominal state, and then designing an optimal estimator based on process and sensor noise covariances ($N_x$ and $N_y$) using standard procedures ("lqe" command in Matlab, The MathWorks, Natick, MA). This yields a set of gains that minimize mean-square estimation error ($\boldsymbol{x} - \hat{\boldsymbol{x}}$), for an infinite horizon and linear dynamics. The constant gain was then applied to the nonlinear system in simulation, with the assumption that the resulting estimator would still be nearly optimal in behavior. Another sensory input to the system is ground contact $\mathrm{GC}_i$, a boolean variable. The state estimator ignores measured $\mathrm{GC}_i$ for pure feedforward control (zero feedback gain $L$), but for all other conditions (non-zero $L$), any sensed change in ground contact overrides the estimated ground contact $\hat{\mathrm{GC}}_i$. When the estimated ground contact state changes, the estimated angular velocities are updated according to the same collision dynamics as the walking model (Eq. 2.5 except with estimated variables).

The state estimate is applied to the state-based motor command (Eq. 2.6). Although the walking control was designed for actual state information ($\theta_i, \mathrm{GC}_i$), for walking simulations it uses the state estimate instead:

$$T_i(s, \hat{\theta}_i, \hat{\mathrm{GC}}_i) = -(k_{st} + \mu_{st} s) \cdot \hat{\mathrm{GC}}_i - (k_{sw} \hat{\theta}_i) \cdot (1 - \hat{\mathrm{GC}}_i) \qquad (2.8)$$

As with the estimator gain, this also requires an assumption. In the present nonlinear system, we assume that the state estimate may replace the state without ill effect, a proven fact only for linear systems (certainty-equivalence principle,(Bryson, 1975; Simon, 1956)). Both assumptions, regarding gain $L$ and use of state estimate, are tested in simulation below.

## Theoretical equivalence between neural oscillator and state estimator

Having fully described the walking model in terms of control systems principles, the equivalent half-center oscillator model may be determined (Fig. 2.4B). The identical behavior is obtained by re-interpreting the neural states in terms of the dynamic walking model states,

$$u_1 \triangleq \dot{\hat{\theta}}_1, v_1 \triangleq \hat{\theta}_1, u_2 \triangleq \dot{\hat{\theta}}_2, v_2 \triangleq \hat{\theta}_2 \tag{2.9}$$

along with the neural output function defined as identity,

$$q_1 = g(u_i) \triangleq u_i. \tag{2.10}$$

In addition, motor command and ground contact state are defined to match state-based variables (Eq. 2.6):

$$\alpha_1 \triangleq T_1, \alpha_2 \triangleq T_2, c_1 \triangleq \mathrm{G}\hat{\mathrm{C}}_1, c_2 \triangleq \mathrm{G}\hat{\mathrm{C}}_2. \tag{2.11}$$

The synaptic weights and higher-order functions (Eqs. 2.1–3) are defined according to the internal model equations of motion (Eq. 2.7),

$$\begin{bmatrix} a_1 & w_{12} \\ w_{21} & a_2 \end{bmatrix} = \mathrm{M}^{-1}\mathrm{C} \tag{2.12}$$

$$\begin{bmatrix} b_1\hat{\theta}_1 - f_1(\boldsymbol{\theta}, \dot{\boldsymbol{\theta}}, \hat{\mathbf{GC}}) \\ b_2\hat{\theta}_2 - f_2(\boldsymbol{\theta}, \dot{\boldsymbol{\theta}}, \hat{\mathbf{GC}}) \end{bmatrix} = \mathrm{M}^{-1}\mathrm{G} \tag{2.13}$$

$$\begin{bmatrix} h'_{11} & h'_{12} \\ h'_{21} & h'_{22} \\ h_{11} & h_{12} \\ h_{21} & h_{22} \end{bmatrix} = \mathrm{L} \tag{2.14}$$

$$\begin{bmatrix} r_{11} & r_{12} \\ r_{21} & r_{22} \end{bmatrix} = \mathrm{M}^{-1} \tag{2.15}$$

$$a'_1 = a'_2 = 0 \tag{2.16}$$

Because the mass matrix and other variables are state dependent, the weightings above are state dependent as well. The functions $f_1$ and $f_2$ are higher-order terms, which could be considered optional; omitting them would effectively yield a reduced-order estimator.

The result of these definitions is that the half-center neuron equations (Eqs. 2.1–3) may be rewritten in terms of $\theta_i$ and $\dot{\theta}_i$, to illustrate how the network models the leg dynamics and receives inputs from sensory feedback and efference copy:

$$\ddot{\hat{\theta}}_i + a_i \dot{\hat{\theta}}_i = -b_i \dot{\hat{\theta}}_i + \sum_{j=1}^{2} -w_{ij} \hat{\theta}_j + \sum_{j=1}^{2} h_{ij} e_j + \sum_{j=1}^{2} r_{ij} \alpha_j(s, \hat{\theta}_j, \hat{\mathrm{GC}}) + f_i(\hat{\boldsymbol{\theta}}, \dot{\hat{\boldsymbol{\theta}}}, \hat{\mathbf{GC}}) \tag{2.17}$$

$$\dot{\hat{\theta}}_i + a'_i \hat{\theta}_i = \dot{\hat{\theta}}_i + \sum_{j=1}^{2} h_{ij} e_j \tag{2.18}$$

The above may be interpreted as an internal model of the stance and swing leg as pendulums, with pendulum phasing modulated by error feedback $e_j$ and efference copy of the motor command (plus small nonlinearities due to inertial coupling of the two pendulums).

The result is that the entire neural circuitry and parameters are fully specified by the control systems model. In Eqs. 2.17–18), all of the quantities except motor command $\alpha$ are determined by a state estimator (Eq. 2.7) with optimal gains (determined by single Matlab command 'lqe'.) For example, higher-order terms $f_i(\hat{\boldsymbol{\theta}}, \dot{\hat{\boldsymbol{\theta}}}, \mathbf{G}\hat{\mathbf{C}})$ are defined by Eq. 2.13). The only aspect of the system not determined by optimal estimation was the motor command $\alpha$, equal to the state-based motor command (Eq. 2.8). This was designed ad hoc to produce alternating stance and swing phases with high robustness to perturbations.

## Parametric effect of varying sensory feedback gain L

The sensory feedback gain is selected using state estimation theory, according to the amount of process noise and sensor noise. High process noise, or uncertainty about the dynamics and environment, favors a higher feedback gain, whereas high sensor noise favors a lower feedback gain. The ratio between the noise levels determines the optimal linear quadratic estimator gain $L^*_{\text{lqe}}$ (Matlab function "lqe"). A constant gain was determined based on a linear approximation for the leg dynamics, an infinite horizon for estimation, and a stationarity assumption for noise. In simulation, the state estimator was implemented with nonlinear dynamics, assuming this would yield near-optimal performance.

It is thus instructive to evaluate walking performance for a range of feedback gains. Setting $L$ too low or too high would be expected to yield poor performance. Setting $L$ equal to the optimal LQE gain $L^*_{\text{lqe}}$ would be expected to yield approximately the least estimation error, and therefore the most precise control (e.g. Rebula et al. (2017)). In terms of gait, more precise control would be expected to reduce step variability and mechanical work, both of which are related to metabolic energy expenditure in humans (e.g.,O'Connor et al. (2012)). The walking model is also prone to falling when disturbed by noise, and optimal state estimation would be expected to reduce the frequency of falling.

We performed a series of walking simulations to test the effect of varying the feedback gain. The model was tested with 20 trials of 100 steps each, subjected to pseudorandom process and sensor noise of fixed covariance ($W$ and $V$, respectively). In each trial, walking performance was assessed with mechanical cost of transport (mCOT, defined as positive mechanical work per body weight and distance travelled; e.g.,(Collins et al., 2005)), step length variability, and mean time between falls (MTBF) as a measure of walking robustness (also referred to as Mean First Passage Time(Byl and Tedrake, 2009)). The sensory feedback gain $L^*_{\text{lqe}}$ was first designed in accordance with the experimental noise parameters, and then the corresponding walking performance was evaluated. Additional trials were performed, varying sensory feedback gain $L$ with lower and higher than optimal values to test for a possible performance penalty. These sub-optimal gains were determined by re-designing the estimator with process noise $\rho W$ ($\rho$ between $10^{-4}$ and $10^{0.8}$, with smaller values tending toward pure feedforward and larger toward pure feedback). This procedure guarantees stable closed-loop

estimator dynamics, which would not be the case if the matrix $L^*_{\text{lqe}}$ were simply scaled higher or lower. For all trials, the redesigned $L$ was tested in simulations using the fixed process and sensor noise levels. The overall sensory feedback gain was quantified with a scalar, defined as the L2 norm (largest singular value) of matrix $L$, normalized by the L2 norm of $L^*_{\text{lqe}}$.

We expected that optimal performance in simulation would be achieved with gain $L$ close to the theoretically optimal LQE gain, $L^*_{\text{lqe}}$. With too low a gain ($L = 0$, feedforward Fig. 2.1A), the model would perform poorly due to sensitivity to process noise, and with too high a gain ($L \to \infty$, feedback Fig. 2.1C), it would perform poorly due to sensor noise. And for intermediate gains, we expected performance to have an approximately convex bowl shape, centered about a minimum at or near $L^*_{\text{lqe}}$. These differences were expected from noise alone, as the model was designed to yield the same nominal gait regardless of gain $L$. Simulations were necessary to test the model, because its nonlinearities do not admit analytical calculation of performance statistics.

## Evaluation of fictive locomotion

We tested whether the model would produce fictive locomotion with removal of sensory feedback. Disconnection of feedback in a closed-loop control system would normally be expected to eliminate any persistent oscillations. But estimator-based control actually contains two types of inner loops (Fig. 2.7A), both of which could potentially allow for sustained oscillations in the absence of sensory feedback. However, the emergence of fictive locomotion and its characteristics depend on what kind of sensory signal is

removed. We considered two broad classes of sensors, referred to producing error feedback and measurement feedback, with different expectations for the effects of their removal.

Some proprioceptors relevant to locomotion, including some muscle spindles and fish lateral lines(Straka et al., 2018), could be regarded as producing error feedback. They receive corollary discharge of motor commands, and appear to predict intended movements, so that the afferents are most sensitive to unexpected perturbations. The comparison between expected and actual sensory output largely occurs within the sensor itself, yielding error signal $e$ (Fig. 2.7B). Disconnecting the sensor would therefore disconnect error signal $e$, and would isolate an inner loop between state-based command and internal model. The motor command normally sustains rhythmic movement of the legs for locomotion, and would also be expected to sustain rhythmic oscillations within the internal model. Fictive locomotion in this case would be expected to resemble the nominal motor pattern.

Sensors that do not receive corollary discharge could be regarded as direct sensors, in that they relay measurement feedback related to state. In this case, disconnecting the sensor would be equivalent to removing measurement $y$. This isolates two inner loops, both the command-and-internal-model loop above, as well as a sensory prediction loop between sensor model and internal model. The interaction of these loops would be expected to yield a more complex response, highly dependent on parameter values. Nonetheless, we would expect that removal of $y$ would substantially weaken the sensory input to the internal model, and generally result in a weaker or slower fictive rhythm.

We tested for the existence of sustained rhythms for both extremes of error feedback and measurement feedback. Of course, actual biological sensors within animals are vastly more diverse and complex than this model. But the existence of sustained oscillations in extreme cases would also indicate whether fictive locomotion would be possible with some combination of different sensors within these extremes.

## Code availability

The source code for the simulation, supplementary table and video are available in a public repository at:

https://github.com/hansolxryu/CPG_biped_walker_Ryu_Kuo

(https://doi.org/10.5281/zenodo.4739744).

# Chapter 3

# What loss functions do humans optimize when they perform regression and classification

## 3.1 Abstract

Understanding how humans perceive patterns in visually presented data is useful for understanding data-based decision-making and, possibly, visually mediated sensorimotor control under disturbances and noise. Here, we conducted human subject experiments to examine how humans perform the simplest machine learning or statistical estimation tasks: linear regression and binary classification in data presented visually as 2D scatter plots. We used simple inverse optimization to infer the loss function humans optimize when they perform these tasks. In classical machine learning, common loss functions for regression are mean squared error or summed absolute error, and logistic loss or hinge loss for classification. For the regression

task, minimizing the sum of error raised to the power of 1.7 on average best described human subjects performing regression on sparse data consisting of relatively fewer data points. Loss functions with lower exponents, which would reject outliers more effectively, were better descriptors for regression tasks performed on less sparse data. For the classification task, minimizing a logistic loss function was on average a better descriptor of human choices than an exponential loss function applied to only misclassified data. People changed their strategies as data density increased, such that loss functions with lower exponents described empirical data better. These results represent overall trends across subjects and trials but there was large inter- and intra-subject variability in human choices. Future work may examine other loss function families and other tasks. Such understanding of human loss functions may inform designing computer algorithms that interact with humans better and imitate humans more effectively.

## 3.2 Introduction

Understanding how humans perceive patterns in visually presented noisy data is useful for understanding data-based decision-making (Keim et al., 2006; Moore, 2017; Kahneman et al., 2021), sensorimotor control under uncertainty caused by disturbance and noise (Körding and Wolpert, 2004a; Srinivasan, 2009; Körding and Wolpert, 2004b; Todorov and Jordan, 2002), and indeed, more directly, just visual perception (Glass and Pérez, 1973; Glass and Switkes, 1976; Dittrich, 1993). Examples of humans interpreting visually presented data include examining medical images (Lewandowsky and Spence, 1989), driving a car (Hills, 1980), playing a sport (Davids et al.,

2005), or living life in general (Palmer, 1975). On the simpler end of this spectrum of task and data complexity is interpreting 2D scatter plots of scientific data. Here, we study humans performing two simple types of visual pattern recognition tasks involving scatter plots, coinciding with fundamental machine learning and statistical inference problems: 1) linear regression (or "fitting"), that is, finding a curve that best represents continuous-valued input-output data (figure 3.1A); and 2) binary classification, that is, finding a decision boundary that separates data already labeled as belonging to two categories (figure 3.1B).

Classical machine learning algorithms for regression and classification usually find a solution that minimizes a loss function (Bishop and Nasrabadi, 2006). For regression problems, a commonly used loss function is the mean squared error (Luenberger, 1997; Bishop and Nasrabadi, 2006), equivalently, the $L_2$ norm of the error, resulting in the ordinary least squares (OLS) regression. Other commonly used loss functions are mean absolute errors (equivalently, $L_1$ norm) and the mean perpendicular distance between the regression surface and data (orthogonal regression). For binary classification problems, common loss functions used include cross-entropy, also called logistic loss function or log loss (Shore and Gray, 1982), and hinge loss function, used for support vector machines (Drucker et al., 1996). Loss functions are chosen for their favorable properties including robustness to outliers, avoiding over-fitting, convexity, and uniqueness of the solution (Wang et al., 2022). Here, we examine whether human behavior in manual regression and binary classification tasks can be described as a solution of an optimization problem minimizing a loss function, and aim to characterize the loss function through human experiments (figure 3.3). Different

loss functions make different predictions depending on the data distribution (figure 3.2), and we use this fact to determine the loss function that best predicts observed human behavior, a process sometimes called inverse optimization (Tarantola, 2005; Liu et al., 2005).

Some studies have attempted to characterize the strategies human subjects use in such simple tasks (Lewandowsky and Spence, 1989), but most studies did not seek to provide quantitative descriptions of the loss function. For instance, it has been reported that human subjects were able to reject outliers when performing regression (Correll and Heer, 2017), sometimes better than some mathematical methods (Wainer and Thissen, 1979). For fitting a straight line to data, subjects selected the slope closer to that of the first principal component, instead of the one with the least mean squares (Mosteller et al., 1981). Subjects with formal regression training selected lines closer to the least square fit, whereas subjects without regression training seemed to use other heuristics (Gillan, 2020). These studies compared human choices to the solutions of a few discrete strategies, rather than considering strategies on a continuum using inverse optimization approaches. These studies are also limited to the particular datasets used: for instance, the scale of the data axis was observed to affect human perception (Cleveland et al., 1982). Another study performed inverse optimization in a sensorimotor task for a narrow set of conditions (Körding and Wolpert, 2004a).

Relatively little has been done on inferring loss functions from human classification, as human labels are usually regarded as ground truth for machine learning and not analyzed independently. In one study, the support vector machine best predicted human behaviors among four algorithms

considered for gender classification tasks from human facial images (Graf et al., 2006). Another study observed how subjects perceive transforming geometric shapes, describing when humans start to classify a transforming shape into a different shape (Gopsill et al., 2021). A study investigating the classification of scatter plot data reported high failure rates of about 50%, when evaluating an algorithm's performance via manual inspections (Sedlmair et al., 2012). Thus, this study showed discrepancies between algorithmic output and human choices, but did not aim to characterize human behavior during classification tasks.

In real-world applications, regression and classification problems can be high-dimensional both in terms of data dimensionality and in terms of requiring high model complexity (such as via neural networks). Solving them not only requires minimizing errors in describing the data presented (training error) but often also requires considering related issues of model complexity, generalization, and avoiding over-fitting. Here, we intentionally ignore these latter issues by considering the simplest one degree of freedom regression and binary classification problems (figure 3.1), which are minimally sufficient to infer how humans penalize errors of different magnitudes via a loss function. Secondly, we examine whether human perception of the pattern depends on data sparsity. Computer algorithms are less likely to change the loss function based on the amount of data, but humans may perceive different data amounts as qualitatively different. Classifying a sparse, handful of dots into two groups could appear to be different from classifying thousands of dots into two groups, which resembles identifying and separating two visually distinct areas in a digital image. So, here, we inferred regression and classification loss functions from human experiments

with different visual data sparsity, showing how visual sparsity can affect behavior.

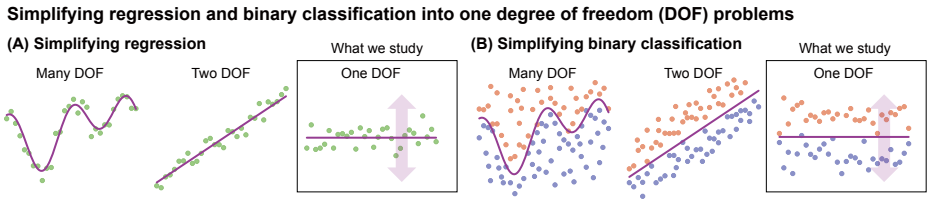


Figure 3.1: **Simplifying regression and classification.** A) Regression problems of decreasing complexity  many degrees of freedom, two degrees of freedom, and one degree of freedom. We consider the simplest regression problem where the output function is a constant, so that there is only one degree of freedom as shown in the third panel. B) Classification problems of decreasing complexity: many degrees of freedom, two degrees of freedom, and one degree of freedom. Similarly, we consider the simplest binary classification problem where the classifier is a constant function, so there is only one degree of freedom. The one degree of freedom problem is sufficient to infer how prediction errors are penalized by the loss function, while deliberately ignoring issues such as model complexity, generalization, and over-fitting.

## 3.3 Methods

### Experiments

Subjects participated with informed consent and the experimental protocol was approved by the Ohio State University Institutional Review Board. Subjects performed two types of tasks: 1) a regression task ($N_{\text{subjects}} = 23$ subjects) and 2) a binary classification task ($N_{\text{subjects}} = 23$ subjects; one subject's medium sparsity data and one subject's low sparsity data was corrupted, thus excluded). For regression, we showed dots of a single color on a computer screen, and asked "What is the horizontal line that best describes

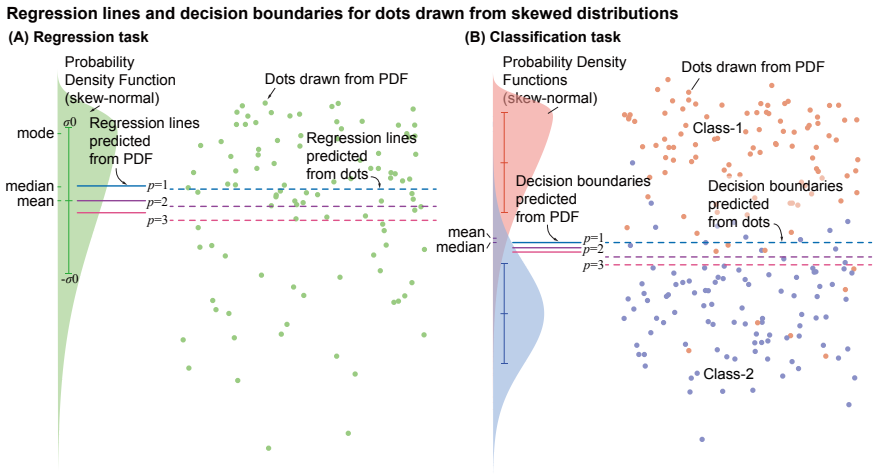


Figure 3.2: **Regression lines and decision boundaries that minimized various objective functions on skewed probability distributions.** (A) A skew-normal distribution (green shaded) was used to generate regression test dataset. (B) One skew-normal (orange shaded) and one normal distribution (blue shaded) were used to generate classification task test data. Probability distribution functions (PDFs, shown as shaded graphs) of skew-normal distributions have distinct mode, median, and mean. Error bars represent mean ± variance of each PDF. Vertical locations of the dots were drawn from the PDFs. The location of the regression lines or decision boundaries depends on the exponent parameter $p$ of the loss function they minimize. These locations calculated from the PDFs and from the actual dot locations are close to each other, but do not perfectly match when there are only a finite number of dots.

the dots?" (figure 3.3A). For classification, we showed dots of two colors, with various amounts of overlapping, and asked "What is the horizontal line that best separates the dots into two groups based on their colors?" (figure 3.3B). Subjects used either a keyboard or mouse to select the vertical location of the horizontal line that best fit or classified the dots. Subjects could re-select the lines as many times as they wanted without a time limit. Subjects performed the test either on the experimenter's computer or on their own. After the test, subjects optionally filled out a questionnaire about

what their strategies were for each sparsity level and whether they were familiar with regression or classification algorithms.

Subjects performed tests with data of different sparsity and skewness, drawn from specific probability distributions (figure 3.3C). There were 40 trials per sparsity condition and 120 trials total per subject. About two-thirds of the subjects ($N_{\text{subjects}} = 16$ for both tasks) were tested with a partially randomized order: they performed the task on high sparsity data first, then medium, and then the low sparsity, while skewness and other conditions within each sparsity condition were randomized. Other subjects were tested in a fully randomized order including the sparsity. We made this decision to keep most of the subjects unaware of the underlying probability density distribution when they perform a task on high sparsity data, because the underlying distribution could become more obvious when they have seen the dots of lower sparsity and this could be used as a priori knowledge. We found no evidence that the different randomization had a significant effect, but given the high variability of the results, order effects could be studied with a bigger sample size.

## Probability distributions for the testing data

### Datasets for regression task

We drew testing data from skew probability distributions, so that minimizing different loss functions predicts different regression lines (figure 3.2). We used skew-normal distributions $\mathcal{SN}(\lambda)$ given by:

$$y = \frac{\xi}{\sqrt{1+\lambda^2}}(\lambda|u_1| + u_2) \sim \mathcal{SN}(\lambda), \quad \text{where } u_1, u_2 \sim \mathcal{N}(0, \sigma_0^2), \tag{3.1}$$

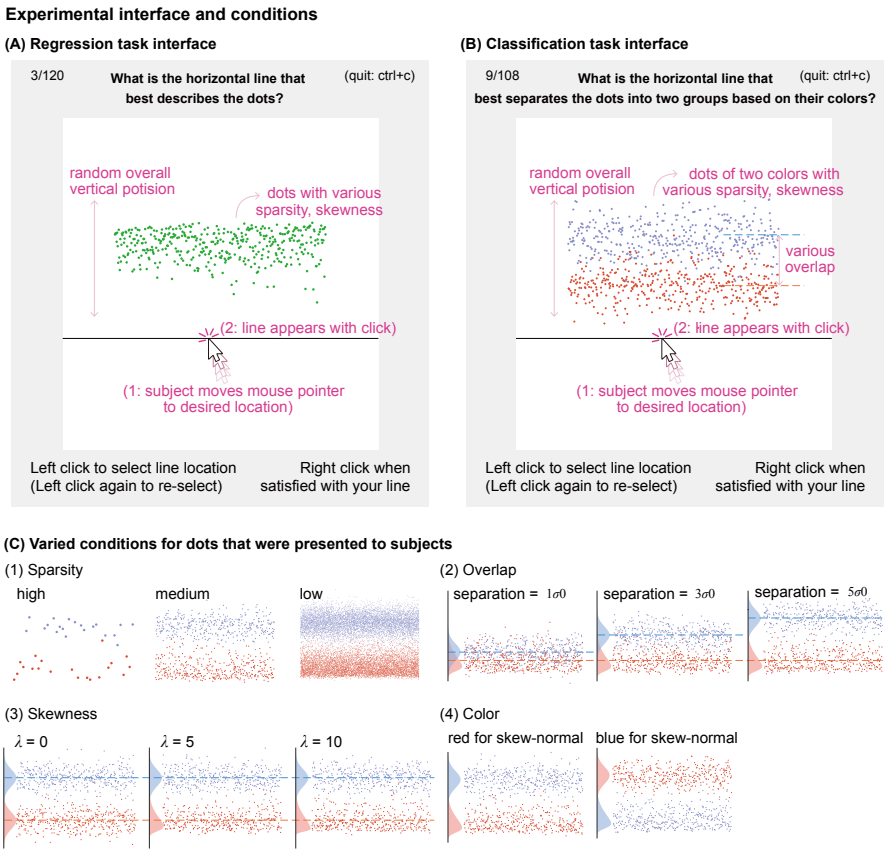


Figure 3.3: **Testing interface** for (A) regression and (B) classification tasks, and (C) conditions that were varied when dots were generated, to be used as testing datasets. On the testing interface (A and B), the task goal was shown on the top of the testing interface with the trial number and termination instruction on the side. Instructions on how to select a line and move to the next trial were shown on the bottom as text. Dots are shown in the white window of the test interface, and when a subject selects a line location by clicking the left button of the mouse, a horizontal line appears at that location. Subjects were free to select the line again as many times as they wanted. Pink labels are added only for the paper and are not shown to subjects, and some components have been re-sized here for illustrative purposes. The vertical locations of the dots were generated from probability distributions of varied conditions as shown in panel (C). Four conditions, (1) sparsity (2) overlap (3) skewness, and (4) color, were changed to generate testing data for classification tasks. The conditions used for the regression were subsets of those shown.

when $\lambda$ is a shape parameter (Azzalini, 1985; Henze, 1986). Shape parameter $\lambda = 0$ gives normal distribution $\mathcal{N}(0, \sigma_0^2)$ with a mean 0 and variance $\sigma_0^2$ and increasing $|\lambda|$ increases skewness. The normalization constant $\xi = \sqrt{1 - \frac{2\lambda^2}{\pi(\lambda^2+1)}}$ ensures that the variance remains $\sigma_0^2$ regardless of $\lambda$. We used shape parameter values $\lambda = 0, \pm5, \pm10, \pm40$ (figure 3.3C-3). For the skew-symmetric distributions ($\lambda \neq 0$), the mode is at the head of the distribution where probability density is the highest, and the median and the mean were located on the longer tail (figure 3.2). When the distribution is symmetric and unimodal ($\lambda = 0$), regression using typical loss functions mostly yields the same solution: the mean, median and mode are all identical. We still included $\lambda = 0$ trials, but trials with $\lambda \neq 0$ provide more information on human loss functions.

**Datasets for classification task**

We generated dots of two colors for the binary classification task, one from a normal distribution and the other from a skew-normal distribution, so different loss functions yield different classification boundaries (figure 3.2). We use the same skew-normal distributions as for the regression task with $\lambda = 0, \pm5, \pm10$ (figure 3.3C-3). We changed the overlap between two distributions, separating the theoretical means of the two distributions by $\sigma_0$, 3 $\sigma_0$, 5 $\sigma_0$ (figure 3.3C-2). The normal distribution ($\lambda = 0$) was always on the skew-normal distribution's longer-tail side and ensured overlap of the two sets: we re-generated the data until the lowest dot of the upper distribution was lower than the highest of the lower distribution by 0.05 $\sigma_0$. We included $\lambda = 0$ trials, but $\lambda \neq 0$ trials, when different loss functions have different predictions, are more informative.

### Sparsity

For both regression and classification task, we tested high-, medium-, low-sparsity datasets, respectively, using $N_{\text{data}} = 20, 400, 8000$ dots of each color (figure 3.3C-1). Only the vertical positions of the dots were randomly drawn from the specified distributions; the horizontal positions were evenly spaced. The size of the dots was scaled across the different sparsity conditions such that the area of each dot multiplied by the number of dots stays the same. We changed overall vertical position of the dots on the display each trial to minimize the effect of the previous trial. We used orange and blue colors for the classification task, which are usually distinguishable with some color vision deficiency (Wong, 2011). We randomized the vertical order of the normal and skew-normal distribution, and the color of the top versus bottom distribution (figure 3.3C-4).

## Loss function models to predict regression lines and classification decision boundaries

### Loss functions for regression

The loss function $J_\mu(\hat{y}, \boldsymbol{y})$ is a function of the data points $\boldsymbol{y}$, a candidate vertical location of the regression line $\hat{y}$, and possibly other hyperparameters $\mu$, such that the optimal regression line location $\hat{y}^*$ is obtained by minimizing this loss function as follows:

$$\text{Regression line } \hat{y}^* = \arg\min_{\hat{y}} J_\mu(\hat{y}, \boldsymbol{y}). \tag{3.2}$$

We may denote $\hat{y}^*$ as $\hat{y}^*(J_\mu, \boldsymbol{y})$ to show dependence on both the loss function $J_\mu$ and the data $\boldsymbol{y}$. In this study, we considered loss functions that are sums of the absolute regression error raised to various exponents $p$ (figure 3.4A-1). Regression error here refers to the difference between the regression line and each data point. When the vertical location of the $i$-th dot is $\boldsymbol{y}(i)$, and the regression error of the dot is $\boldsymbol{x}(i) = \boldsymbol{y}(i) - \hat{y}$, the regression loss function with exponent parameter $p$ is given by:

$$J_{\mathrm{reg},p}(\hat{y}, \boldsymbol{y}) = \sum_{i=1}^{N} |\boldsymbol{y}(i) - \hat{y}|^p = \sum_{i=1}^{N} |\boldsymbol{x}(i)|^p, \tag{3.3}$$

equivalent to using the error vector's $L_p$ norm. The individual summand in the loss function (figure 3.4A-1), $|x|^p$, defines how error from each point contributes to the total loss (figure 3.4B). It is symmetric with respect to zero error, so that error on either side of the regression line has the same loss.

The effect of the exponent $p$ on the overall loss could be understood in terms of how larger regression errors are penalized relative to the small errors. For example, regression loss function summand $|x|^2$ grows faster than $|x|^1$, thus penalizing larger error relatively more (figure 3.4A-1). So, minimizing $J_{\mathrm{reg},2}$ results in a regression line more towards the tail of the distribution compared to minimizing $J_{\mathrm{reg},1}$ on a skew-normal distribution (figure 3.2A), because moving the regression line towards the tail of the distribution reduces larger errors that come from the further points.

### Loss functions for binary classification

The loss function for binary classification $J_\mu(\hat{y}, \boldsymbol{y}_1, \boldsymbol{y}_2)$ is a function of the candidate decision boundary $\hat{y}$ location and the data points $\boldsymbol{y}_1$ and $\boldsymbol{y}_2$, belonging to the two classes (two colors), class-1 and class-2 respectively.

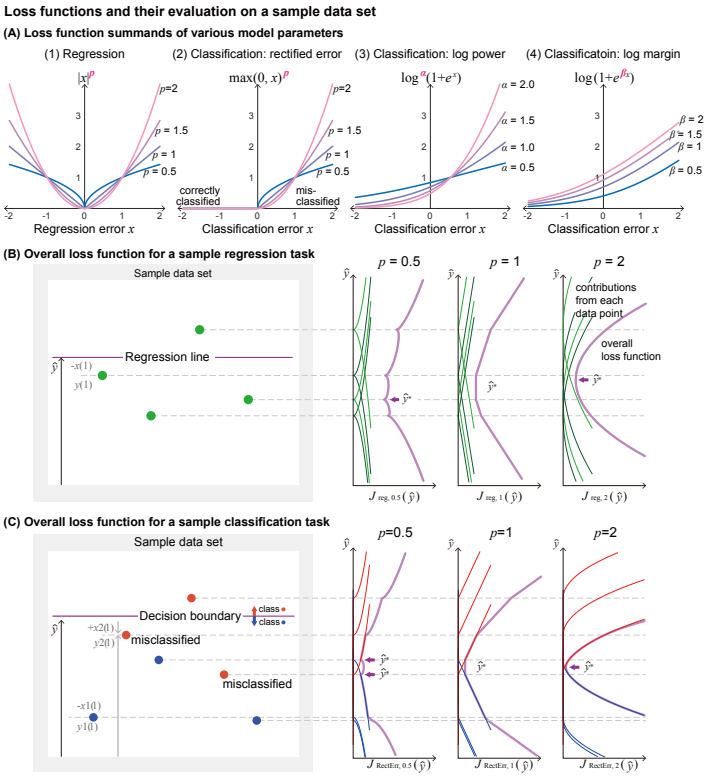


Figure 3.4: **Demonstration of various loss functions for regression and classification tasks.** (A) Loss function summands of various parameters, as functions of (1) regression error $x$ for regression task, or functions of (2-4) classification error $x$ for classification task. (1) Regression loss function with exponent parameter $p$. (2) Rectified error loss function, with exponent parameter $p$. (3) Log power loss function with power parameter $\alpha$. (4) Log margin loss function with margin parameter $\beta$. (B) Evaluation of overall regression loss for a sample regression task dataset $\boldsymbol{y}$, as a function of the regression line location $\hat{y}$, with various exponent parameters. The overall loss (purple thick line) is a sum of contributions from each data point (green thin lines). (C) Evaluation of overall rectified error loss for a sample classification task dataset $\boldsymbol{y}_1, \boldsymbol{y}_2$, as a function of the regression line location $\hat{y}$, with various exponent parameters. The overall loss (purple thick line) is a sum of contributions from orange class (orange thin lines) and blue class (blue thin lines) data points. Orange dots have positive classification errors when the decision boundary is above them (two orange dots marked as "misclassified" have positive losses for the decision boundary shown in the illustration), and blue dots have positive classification errors when the decision boundary is below them. $\hat{y}^*$ indicates global minima.

The decision boundary divides the data points into two groups, so that data above the boundary is classified as class-1 and data below the boundary is classified as class-2. The optimal decision boundary $\hat{y}^*$ is defined as minimizing the loss function $J_\mu$ (figure 3.4C) as follows:

$$\text{Decision boundary } \hat{y}^* = \arg\min_{\hat{y}} J_\mu(\hat{y}, \boldsymbol{y}_1, \boldsymbol{y}_2). \tag{3.4}$$

We may denote $\hat{y}^*$ as $\hat{y}^*(J_\mu, \boldsymbol{y}_1, \boldsymbol{y}_2)$ to show dependence on both the loss function and the two datasets.

Loss functions for classification are defined such that misclassified points increase the loss more than correctly classified points do (Bishop and Nasrabadi, 2006). We consider two types of loss functions: those that only penalize misclassified points and are not affected by correctly classified points, and those that also account for correctly classified points. Our datasets were not linearly separable and always had misclassified points. Let the location of the $i$-th member of the two classes be $\boldsymbol{y}_1(i)$ and $\boldsymbol{y}_2(i)$. Members of $\boldsymbol{y}_1$ but located above a candidate decision boundary $\hat{y}$ (i.e., $\boldsymbol{y}_1(i) - \hat{y} > 0$), and members of $\boldsymbol{y}_2$ but located below the boundary (i.e., $\hat{y} - \boldsymbol{y}_2(i) > 0$), are misclassified by the decision boundary $\hat{y}$. We define classification error $\boldsymbol{x}_c$ for for $c = 1, 2$ as follows: for data points in class-1, $\boldsymbol{x}_1(i) = \boldsymbol{y}_1(i) - \hat{y}$ and for data points in class-2, $\boldsymbol{x}_2(i) = \hat{y} - \boldsymbol{y}_2(i)$, ensuring that the classification error $\boldsymbol{x}_c(i)$ is positive when misclassified. We now describe specific loss functions considered.

**Rectified error classification loss function.** As an example of a loss function that only penalizes misclassified points, we investigated the effect of the exponents on the positive part of the classification error ("rectified error",

figure 3.4A-2). We define the rectified error classification loss function with exponent parameter $p$ as:

$$J_{\text{RectErr},p}(\hat{y}, \boldsymbol{y}_1, \boldsymbol{y}_2) = \sum_{i=1}^{N} \max\left(\boldsymbol{y}_1(i) - \hat{y}, 0\right)^p + \sum_{i=1}^{N} \max\left(\hat{y} - \boldsymbol{y}_2(i), 0\right)^p$$
$$= \sum_{c=1}^{2} \sum_{i=1}^{N} \max\left(\boldsymbol{x}_c(j), 0\right)^p, \tag{3.5}$$

where the positive part or rectification function $\max(x, 0)$ is the ReLU function. The exponent parameter $p$ has a similar effect to that in the regression loss function. A loss function with bigger $p$ penalizes bigger errors relatively more than a loss function with smaller $p$ does. For distributions used here, since the skew-normal distribution has a heavier tail than a normal distribution on the overlapping side, decision boundaries tend to move towards the tail of the skew-normal distribution when the exponent $p$ of the loss function increases (figure 3.2B). When $p = 1$, the decision boundary divides data points such that there are equal numbers of misclassified points on both sides, analogous to a median.

**Log power classification loss function and log margin classification loss function.** For loss functions that also take into account correctly classified points, as the distance between the correctly classified points and the decision boundary increases, the classification becomes "more correct, and thus gives a better margin for the decision boundary. However, the loss still needs to increase more with misclassified points, in order to have sensible classification. In this study, we used two one-parameter family of functions derived from the logistic loss function, in which loss smoothly increases with positive classification error (from misclassified data) and decreases with negative error (from correctly classified data). The "Log power"

classification loss function with power parameter $\alpha$ is given by:

$$J_{\text{logPower},p}(\hat{y}, \boldsymbol{y}_1, \boldsymbol{y}_2) = \sum_{i=1}^{N} \log^{\alpha}\left(1 + e^{(\boldsymbol{y}_1(i)-\hat{y})}\right) + \sum_{i=1}^{N} \log^{\alpha}\left(1 + e^{(\hat{y}-\boldsymbol{y}_2(i))}\right)$$
$$= \sum_{c=1}^{2}\sum_{j=1}^{N} \log^{\alpha}\left(1 + e^{\boldsymbol{x}_c(j)}\right), \tag{3.6}$$

and the "log margin" classification loss function with margin parameter $\beta$ is given by:

$$J_{\text{logMargin},\beta}(\hat{y}, \boldsymbol{y}_1, \boldsymbol{y}_2) = \sum_{i=1}^{N} \log\left(1 + e^{\beta(\boldsymbol{y}_1(i)-\hat{y})}\right) + \sum_{i=1}^{N} \log\left(1 + e^{\beta(\hat{y}-\boldsymbol{y}_2(i))}\right)$$
$$= \sum_{c=1}^{2}\sum_{j=1}^{N} \log\left(1 + e^{\beta\boldsymbol{x}_c(j)}\right). \tag{3.7}$$

We analyzed the effect of the exponent in the"log power" loss (figure 3.4A-3) and the margin parameter in the "log margin" loss (figure 3.4A-4, Masnadi-Shirazi and Vasconcelos (2015)). In addition to these three one-parameter families of cost functions, we considered two standard cost functions: the hinge loss for support vector machines and the logistic or cross entropy loss function of logistic regression (Wang et al., 2022).

**Inverse optimization to infer loss functions from subjects' responses**

To evaluate which loss function best describes each subject's responses, we minimized the mean squared distance between the subject's responses and model-predicted regression lines or decision boundaries for each trial, averaged across all trials. Let the model predicted regression line (eq. (3.2)) or decision boundary (eq. (3.2)) on the $k$-th trial be ${}^{k}\hat{y}^{*}$. Let the subject's response on the $k$-th trial be ${}^{k}\gamma$. Then, the root mean squared error between

human response and model prediction is:

$$\text{RMSE} = \left( \frac{1}{\#\text{trials}} \sum_{k=1}^{\#\text{trials}} |{}^{k}\hat{y}^{*} - {}^{k}\gamma|^{2} \right)^{\frac{1}{2}} \tag{3.8}$$

For each trial, the model prediction ${}^{k}\hat{y}^{*}$ depends on the loss function $J_{\mu}$ used, the hyperparameters $\mu$ of the loss function, and the particular dataset from the $k$-th trial. So, we may denote the mean squared error in eq. (3.8) as RMSE($\mu$), focusing on the dependence on the loss function hyperparameters $\mu$, suppressing the dependence on the datasets used and the particular loss function $J_{\mu}$ for simplicity. For the four parameterized loss functions considered, the hyperparameters $\mu$ are $p$ for the regression loss function, and $p$, $\alpha$, and $\beta$, respectively, for the three classification loss functions. Within a given one-parameter family of loss functions $J_{\mu}$, the best describing loss function is determined by computing the best-describing loss function parameter $\mu^{*}$ as minimizing RMSE($\mu$):

$$\text{best-describing loss function parameter } \mu^{*} = \arg\min_{\mu} \text{ RMSE}(\mu). \tag{3.9}$$

We used a quasi-newton algorithm (MATLAB fmincon) to find the location $\hat{y}^{*}$ for most of the cases, as the loss function usually has a unique global minimum without other local minima. The exceptions were for exponents $p$ equal to or smaller than 1 ($p <= 1$ in eq. (3.3) and eq. (3.5)), as there could be multiple local minima. We used $p = 1.001$ as a proxy for $p = 1$, as $p = 1$ could produce infinitely many minima. For $p < 1$, we evaluated the loss function at the testing data point locations, as the minima will appear at those places (figure 3.4B and C, $p < 1$). When we found two global minima with identical values ($p < 1$ in classification), we picked the model prediction $\hat{y}^{*}$ to be the minimum closer to the subject selection.

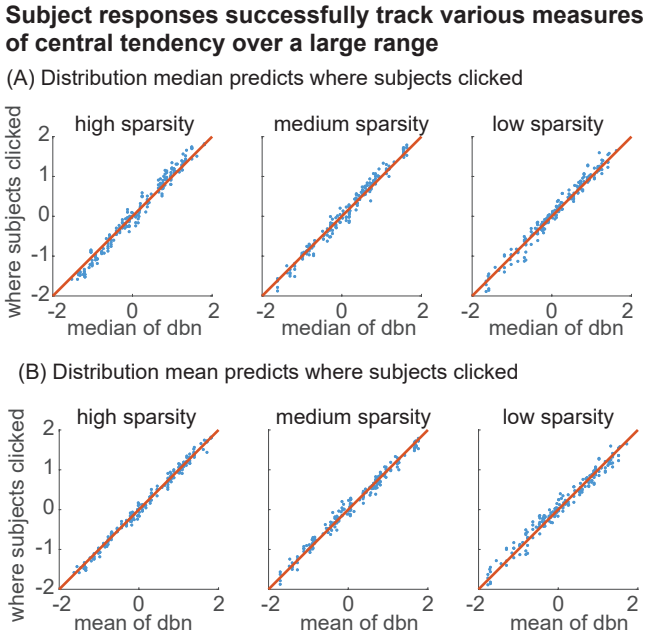


Figure 3.5: **Subject responses compared to various centers of the distributions.** Subjects effectively tracked standard measures of central tendency. The location of the median and the mean varied substantially on the screen, and subjects systematically tracked these.

## 3.4 Results

### Regression: subjects effectively track measures of central tendency

Subjects effectively tracked standard measures of central tendency of the data shown in each trial (figure 3.5). Specifically, the location of the mean, the median, and other measures of central tendency changed substantially between trials, and the locations of the mean and the median were highly predictive of where the subjects clicked. The linear model from the mean of the distribution to where the subjects clicked had 97.1% $R^2$ value and the median of the distribution to where the subjects clicked had 97.3% $R^2$

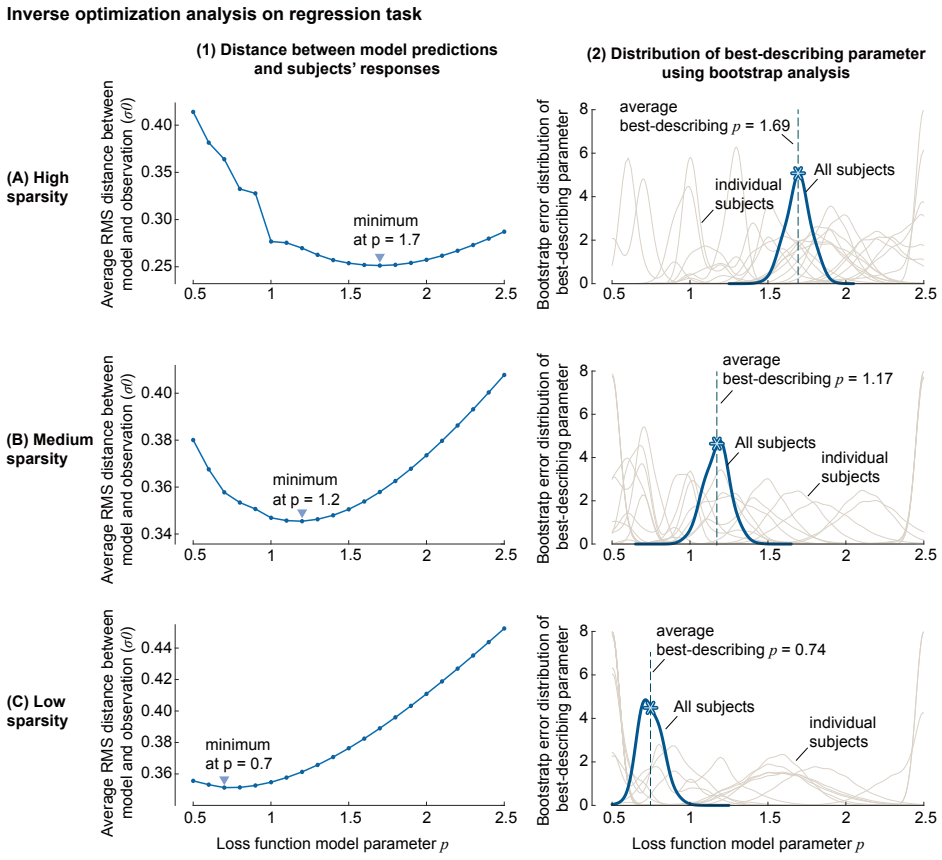


Figure 3.6: **Comparison of subjects' responses to the predicted regression lines.** Regression lines were predicted using loss function models of various exponent parameter $p$, for different sparsity levels (top to bottom). On the left are the RMS distances between the predicted regression lines and the subject's response, normalized by PDF variance $\sigma_0$, and the downward triangle indicated the loss function parameters that had minimum RMS distances for the given sparsity. On the right are the distributions of best-describing loss function parameters inferred from the RMS distance, using bootstrap method. Thin lines indicate best-describing loss function parameter for each subject, and the thick black line shows that of the entire subjects. The asterisk on the tick line indicates the average of the best-describing loss function parameter from each bootstrap sample.

value, when averaged across all subjects and all trials. Thus, subjects are able to track the overall location of the distribution well. The rest of the results section is about the small but significant differences between how well different measures of central tendency, or equivalently, minimizing different loss functions, predict the subject responses.

## Regression: loss function exponent reduces with reducing sparsity

The mean RMS error (eq. (3.8)) between the subjects' responses and the model-predicted regression lines, averaged across all subjects and all trials for a given sparsity, has a U-shaped curve with respect to the $L_p$ exponent $p$ (figure 3.6 left). We obtained the best describing exponent $p^*$ by minimizing the overall RMSE for each sparsity. The best-describing parameters were different for different sparsity levels. We found that $x^{1.7}$ for high sparsity (20 dots), $x^{1.2}$ for medium sparsity (400 dots), $x^{0.7}$ for low sparsity (8000 dots) best predicted human regression lines on average. Thus, as sparsity decreased, or in other words, as the data density increased, subjects tended to choose regression lines described by a loss function with a smaller exponent.

To compute the uncertainty in these estimates, we performed bootstrap resampling of trials from all subjects and all trials of a given sparsity and recomputed the best-describing exponent $p^*$ for each sample to obtain bootstrap-based error distributions for $p^*$ (figure 3.6 right). The average best-describing loss function parameters obtained from this bootstrap analysis were 1.69, 1.17, 0.74 for high, medium, low sparsity, with relatively clear peaks at those parameter values, and error standard deviations of about

0.15 for each sparsity. We note, however, that the RMS error landscape near $p^*$ is quite flat, that is, has low curvature (figure 3.6 left), indicating that substantially different exponents predict a small increase in error, partly an indication of inter- and intra-subject variability in responses, as described later.

## Classification: rectified error loss had worst performance and exponent changed with sparsity

RMSE using rectified error loss function had the worst performance among the loss functions we considered (figure 3.7 left). Commonly used loss functions, logistic regression and support vector machines (SVM) were closer to subjects' responses than rectified error, with SVM being closer than logistic regression. The other two parameterized loss functions were also systematically better. This provides limited evidence that subjects do not just consider error in misclassified points while performing the classification task, as rectified error loss function is the only one of our loss functions that only used misclassified points for computing loss.

RMSE using rectified error loss function averaged across all subjects and all trials had minima within the parameter range we searched, and the best-describing parameter changed systematically with the sparsity of the dots (figure 3.7 left). Rectified error to the power of $p^* = 0.9, 0.5, 0.2$ were the best descriptors of subjects' responses for each sparsity using rectified error loss functions. Rectified error loss function to the power of $p^* = 1$ yields a decision boundary that splits dots into two groups in a way that the numbers of misclassified dots are identical from both groups, analogous

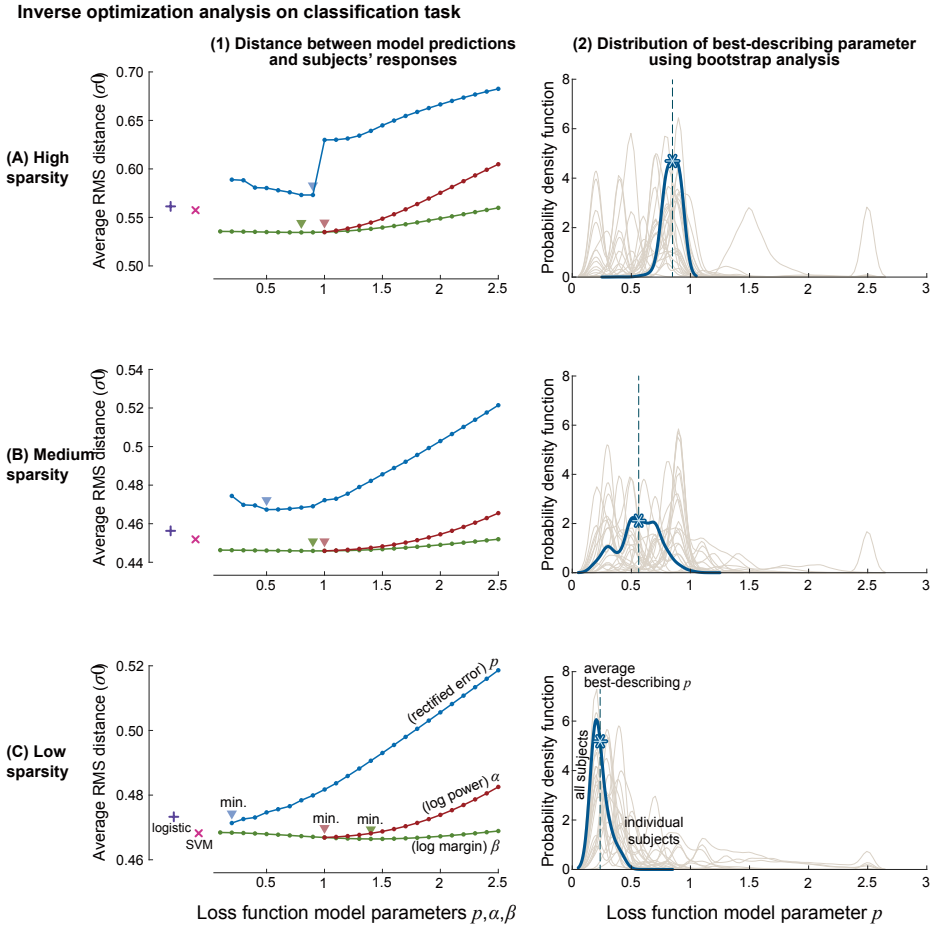


Figure 3.7: **Comparison of subjects' responses to the predicted decision boundaries.** Decision boundaries were predicted using rectified error (blue), log power (red), and log margin loss functions (red), with their model parameter $p$, $\alpha$, $\beta$, for different sparsity levels (top to bottom). Distances from the decision boundaries obtained from logistic regression classifier (plus mark) and SVM (x mark) are also shown as a reference. On the left are the RMS distances between the subject's response and the decision boundaries obtained by minimizing loss functions, normalized by PDF variance $\sigma_0$, and the downward triangle indicated the loss function parameters that had minimum RMS distances for the given sparsity. On the right are the distributions of best-describing exponent parameter $p$ for rectified error loss function, inferred from the RMS distance, using bootstrap method. Thin lines indicate best-describing loss function parameter for each subject, and the thick black line shows that of the entire subjects. The asterisk on the tick line indicated the average of the best-describing loss function parameters from each bootstrap samples.

to a median. Smaller $p$ is in general associated with the decision boundary being closer to the skew-symmetric distribution; in other words, more dots from skew-symmetric distribution tend to be misclassified than dots from the symmetric distribution. Our observation of smaller best-describing $p^*$ for lower sparsity roughly means that subjects chose decision boundaries closer to the skew-symmetric distribution when sparsity decreased.

Best-describing parameters obtained from bootstrap analysis had similar results. Parameter for rectified error loss function $p = 0.85, 0.75, 0.23$ (figure 3.7 right) with standard deviations about 0.15, 0.33 and 0.15 respectively. Performing subject-specific analysis, we find that most of the subjects had best-describing exponent $p^*$ lower than 1, which in general means that they drew the decision boundary closer to the skew-symmetric distribution, and more so as the sparsity decreased.

The RMSE curve for rectified error loss function at high sparsity had a distinct jump between $p = 0.9$ and 1.001 (figure 3.7 left), because $p <= 1$ could have multiple global minima (as seen in figure 3.4C $p = 0.5$ and 1) and we used the one that is closer to the subjects' response for the analysis. Such discrepancy also exists in medium and low sparsity, but the effect is less noticeable because multiple minima, which can only exist between adjacent dots, are closer to each other as sparsity decreases.

## Classification: log margin loss function best describes human responses

We considered two one-parameter families of loss functions — sum of log power (eq. (3.6)), sum of log margin (eq. (3.7)) — that considered error

in both correctly classified and misclassified points. Their hyperparameters were an exponent parameter $\alpha$ and margin parameter $\beta$ respectively. Log margin and log power in general had smaller RMS distances and, thus were better descriptors of subjects' behavior than rectified error loss function, while log margin was the best descriptor among the three functions in the range we considered. Log margin at its minima also yielded decision boundaries closer to subjects' behaviors than SVM and logistic regression did.

Log margin loss function model had minima within the parameter range we searched, and the best-describing parameter changed systematically with the sparsity of the dots (figure 3.7 left). Specifically, increased margin logistic function with margin parameter $\beta^* = 0.8, 0.9, 1.4$ were the best descriptors for each sparsity (figure 3.7 left), although RMSE curve is shallow for the wide range of the parameter for this loss function. The RMSE using log power had minima at $\alpha^* = 1.001$ for all three sparsity conditions. This $\alpha^* = 1.001$ was at one extreme of our evaluation range, as we did not evaluate values below $\alpha = 1.001$ (a proxy for $\alpha = 1.0$).

Best-describing parameters obtained from bootstrap analysis had similar results. Parameter for log power loss function $\alpha^* = 1.00, 1.04, 1.05$ (Figure 3.8 left) and parameter for log margin loss function $\beta^* = 0.74, 0.94, 1.46$ (Figure 3.8 right) were best-describing parameters obtained from the bootstrap analysis, with standard deviations of about 0.35, 0.6, and 0.7 respectively.

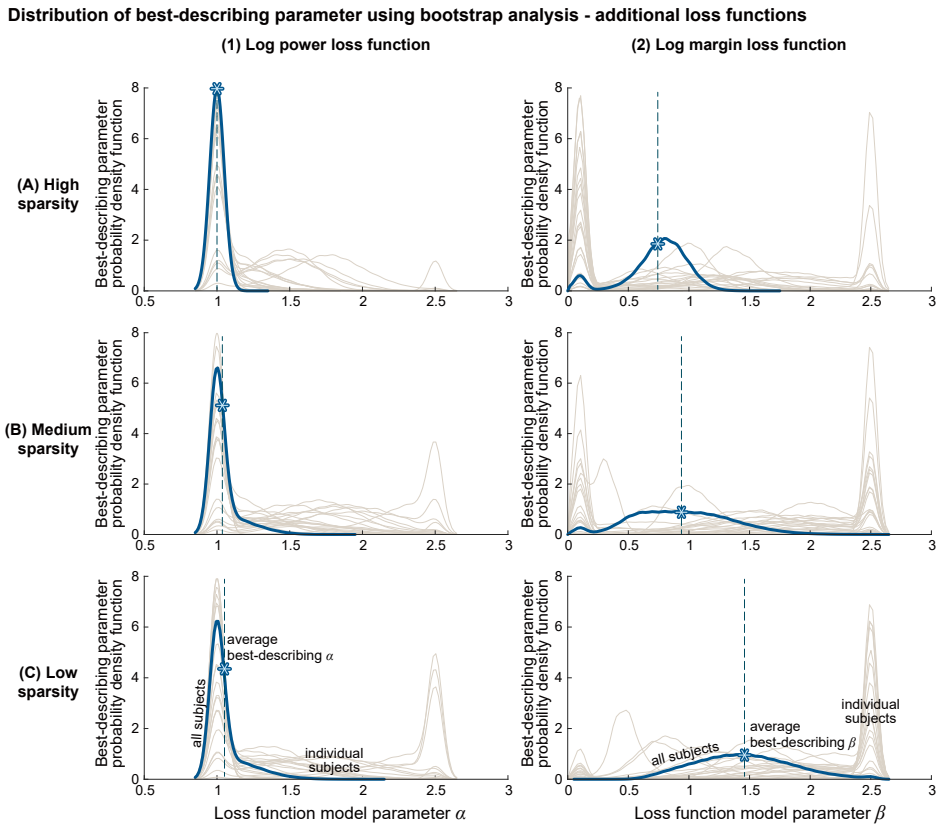


Figure 3.8: Best-describing parameters for log power and log margin loss function. Distributions of best-describing exponent parameter $\alpha$ and $\beta$ were inferred from the RMS distance by applying bootstrap method. Thin lines indicate best-describing loss function parameter for each subject, and the thick black line shows that of the entire subjects. The asterisk on the tick line indicates the average of the best-describing loss function parameters from each bootstrap sample.

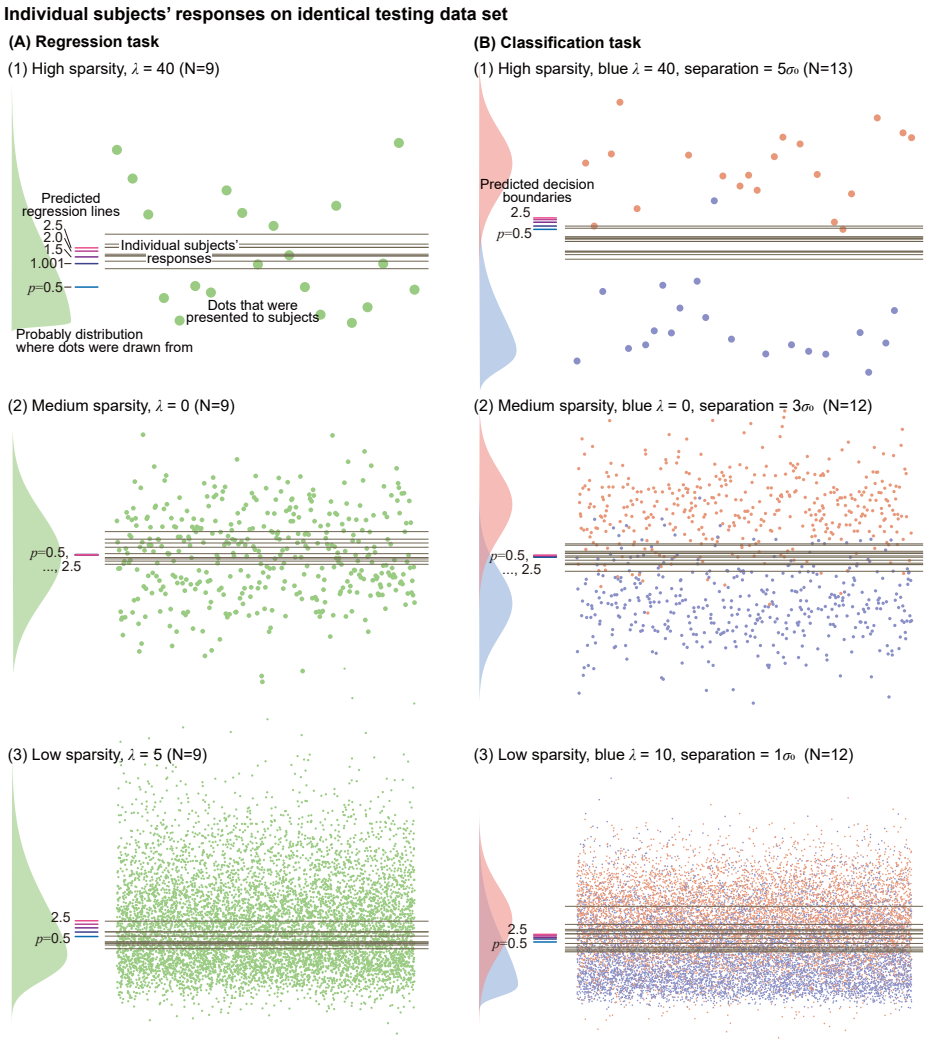


Figure 3.9: **Various responses from multiple subjects on identical testing datasets.** Responses from (A) regression task and (B) classification task, from representative trials of various conditions. The dots on each panel were drawn from the PDFs(s) shown on the left side of the panel. Regression lines that minimize regression loss functions of various exponent parameter $p$, and decision boundaries that minimize rectified loss functions of various exponent parameter $p$ are indicated with the thick, short horizontal lines as references. The longer, thin lines on top of the dots are the responses from each subject.

## Regression and classification: large inter-subject variabilities in responses and in loss functions

We obtained the best-describing regression and classification loss function hyperparameters for each subject and constructed a subject-specific bootstrap distribution of the best-describing hyperparameters. We found substantial inter-subject variability — seen in the wide ranges of peak locations among different thin lines in figures 3.6-3.7 (right), indicating best-describing parameters for individual subjects were not consistent across them. Furthermore, when we analyze their behavioral variability, the results also indicate substantial intra-subject variability — evident in the wide ranges covered by each of the thin lines in figures 3.6-3.7 (right), indicating best-describing parameters were not highly consistent across trials within the same subject. Parameters for rectified error in the classification task had fairly large inter- and intra-subject variability, although it was smaller than the variability observed in the regression task.

To more directly observe the inter-subject variability, a subset of our subjects (9 for the regression task, 13 for the classification task) were tested with the exact same arrangements of dots. Subjects' responses (figure 3.9 thin lines) varied to a large degree, often more than the range of regression lines that are calculated by minimizing loss functions of various parameters (figure 3.9 thick lines). Even for the dots that were generated from symmetric probability density function(s) (figure 3.9 middle rows), where regression lines calculated using various loss functions lie close to each other at the middle of the distribution(s), (thicker lines on top of each other), subjects' responses varied to a large degree.

### Regression and classification: a weak trend of longer time for sparser trials

Subjects ($N_{\text{subjects}} = 7$) who were tested with fully randomized orders for regression task took 6.4 ± 20.3, 4.9 ± 10.9, 3.8 ± 4.2 (average ± standard deviation) seconds to complete a regression task trial for high, medium, low sparsity. Both the mean and standard deviation of the completion time decreased on average with decreasing sparsity. Subjects ($N_{\text{subjects}} = 7$) who were tested with fully randomized orders for the classification task took 4.0 ± 6.0, 3.7 ± 8.8, 3.6± 9.1 seconds for high, medium, low sparsity. The average completion time slightly decreased with decreasing sparsity, but the standard deviation increased. We did not perform explicit statistical significance tests.

## 3.5 Discussion

We applied inverse optimization analysis on humans performing regression and classification tasks in visually presented data. For the regression task, minimizing the sum of error raised to the power of 1.69, 1.17, 0.74 were the best descriptions of the average subjects' decisions for high, medium, and low sparsity data. For classification task, minimizing the sum of increased margin logistic classification error was a better descriptor among various types of loss functions we considered, with its best-describing margin parameters $\beta$ being 0.74, 0.94, 1.46 for high, medium, low sparsity data. Among the loss function models that sum error powers of only misclassified data, exponents of $p = 0.85, 0.75, 0.23$ were the best descriptors, while logistic

error functions that also take into account correctly classified data were in general better. These changes to the best-describing loss functions with decreasing sparsity had a common tendency: the regression line or decision boundary subject chose moved towards the mode of the skew-symmetric distribution, or in other words, towards the densest part of the dataset, as the data became denser.

These results qualitatively agree with some previous findings. A study that tried to infer a human loss function from a pointing task (Körding and Wolpert, 2004a) reported that minimizing the sum of distances raised to the power of 1.69 was the best descriptor of the average subjects' behavior, when subjects observed about 60 data points during each trial. Our trials with the sparsest data consisted of 20 data points, and the best-describing loss function for the regression task was distance raised to 1.69, which is a close match with the previous finding. This exponent of 1.69 is also reasonably close to 2, which is used for least mean squared method, so is in alignment with the study (Gillan, 2020) reporting that students with statistics training were more likely to choose a regression line based on least square method among other specific alternative heuristics, when tested with scatter plots of 5 to 20 data points. This previous study however does not provide a best exponent as an outcome of an inverse optimization analysis, and instead, compared a few different methods which are not on a continuum.

There are studies reporting that there is a central tendency (Hollingworth, 1910) when humans perceive a dataset. Many of our subjects indeed responded to our optional questionnaire that their strategy was to "put the line at the center of the distribution" when they performed the regression or classification task, but the best-describing loss functions varied to a large

degree even between these subjects. The definition of “central” differs from study to study when referring to central tendency. For example, the mean, median, and mode of the data could all be reasonably defined to be the center of a distribution. The best-describing parameters we found from the experiment could be interpreted in terms of these statistical quantities of the distribution, because finding the median and mean are mathematically equivalent to finding a regression line that minimizes the sum of absolute regression error and error squared. Using this equivalent description, our inverse optimization result on the regression task is that, people on average chose a regression line near mean for high sparsity data, near median for medium sparsity data, and between median and mode for low sparsity datasets. While "central" is even less well-defined for two distributions for binary classification tasks, our result from classification shows that there was a similar shift with the sparsity of the data. The average decision boundary moved towards the skew-symmetric distribution as sparsity decreased. Our results provide some insights into central tendency theory, suggesting that "central" could be highly context-dependent and highly variable across people.

Traditional computational algorithms normally do not change their strategies based on the size of the data, but we observed noticeable shifts in average strategy when humans perform regression and classification. Potential explanations for the shift we observed include: when more data points were presented, (1) people could infer the underlying structure of data better, and thus made different judgments on the importance of each data point; (2) people may perceive the nature of the dataset differently, e.g., less sparse data (dense data points) might be perceived as a contiguous area,

whereas sparse data would be perceived as a set of individual dots; (3) it becomes more challenging to consider individual data simply because there are a lot of them, thus people switched to different heuristics. The third point seemed to be more apparent for the regression task, where subjects took longer times to complete a high sparsity task that had fewer dots than a lower sparsity task that had more dots. These shifts in behaviors, both in terms of the decision itself and the time taken to make the decision, provide insights into how humans perceive patterns differently in data of different sizes.

Commonly used loss functions for regression or classification algorithms are mostly convex, so that the loss function is smooth and there is a single global minimum. For example, the sum of distances raised to the exponent smaller or equal to 1 could have a non-smooth loss function, and could result in multiple local and global minima (figure 3.4), and thus are not desirable for machine learning algorithms. However, many subjects chose regression lines and decision boundaries in the range that was only reached by loss function models that were non-convex, at least among the loss function models we considered in this study. Another limitation that comes from using only convex loss functions is that the contributions from the outliers are bound to be bigger than a certain value. Loss functions that are relatively robust to outliers, such as Huber loss and log-cosh loss, have smaller increases in slope at the extremes, but only to the degree that the overall loss function is still convex. Although convexity and other traits are desirable for machine learning algorithms, it is conceivable that computational and mathematical simplicities are not as strictly required for humans. Therefore, developing a machine learning algorithm that closely mimics

human perception of patterns may necessitate the use of loss functions that are not conventionally used.

Unlike computational optimization, "noise" can be a factor in how humans actually perform pattern recognition, even when they have a consistent criterion (which is not necessarily guaranteed). Our experimental results exhibited high intra-subject variability, and noise could be one possible explanation. Noise in the human selection (Kahneman et al., 2021), arising from sources such as limitations on calculation precision, inaccurate motor execution of selecting a line, and even effects of optical illusion, are hoped to be canceled out if we increase the experimental sample size and look for an average behavior across samples. However, loss functions of some types could result in the ill-posedness of the inverse optimization problem, which may not be rectified by simply adding more samples to the analysis. Consider the case when a loss function is very flat near the minima, or when it has multiple local minima that have loss values close enough (or even exactly the same) to the global minimum (e.g., figure 3.4). Even if a subject is consistently using the specific loss function, they may still make a final decision that is not exactly at the global minimum, but at other reasonable alternatives like at one of the local minima. In this case, the loss function could falsely appear to be an inadequate descriptor of subjects' decisions. We partially addressed this issue by considering multiple global minima locations for p<=1 and by assuming that the location that was closer to what subjects selected was the location they were aiming for. However, this assumption may have given p<=1 an unfair advantage against p>1. In addition, this still does not address the case of humans selecting a location that is close enough to the global minimum but numerically not

identical. Further studies would be needed to improve inverse optimization analysis when the proximity between the observed decision and the specific optimization criterion is an ill-behaved function like this.

There was high inter-subject variability in our experimental results. Sometimes patterns in the visually presented data seem obvious (Wertheimer, 1938) and can be easily agreed between different people. However, the high inter- and intra-subject variability that we observed on relatively simple tasks leads to a suspicion that there might be no single commonsensical "ground truth" to many of the regression and classification problems. As some authors point out, (Von Luxburg et al., 2012), some pattern recognition may need to be viewed more like art than science.

There were some limitations to our current study. We imposed the patterns to be one-dimensional, but higher dimensional problems may result in different results. We also cannot test overfitting with one-dimensional problems, but in future studies, we could consider introducing a higher degree of freedom to see what people do. Most of our subjects had a science and engineering background, and had some previous experience with regression techniques, while fewer had an experience with classification techniques. Our optional questionnaire shows that about half of the subjects could perform a regression method they learned, and half of the subjects at least learned about it in the past, whereas about half of the subjects never heard about classification algorithm and very few subjects responded that they could perform a classification method. As shown in a previous study (Gillan, 2020), people with statistics training seem to use a different method to perform regression than people with training, and we also expect that our result is dependent on the subject group. Results might also be dependent

on the instruction, and specific details of the test such as the scaling of the task interface on the computer screen (as it was reported in a previous study that the scaling of the graph affected subjects' decisions (Cleveland et al., 1982)), color and size of the dots, and the order of the trials. We applied the inverse optimization approach to loss functions that sum up contributions from each data point, but it would be also interesting to test other forms of loss functions.

We calculated model-predicted regression lines and decision boundaries for each trial using actual testing datasets of each trial, rather than using the probability distribution from which the dataset was drawn. Statistics of the sample data are different from the statistics of the PDF from which the dots were drawn from, thus regression lines or decision boundaries that are calculated based on sample data are also different from the calculations based on the PDF (figure 3.2). These discrepancies are bigger when we draw a smaller number of dots. If humans are updating a Bayesian prior during the experiment to make decisions based on a mixture of their estimated prior and the current dataset, we might expect systematic deviations toward the center of the visual area, which we do not see in the data (figure 3.10).

We designed datasets to study what loss functions humans optimize for when they perform regression and classification, and obtained loss functions that were on average best descriptors of subjects' responses. However, the result was not as simple as simply reporting what was "the" loss function humans optimize. Instead, we learned that the loss function could be context-dependent, and that there are high subject variabilities when humans perform visual pattern recognition tasks. It would be interesting to see what are the other factors that contribute to the human inconsistency,

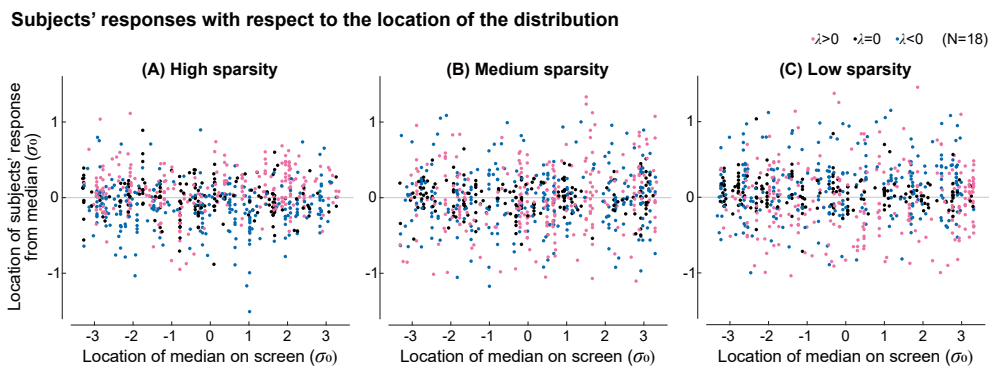


Figure 3.10: **Error dependence on location on screen.** The error with respect to the median or any other $L_p$ optimum does not depend on the location of the distribution's median on the screen.

as well as measuring the inconsistency itself more closely, for example by repeating the same test again. More in-depth investigation of how humans perform an individual trial could also provide useful insights. Eye tracking could show what points each subject considered while performing the task and may especially provide insights into outlier processing. We could also ask people to speak out what their thoughts are while perceiving the dots. Another direction for a future study could be to use specially designed probability distributions where dots are drawn from, so that specific hypotheses could be tested. The way data is presented could be also altered. For example, one could present a target line and ask people to move the set of dots to best hit the target line. One could present some dots each moment and refresh the dot locations with some time interval, investigating the history effect on pattern perception. These tests could be also integrated with motor control tasks, for example, humans performing aiming, reaching, or catching tasks, while target objects to interact with have some probability distribution in terms of their position or velocity.

We obtained average loss functions that human subjects use when they

perform regression and classification tasks, while observing a large variability. This observation would contribute to the understanding of human visual perception and motor control using visual perception, and would provide insights into developing machine learning techniques. Understanding how humans perform such pattern recognition tasks can be useful as ground truth to train machine learning algorithms aimed at reproducing human intelligence (Foncubierta Rodríguez and Müller, 2012), as an inspiration to develop new algorithms, since humans seem capable of performing complicated pattern recognition tasks, to identify common mistakes humans make and systematic biases that humans have, so as to educate people (Tschandl et al., 2019; Kahneman, 2011), and more broadly, to study how human nervous system functions (Körding and Wolpert, 2004a; Schwab and Nusbaum, 2013; Caelli et al., 1987).

# Chapter 4

# Human force control may trade-off force error with central tendency and recency biases.

## 4.1 Abstract

Understanding how humans control force is useful for understanding human movement behaviors and sensorimotor control. However, it is not well understood how the human nervous system handles different control criteria such as accuracy and energetic cost. We conducted force tracking experiments where participants applied force isometrically while receiving visual force feedback, tracking step changes in target forces. The experiments were designed to disambiguate different plausible objective function components. We found that force tracking error was largely explained by a trade-off between error-reducing tendency and force biases, but we did not need to include an effort-saving tendency. Central tendency bias, which is a

shift towards the center of the task distribution, and recency bias, which is a shift towards recent action, were necessary to explain many of our observations. Surprisingly, we did not observe such biases when we removed force requirements for pointing to the target, suggesting that such biases may be task-specific. This study provides insights into the broader field of motor control and human perceptions where behavioral or perceptual biases are involved.

## 4.2 Introduction

We interact with the world by applying forces. For example, we push the ground to walk, press pedals to ride a bicycle, and even apply muscle forces onto our own body parts to breathe, sing, and reach out a hand. Understanding how people control forces would be beneficial in understanding how the nervous system performs sensorimotor control, and insightful in designing robots and biomechanical simulations. One way to model sensorimotor control is to view it as an optimization problem, that there are objective functions that are optimized for and constraints that are needed to be satisfied while executing the task (Baron and Kleinman, 1969; Kleinman et al., 1970). There often are multiple objectives and constraints in many sensorimotor tasks and robotics applications (Dao et al., 2016; Jin et al., 2021). Our goal was to observe human subjects' behaviors when they perform simple force tracking tasks, and to investigate objective functions that could explain the observed behaviors.

In biomechanics simulations and robotics, researchers often formulate an objective function as a sum of error (or performance) term and effort

(or energy cost, control energy) term. Such formulations are used to model human motor control (Emken et al., 2007; Izawa et al., 2008; Mi et al., 2009), in biomechanics simulations (De Groote et al., 2016; Lee and Umberger, 2016), and in robotics (Kalakrishnan et al., 2013; Miao et al., 2021). In optimal control theory, cost function of a linear quadratic regulator ("LQR", Kalman et al. (1960)) is often formulated as a sum of quadratic functions of state and control input.

Having an error term in the objective function ensures that the goal is achieved to a certain degree. In addition to the error term, there are several reasons to include an effort term, including: 1) To handle the redundancy problem: there are usually redundancies in the system, meaning there are multiple ways to achieve the goal, so additional criteria are needed (as discussed in De Groote and Falisse (2021)). 2) To better mimic biological systems: there are pieces of evidence suggesting that biological systems minimize energetic cost, so having the term allows simulation and robot to behave more like biological systems and thus provides more insights into understanding them (e.g., Srinivasan (2011)). 3) For practical reasons: Robots often need to be efficient because power or energy consumption are some of the major concerns (e.g., Liu and Sun (2013); Pellegrinelli et al. (2015)).

However, those functions and their relative weightings are usually arbitrarily designed and tuned until they produce acceptable outcomes. Some researchers refer to biological measurements to formulate some components of the objective function (e.g., Körding and Wolpert (2004b) studied error, Berret et al. (2011) studied cost), but such investigations have not been considered in the context of human force tracking.

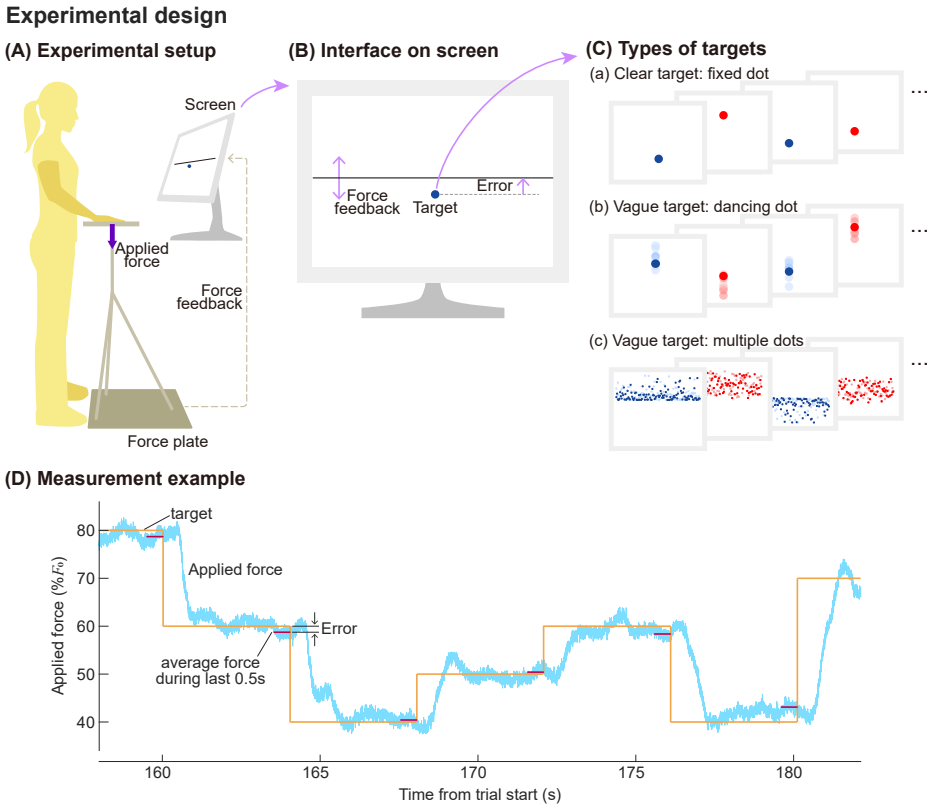


Figure 4.1: **Experimental design.** (A) Subjects applied force on the platform in front of them while looking at a screen. The vertical force they applied was measured through a ground-mounted force plate, and the force was relayed to a (B) screen that displayed the applied force as a horizontal bar of a changing vertical location, as well as a target. (C) There were three types of targets. Illustrated are conceptual representations of each sub-trials. (D) An example of a trial, which was a series of sub-trials that changed target force in a random order. Applied force and target force at the time are shown together. Force tracking error was defined as a difference between the average applied force during the last 0.5 seconds of the sub-trial and the mode of the target.

We designed a force tracking experiment that allows us to compare various objective function models to experimental observations. Participants were asked to apply forces isometrically onto the platform in front of them through their hands, while receiving the force feedback as the height of the bar on the screen (figure 4.1A, B). The force targets (figure 4.1C) they tracked were either clearly defined as a fixed single dot, or vaguely defined in two ways, as a single dot that had noise in its location or as a cloud of multiple dots. The targets were shown for 4 seconds (referred to as "sub-trial"), and the next target of the same kind appeared at a random location. We analyzed force error near the end of each sub-trials (figure 4.1D) to quantify the force tracking error.

We hypothesized that the vagueness of the target would result in more shifts in subjects' behaviors towards the effort-saving direction when the force requirement increases. If effort is not a criterion, when subjects see the same distribution of dots simply shifted up to require more force (figure 4.2A), they would increase their force by the same amount. In that case, their behaviors would be largely explained by an error-based objective function alone (figure 4.2B-1). However, as there is some allowance due to the vagueness of the target, they may save effort by increasing the force by a slightly smaller amount than the target shift. In that case, we could model the behavior as a trade-off between error-reducing and effort-saving criteria in the objective function (figure 4.2B-2).

In addition, we used skewed distributions when we defined vague targets to study the error term of the objective function (figure 4.2C). Skewed distributions have distinct mode, median, mean, and half of the range, which are the locations where error raised to power of 0, 1, 2, and infinity are min-

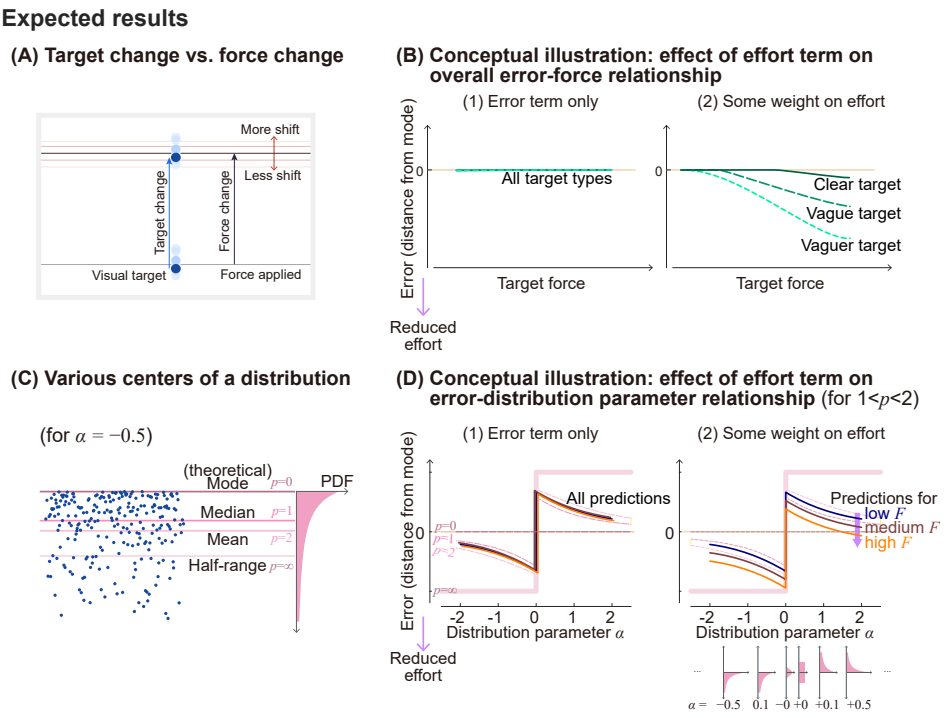


Figure 4.2: **Illustration of expected results for different target types and distributions.**(A) Relative force shifts with respect to the target shift. Subjects may shift by the same degree as the visual target position changes, but they may shift less than the ascending target change if effort becomes a critical factor. (B) Therefore, if minimizing error is the only factor that determines people's behaviors, (1) we expect an average zero error for all force ranges and target types. However, if effort is a consideration too, and if vagueness of the target is an extra allowance to facilitate effort-saving behavior, (2) we expect increasing error towards the effort-saving direction as target vagueness increases. (C) Using targets of different distributions could provide us with extra information about how people perceived the task. As there are many definitions of centers in a skewed distribution, including the mode, median, mean, and half-range, we could study where people were aiming for, and whether this changes with increasing force demands. (D) Combined with effort considerations, if effort does not affect the behavior and people are consistent with what "center" they aim for, (1) we expect to see an error trend across various distribution parameters that is best described by which center they aimed for, and does not change with increased force requirements. If effort is combined with this perception, (2) we expect that people's response will be similar to that of (1) when force requirement is low, but will shift towards effort-saving way as force requirement increases.

imized. For example, if a subject minimized the error raised to about 1.5, on average they would place the force feedback bar between the median and mean of the distributions (figure 4.2D-1). If an effort-saving tendency is added to the same error-reducing criterion in the objective function, we expect that people's behaviors would not change much in a low force range, but it will shift towards a direction that saves effort when the force requirement increases (figure 4.2D-2). We measured how participants changed their force according to the force requirement and given distributions, and applied inverse-optimization analysis to look for an objective function that best describes observed human behaviors.

We observed shifts towards less force in the medium to high force range. However, there also were unexpected findings that looked like people systematically "wasted" effort in the low to medium force range, meaning, they exerted more force than needed for no obvious benefits in reducing errors. We used "central tendency bias" and "recency bias" to explain the results, and conducted additional follow-up experiments on a subset of the participants to test these biases. We use the term "central tendency bias" to describe the shift towards the center of the tasks. That is, if their current force is on a lower side, people tend to make errors towards the center, and end up producing more force than needed. In a similar manner, we use the term "recency bias" to refer to the bias towards the recent past action, meaning people tend to make an incomplete shift to the next target. Surprisingly, an effort term that increases with force, does not seem to have a significant effect on the model prediction. Further, we found that eliminating the force requirement as much as possible eliminated the biases, showing no significant bias in visual perception of the tasks.

4. Human force control may trade-off force error with central tendency and recency biases.

## 4.3 Results

### How humans track step changes in forces

#### Force tracking errors have task-dependent positive and negative biases

Subjects typically took about 0.4 s seconds to initiate the force change after the target location changed, and held the force until the next target was shown (figure 4.1D; average responses can be found in figure 4.8 and figure 4.9). We report distance from the mode of the distribution as the error in this paper unless otherwise noted.

We measured the force tracking error for different target types and force requirements. As we expected, people exerted less force relative to the target when the target force increased, and there was a bigger change when the target was vaguer (figure 4.3A). However, what was unexpected for us was that people tended to exert more force than needed for low-medium range targets. These two observations, 1) negative correlation between error and target force and 2) positive error on the lower target force, were consistent across subjects (figure 4.3B). When targets were grouped based on the distribution parameters, force errors were in general in between the median and half-range of the distributions. Each of the sub-grouped forces errors showed a negative correlation with a target force (figure 4.3C).

#### Force tracking error results are not explained by error and effort minimization

We used two types of objective function models to describe the observations. The objective function we originally formulated was in the form of

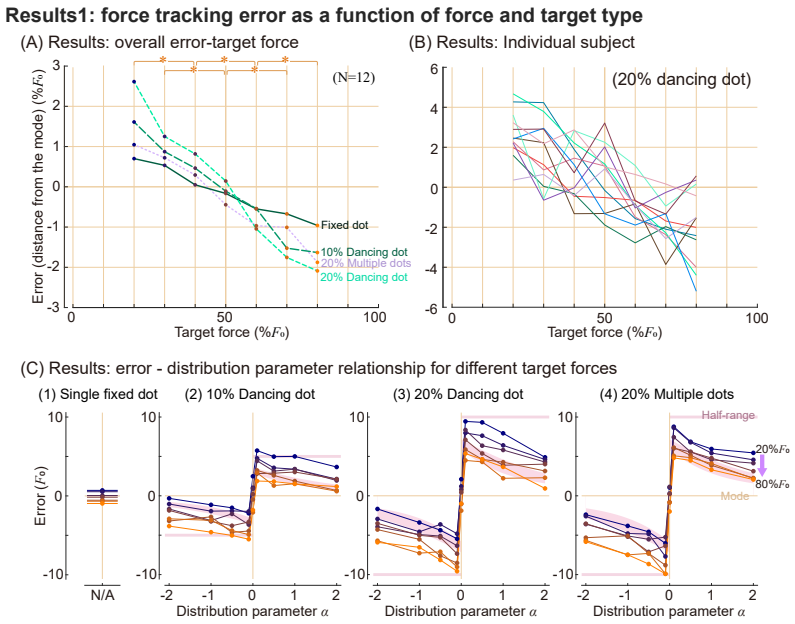


Figure 4.3: **Median values of tracking error for different target force, target types, and distribution parameters.** (A) Error, defined as a distance between the average force people applied during the last 0.5 seconds of sub-trials and a mode of the target, for each target type. Asterisks indicate statistically significant differences (p<0.05) for pairs of the force conditions, for every target type compared separately. (B) Error-force pattern of individual subjects. (C) Median response for each target force and distribution parameter. Pink shaded regions represent the range between the theoretical mean and median of each distribution, and pink horizontal lines represent half of the distribution range.

$\sum \text{error}^p/N + cF^\gamma$, where error is the absolute distance between the target and applied force, $F$ is applied force, $N$ is the number of target dots. Hyperparameters $p$ and $\gamma$ are shape parameters for each functions, and $c$ is a constant that determines the relative weighting between two terms. Since human data is noisy, we aimed to keep the formulation as simple as possible. For simplicity, we used $\sum(\text{error}^p)/N$ to represent performance criteria for targets of different vagueness. The formulation has shallower minima for bigger $N$ if $p < 2$, thus competing terms in the objective function would

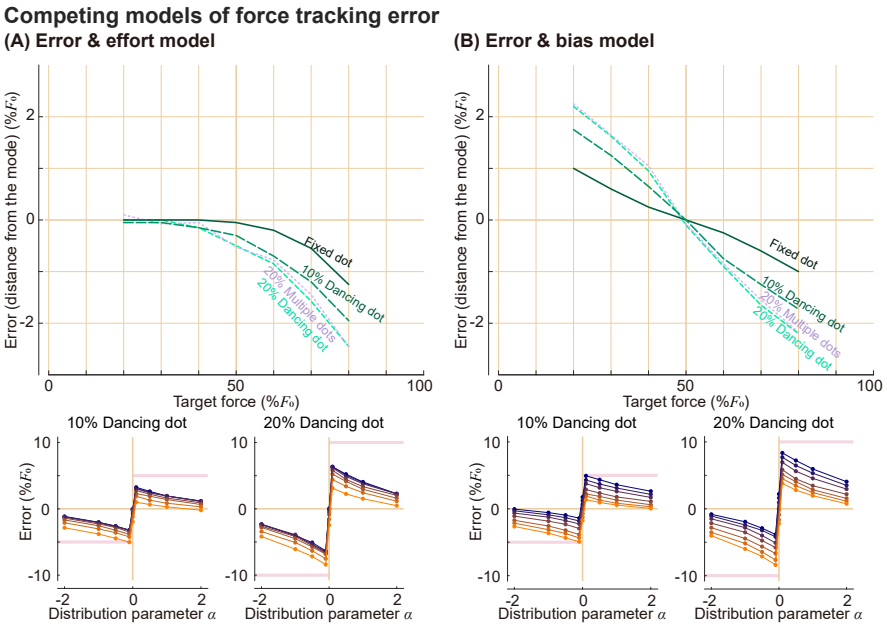


Figure 4.4: **Modeling force tracking errors using (A) error-and-effort model and (B) error-and-bias model.** In error-force plots (top row), different target types are indicated with different line types. In distribution parameter-error plots (bottom row), lighter and more orange colors indicate lower target forces, darker and more blue colors indicate higher target forces. Errors shown on the y-axis in both types of plots are both errors with respect to the mode of the target distribution. Objective function models to generate the model prediction here are $\sum \text{error}^{1.6}/N + 0.06F^5$ for (A) and $\sum \text{error}^{1.6}/N + 0.15\, d^{1.8}_{\text{ctr-bias}}$ for (B).

make the minima shift more for bigger $N$. The effort term in this form has inherent limitations, that it cannot explain positive force errors (figure 4.4A), and thus inverse optimization did not have local minima within our search range. We illustrated a solution that was found on one end of the search range, but even bigger exponents on effort term would further minimize the objective function. Bigger exponents would make low to middle-range errors closer to zero, thus reducing model error. However, this formulation does not predict positive error in any case.

**We investigated which variable predicts force tracking error.**

Force tracking error might be fully determined by the target force or visual representation of the target force. However, there might be a bias that is determined by the temporal relationships between targets. We formulated variants of the objective function models to represent these cases. One of our objective function models was error-and-bias model (figure 4.4B), which had a form of $\sum \text{error}^p/N + b d_{\text{bias}}^{\beta}$, where $d_{\text{bias}}$ represents the distance to some point when there is a tendency to shift towards that point, which will be further explained later. error is absolute distance between the target and applied force. Hyperparameters $p$ and $\beta$ are shape parameters for each functions, and $b$ is a constant that determines the relative weighting between two terms. figure 4.4B shows the error-and-bias model that has a shift towards the average target force.

## Additional experiments to disambiguate different terms

Some of the variables inherently co-varied in the original protocol (referred to as "Protocol 1"), so we designed additional experiments to distinguish some of them and test models accordingly.

The design of the additional protocol and what we found from each of them are listed below. A subset of subjects who participated in the original experiment using Protocol 1 participated in these additional tests, so we compared their responses to those of Protocol 1. We used a single fixed dot as a target in all additional tests to reduce the variability due to the target vagueness.

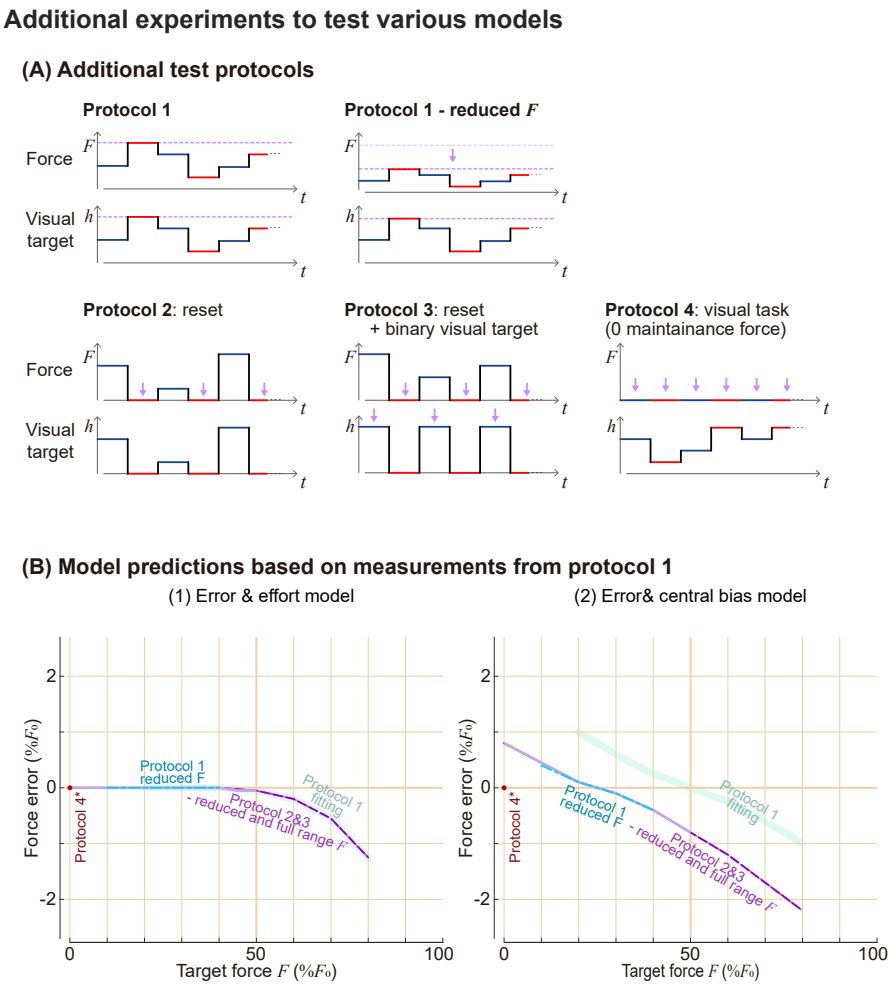


Figure 4.5: **Additional protocols to test different model predictions.** (A) Test protocols in terms of force requirement and its visual representation on the screen. Purple arrows emphasize the main differences between protocols. Protocol 1-reduced $F$ tested for a lower half range of the force, while spanning to a full visual target range. Protocols 2 and 3 had zero re-set period between each non-zero target force. Protocol 3 had binary targets, where the target was alternating between only two locations each indicating zero and non-zero target. This was done by changing the conversion ratio between force and visual target location each time. Protocol 4 was done using a computer mouse, and did not require force to maintain the pointing location. (B) Example of model predictions for these additional protocols. (1) Error-and-effort model, as an example of a model where target forces determine the errors: results from all protocols will match with each other when the target force is the same. (2) Error-and-bias model, as an example of a model that depends on a target force and the experimental contexts. Error-force trend changes for each protocol, and we had specific qualitative expectations for each protocol.

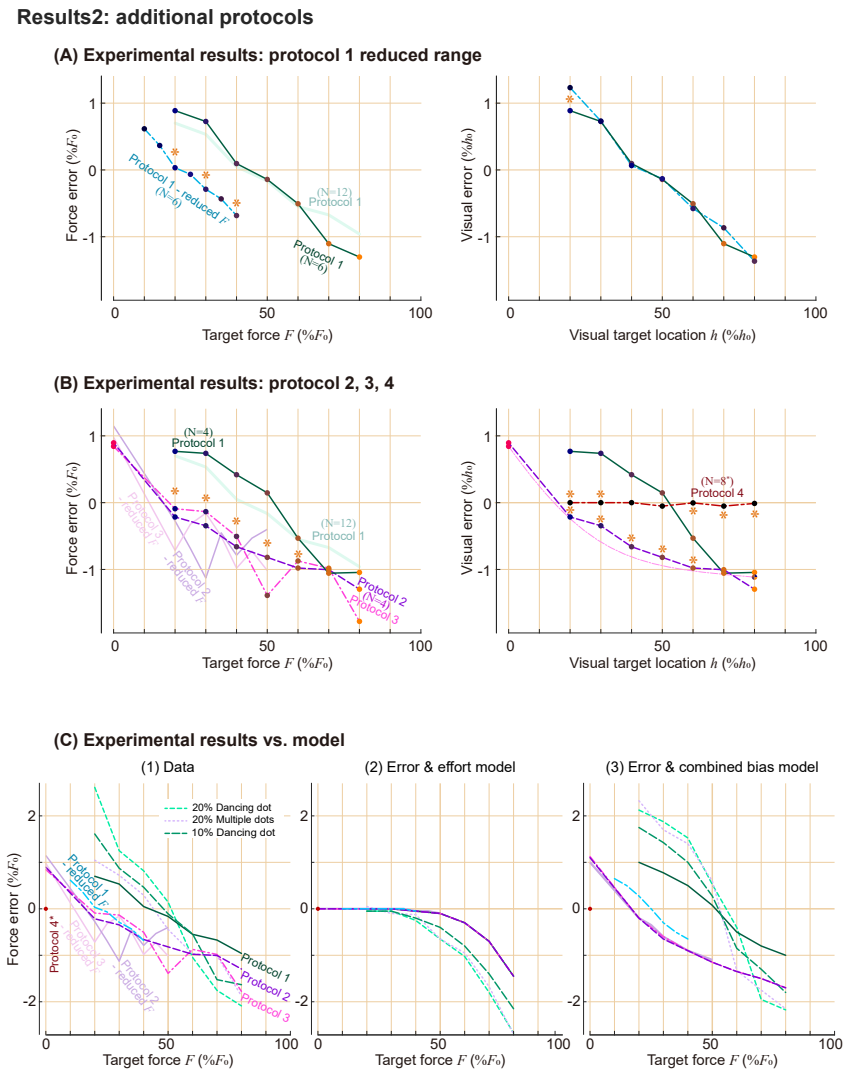


Figure 4.6: **Experimental results of additional protocols and its comparison to model predictions.** Different lines indicate the results of each protocol. As subsets of Protocol 1 subjects participated in additional tests, we represented the results of matching subjects in Protocol 1 as a thick green line here, while showing the results of all subjects as a dimmer line. Matching subjects result of Protocol 4 was omitted for simplicity, because the error was consistently very close to zero for everyone. (A) Protocol 1-reduced $F$ trial had a distinct error trend compared to Protocol 1 in force domain, while its visual domain had a good match. Asterisks indicate statistically significant differences ($p<0.05$) between Protocol1-reduced $F$ and Protocol 1 for matching conditions. (B) Protocols 2, 3, and 4 results, in force and visual domain. Asterisks indicate statistically significant differences between protocols and Protocol 1. (C) Comparison of (1) experimental results and (2, 3) models. Error-and-effort model and error-and-bias model were poor and good predictors of data.

**Protocol 1 – reduced *F* shows that target force alone does not determine error.**

In Protocol 1 – reduced $F$, we tested the lower half range of the force while keeping the range of the visual target fixed (figure 4.5A). Among our 12 subjects who participated in the Protocol 1 experiment, 6 of them participated in this additional protocol experiment on the same day.

**Results:** Testing result shows that force-error relationship was significantly different between Protocol 1 and Protocol 1 – reduced $F$, but visual target location – error relationship in general matched quite well between the two protocols (figure 4.6A).

**Protocol 2 and 3 shows that testing order affects the error, and that visual representation of the target force is not a good descriptor of error.**

We tested the same target force range as Protocol 1, but added zero force reset periods between non-zero force targets (figure 4.5A) to test the order effect. The difference between Protocol 2 and Protocol 3 was the visual representation of the target. In Protocol 2, visual representation was the same as the Protocol 1, i.e., the target location was moved proportional to the required force. In Protocol 3, targets appeared between only two locations, the lower one indicating 0 force and the higher one indicating various non-zero target forces. In this case, the ratio between force and target representation changed each time a new target was presented. On a different day from Protocol 1 testing, 4 participants came back to participate in Protocol 2 and Protocol 3.

**Results:** Testing results suggest that visual representation of the target is also

not a good predictor of the force tracking error. Despite different visual target representations, there were not significant differences between Protocol 2 and Protocol 3 in force-error relationship on all target force conditions (figure 4.6B). Those force-error relationships were significantly different from that of Protocol 1 in most of the target force range. The observations were similar in visual target location–error relationships. Error trends of Protocol 2 and Protocol 3 were similar to each other, but were different from that of Protocol 1. We also tested Protocol 2 - reduced $F$ and Protocol 3-reduced $F$ conditions, where we tested a smaller range of the forces, while not changing the mapping between force and its visual representations. There were no notable differences between Protocols 2 and 3 and their reduced $F$ versions.

**Protocol 4 shows that visual bias does not explain the force bias.**

We asked subjects to track the target using a computer mouse, so that we could investigate the errors coming from visual aspects of the task. They did not need to keep exerting force to keep the mouse position, which is different from all other protocols where they needed to keep applying the force until a new target was shown. Eight out of twelve subjects performed this Protocol 4 experiment on their personal computers.

**Results:** Participants performed the tracking task almost perfectly. Visual tracking errors were overall quite small, and the error relationship was again significantly different from that of Protocol 1 for most of the ranges (figure 4.6B).

**Model with force error and biases captured the experimental results qualitatively**

We reject hypotheses that force or visual representation of the force predicts force tracking error, as force tracking errors were different for some protocols even for the same force or same visual target location. Any objective function model that mainly relies on mere force (e.g., figure 4.6C2) or visual representation to describe error trend would not be suitable to describe the observation. Error-and-bias model was better supported by the data. Error-and-central tendency bias model that fits Protocol 1 predicts the results of additional protocols fairly well (figure 4.6C3). The objective functions that minimized mean RMS error between mean data and mean model prediction on each force condition of different protocols were as follows (figure 4.13):

- Error-and-central tendency bias model:

$$F^* = \arg\min_F \sum_{j=1}^{N} \frac{\text{error}_j^{1.7}}{N} + 0.09 d_{\text{ctr-bias}}^{1.55}$$
$$= \arg\min_F \sum_{j=1}^{N} \frac{|F_{\text{target},j} - F|^{1.7}}{N} + 0.09(\bar{F}_{\text{target}} - F)^{1.55},$$

- Error-and-recency bias model:

$$F^* = \arg\min_F \sum_{j=1}^{N} \frac{\text{error}_j^{1.5}}{N} + 0.15 d_{\text{rec-bias}}^{1.3}$$
$$= \arg\min_F \sum_{j=1}^{N} \frac{|F_{\text{target},j} - F|^{1.5}}{N} + 0.15(F - F_0)^{1.3},$$

- Error-and-combined bias model:

$$F^* = \arg\min_F \sum_{j=1}^{N} \frac{\text{error}^{1.6}}{N} + 0.05 d_{\text{ctr-bias}}^{1.55} + 0.07 d_{\text{rec-bias}}^{1.3},$$

where $F^*$ is the prediction of the applied force based on the given objective function and $F$ is the applied force that is to be optimized. $F_{\text{target},j}$ is the force indicated by $j$-th dot in the sub-trial, when $N$ is the number of dots presented. Bias-related terms $d_{\text{ctr-bias}}$ is a distance to the "center" of the targets associated with central tendency bias, $d_{\text{rec-bias}}$ is a distance to the recent action associated with recency bias. They are determined by $\bar{F}_{\text{target}}$, which is the average (or expected) target force of the whole trial consisting of many sub-trials, and $F_0$, which is the force at the beginning of the sub-trial.

Details of the inverse optimization analysis are described in the Methods section.

## Changes in target forces describe error trends from all protocols.

We further investigated how force tracking error is explained by a tendency to shift towards some point. As we pointed out earlier, the error-target force relationship (figure 4.7A) and the visual error-visual target location relationship had distinct patterns for each of the protocols. However, the expected change in target force (figure 4.7B) and change in target force from the recent past target (figure 4.7C) better describe errors across different protocols. These support the idea of people's tendency to shift towards either the recent past action or the center of the task. Error-and-effort model could not explain the positive error, but error-and-bias models could explain it: central tendency bias predicts positive errors on lower-range target forces as the center of the task is higher than the current force, and recency bias predicts positive error on lower range target forces as their recent past targets were on average higher than the current target.

We defined recency bias as a function of $d_{\text{rec-bias}}$, which is the distance to the recent past action, and central tendency bias as a function of $d_{\text{ctr-bias}}$, which is the distance to the "center" of the targets or the average of the targets. From their definitions, the average of the $d_{\text{rec-bias}}$ is close to $d_{\text{ctr-bias}}$ except for the small discrepancies due to the order effect in Protocols 2 and 3. Therefore, models using recency bias, central tendency bias, or a combination of recency bias and central tendency bias, all yield similar overall error trends (figure 4.13C). We analyzed sub-grouped data to see their separate effects, and found that they both seem to exist, which is presented in the following section.

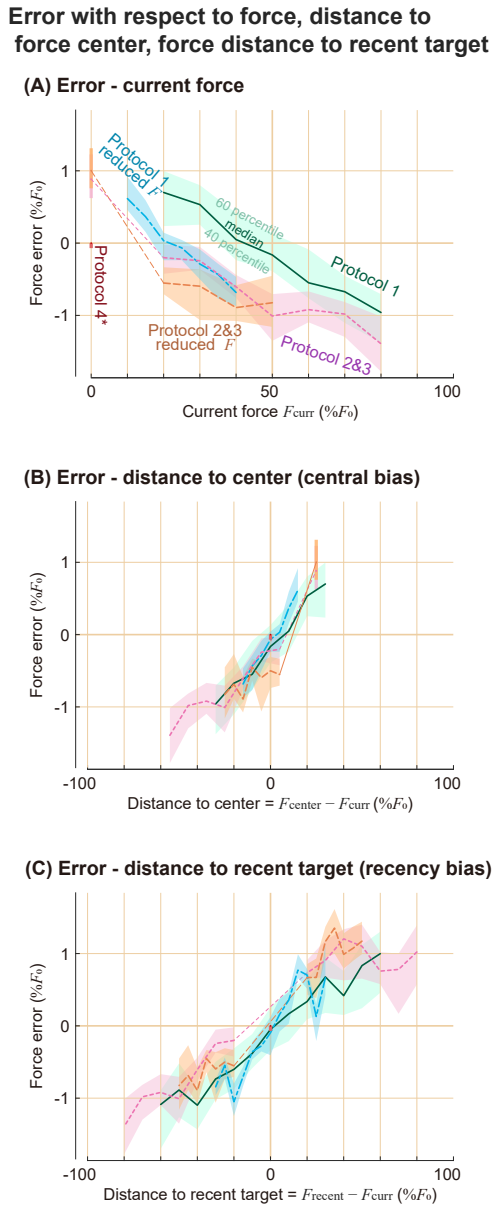


Figure 4.7: **Error trends with force, force transition from the recent target, and expected future force transition.** Force tracking error is plotted against (A) the current target force, (B) distance to the target center from the current target force, which is the expected transition, (C) distance to the recent past target force from the current target force, which is the transition from the past. Shaded areas represent 40 to 60 percentiles of the data at each condition, and the thick lines represent the median of the data. We showed visual error of Protocol 4 on the y-axis as a reference, because force error is undefined. The y-axis is for force error for all other conditions.

## Comparing central tendency bias and recency bias

### Changes in target force affect error when the current target force is fixed.

We grouped data of Protocol 1 – fixed dot target condition to investigate the recency bias effect. If recency bias does not have a notable effect, sub-trials that have the same target force will generally have the same errors, regardless of their recent past target. However, we do see a dependency on where the force started from, even if the target force is the same (figure 4.8A). Errors had negative correlations with force change, even when they were compared against sub-trials that had the same target force.

We considered three types of bias models in the objective function: central tendency bias, recency bias, and a combined model that has both biases. While all three of them do similarly well at capturing the overall error trend with force, the central tendency bias model does not capture the negative correlation between force change and error when the target force is fixed (figure 4.8B). Recency bias and combined model are more suitable to describe this observation.

### Current target force affects the error among sub-trials that underwent the same change in target force.

We now grouped data of Protocol 1 – fixed dot target condition to investigate the central tendency bias effect. Here, we grouped sub-trials into the same target force changes, because analysis on the sub-trials that had the same target forces showed that change in target force affects the force error. If recency bias alone could explain the observations and central tendency

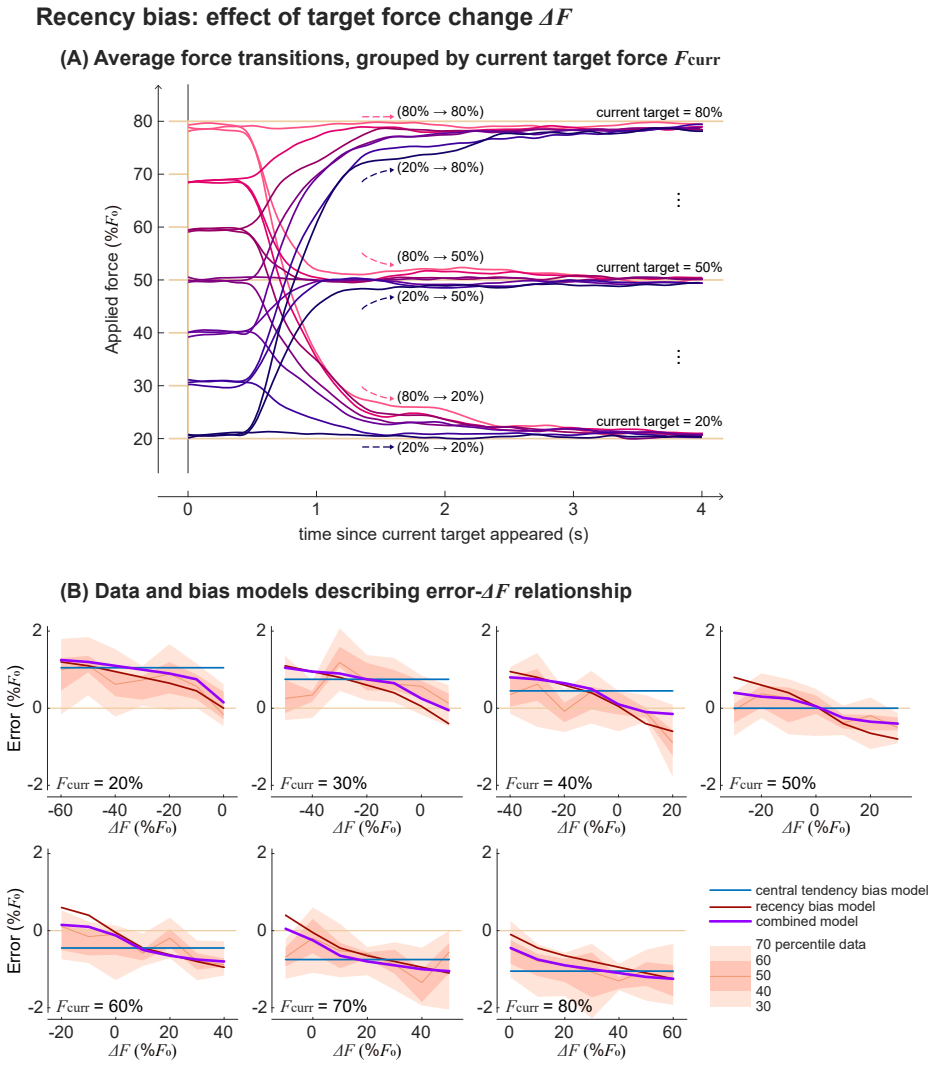


Figure 4.8: **Protocol 1 sub-trials grouped into same target forces.** (A) Averaged force time series grouped based on its recent past target and current target forces. Brighter and more red colors are for higher previous target forces, and darker and more blue colors are for lower previous target forces. (B) Force error as a function of target force change, among sub-trials that had the same current target force. Each sub-panel is for different current target forces. The shaded area represents 30, 40, 50 (=median), 60, 70 percentile data range. Blue, red, and purple lines are predictions using error-and-bias models with only central tendency bias, only recency bias, or central bias and recency bias combined.

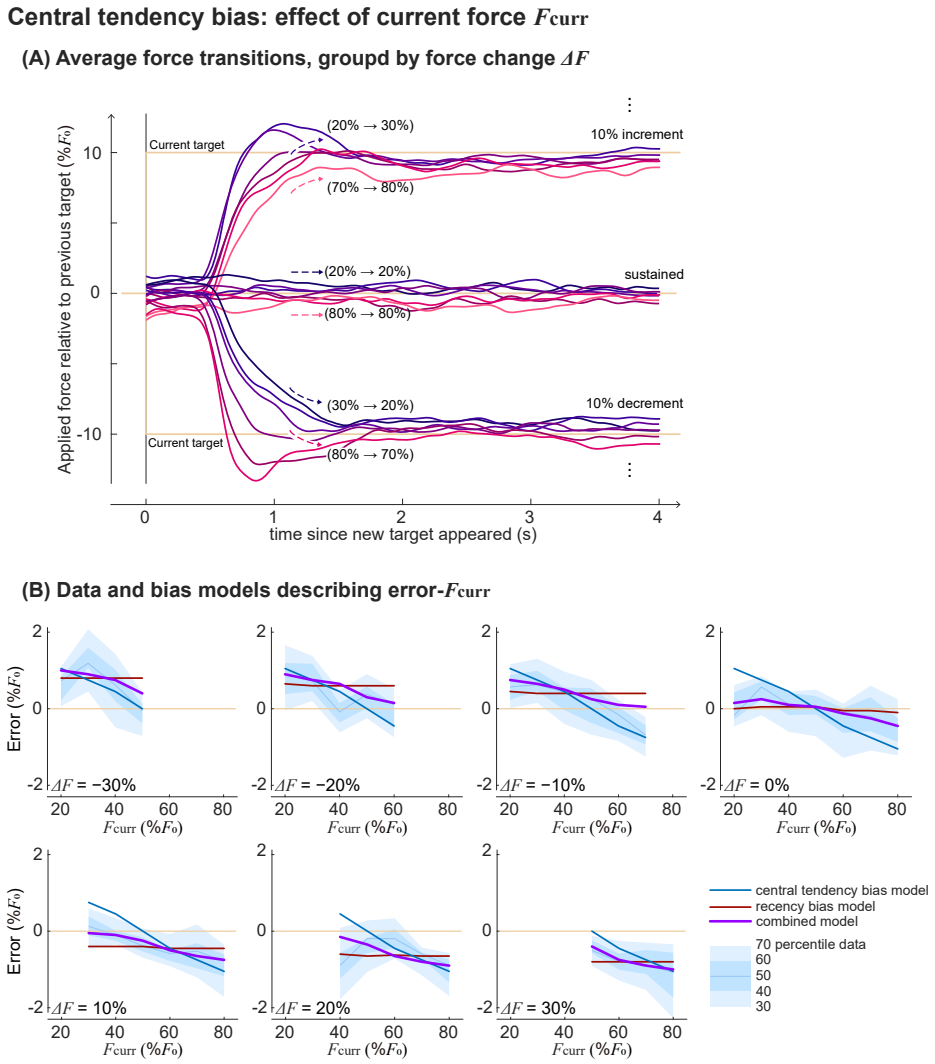


Figure 4.9: **Protocol 1 sub-trials grouped into same changes in target forces.** (A) Averaged force change time series, where the y-axis is a force difference with respect to the recent past target. Shown here are sub-trials that had 10%$F_0$ increment, same, or 10%$F_0$ decrement from the recent past target. Brighter and more red colors are for higher current target force, and darker and more blue colors are for lower current target force. (B) Force error as a function of the current force, among sub-trials that had the same change in the target force. Each sub-panel is for different changes in the target force. The shaded area represents 30, 40, 50 (=median), 60, 70 percentile data range. Blue, red, and purple lines are predictions using error-and-bias models with only central tendency bias, only recency bias, or central bias and recency bias combined.

bias has a negligible effect, groups of data that underwent the same target force change would have a similar error regardless of the current force requirement. However, we do see a dependency on the current target force level, when we compare sub-trials against other sub-trials that had the same target force change (figure 4.9A). Errors had negative correlations with target force in each of the groups that had the same change in target forces. We explained this observation in terms of central tendency bias, that people make positive errors when the center of the task is higher than the current target force, and make negative errors when the center is lower than the current target force.

We again considered three types of bias models in the objective function: central tendency bias, recency bias, and a combined model that has both biases. Since the change of target force is a variable that inherently co-varies with target force on average, all three models capture the overall error trend. However, the recency bias model does not capture the negative correlation between target force and error when the target force change is the same (figure 4.9B). Central tendency bias and combined model are more suitable to describe this observation.

## Purely visual tasks did not have the biases

We have shown that force or visual target locations alone were not good descriptors of error, but force bias could be a good descriptor. Then, if an error could be explained by force bias, there is a chance that it could also be explained by a visual bias. We therefore investigated whether visual bias could be an alternative explanation of the error trend we observed. Since the

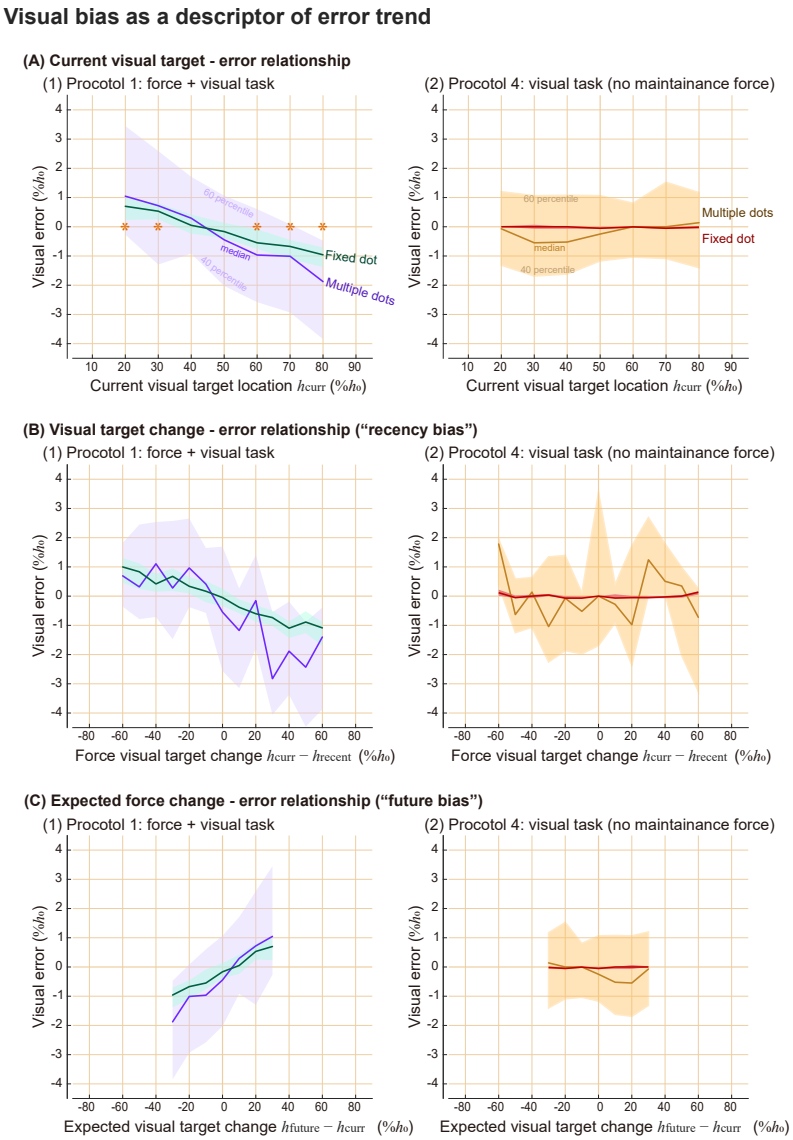


Figure 4.10: **Tracking errors in visual domain, comparing Protocol 1 and Protocol 4.** Results from target type of single dot and multiple dots are shown here. Shaded areas represent 40 and 60 percentile data, and thicker lines in the middle of the area are the median of the data. We represent visual error with respect to (A) the current visual target location, (B) the distance to the center of the visual target, (C) the distance to the recent past target location. Asterisks in the top row sub-panel indicate statistically significant differences from zero for both target types separately. There were no significant differences from zero from Protocol 4.

visual location of the target was proportional to the force in Protocol 1, visual bias could explain the error trend (figure 4.10 left) as much as the force bias does. The most striking counterexample is from Protocol 4, where subjects used a computer mouse to track the targets and did not need to exert force to maintain the pointing location. Although recency bias is commonly studied in visual tasks, we do not observe clear visual biases from Protocol 4 (figure 4.10 right). Subjects made almost no error for single fixed targets when they used a computer mouse to track the target. When they tracked a vague target which is a set of multiple dots, overall variability increased, but there was no significant trend in visual error, and its mean is not significantly different from 0 regardless of the visual target location.

## 4.4 Discussion

We measured force tracking errors while subjects performed tracking tasks of various protocols and modeled their behaviors using an objective function with an error term and force bias term. Our original aim was to measure the trade-off between task performance and effort, but we needed to include bias term(s) rather than an effort term in the objective function to explain the result. The main discrepancy between the observation and our original expectation was that people made consistent positive force errors in some ranges, which is not explainable by either effort-saving tendency or error-reducing tendency. Central tendency bias and recency bias, which means the tendency to shift towards the center of the tasks and towards the recent action, seem to explain the data well when combined with an error model. To our knowledge, these biases in force tracking tasks have not previously

been observed and modeled.

In certain modeling scenarios, refining the control objective function, as demonstrated in this study, can yield significant benefits, while in others, the advantages may be less evident. The usefulness of such refinement may depend on the level of detail at which one examines the phenomenon, and on practical considerations such as computational requirements and analytical solvability. On the other hand, understanding the human tendency to make biases while performing motor tasks could have broader applications in various fields, including human-machine interaction and human factors engineering. Additionally, exploring the connection between these biases and neuromuscular disorders could also provide deeper insights into motor control and hold the potential for various clinical applications, including diagnosis and rehabilitation.

We initially attempted to model the force tracking error using an effort model because it is a common expectation that motor control is usually done in an energetically optimal way. The observation that people apply more force than needed in the low-medium force range seems to be an example that people did not optimize for energy, at least during the experiment. However, could it turn out to be energetically cheaper to make such positive biases? For example, if there is a huge cost associated with force changes, it could be more efficient to spend slightly more energy on maintaining force and save a bigger energy by reducing a force change. Since we did not directly measure the energetic cost during the experiment, we cannot conclusively claim that people's behavior was energetically suboptimal. However, our speculation is that energy saving is not a primary explanation of the biases, because 1) the transient cost people save seems to be small

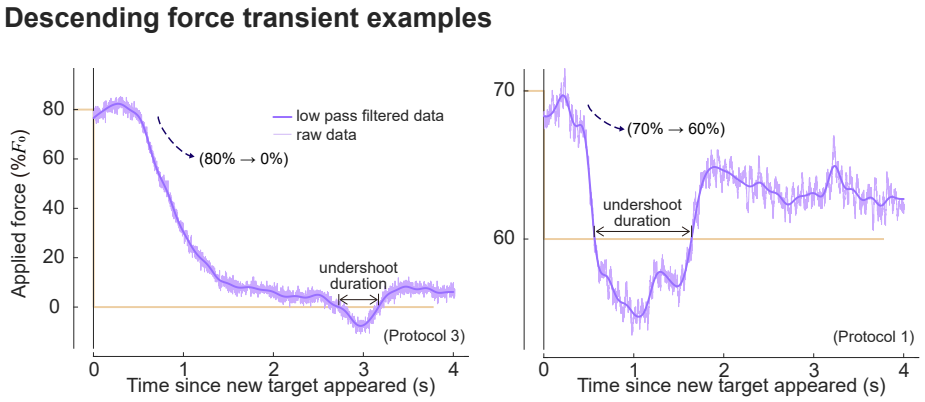


Figure 4.11: **Example force time series during sub-trials that had descending target forces.** Dim horizontal lines indicate the recent past target and the current target. Lighter purple lines show raw data, and darker purple lines show low pass-filtered data that was used in undershoot analysis. We defined undershoot duration as the duration where the applied force was lower than the target force during descending sub-trials.

compared to what they spend throughout the sub-trials while maintaining the force, 2) usually "fast change" is regarded energetically costly, but people did not seem to slow down the transient even when there was no explicit speed requirement, suggesting that transient cost is not of significant consideration, and 3) people often did reach a lower force than the target, and increased the force to again to make positive force error at the end (figure 4.11).

Undershoots in descending sub-trials (where the current target force was lower than the recent past target) are particularly interesting because they provide insights into the underlying reason for the positive force errors. Overshoots and undershoots that go past the target were quite common when we looked at individual sub-trials, although they were less obvious in averaged force transient responses (figure 4.8 and figure 4.9) due to the large variabilities in both amplitude and timing of the responses between

sub-trials. In Protocols 1, 2, and 3 full range and reduced range trials, 72-90% of descending force transients had undershoot of more than 0.2 seconds. Among all descending transients, 67-85% of sub-trials had positive tracking errors at the end. Among descending transients that ended up having positive errors, 68-86% had undershoot of more than 0.2 seconds. There were many sub-trials where the force recovered back to a higher force after an undershoot during descending force transients like the sub-trials shown here, where it did not seem like an unavoidable by-product of a fast response due to physiological constraints, nor a strategy to save transient energy. This suggests that positive biases on low-medium range target forces are not for energetic advantages but for some other benefits.

We modeled force tracking error as an outcome of competing goals of reducing error and biasing towards a center, but there could be alternative models to capture the same phenomenon. We used our bias models to predict errors from additional protocols, but the model is still descriptive in the sense that we did not test for the underlying mechanism or causality of such bias. Our description of biases suggests that people tend to reduce force change, either from the past by making an incomplete shift, or toward the future by making an anticipatory error towards the expected target. However, since we have not proven whether the reduction in force change is the primary cause of the errors, it may turn out to be a secondary change following another one. It would be interesting for future work to investigate the causality of the biases.

Including more terms in the objective function model could capture a broader range of phenomena, but it could also make the inverse optimization problem more underdetermined, potentially leading to an unreliable

solution. Central tendency bias and recency bias exhibit similar effects on the overall trend predictions in our experimental designs; thus, one may not need to model both biases to explain some behaviors, depending on their goals. We did not particularly design experiments to distinguish these two biases, and there were multiple sets of solutions yielding similarly good inverse optimization results (figure 4.13). Our subgroup analysis suggests that both seem to have an effect, but we do not claim that we quantitatively verified recency bias and central tendency bias. It would be interesting to design experiments to further disambiguate the biases that originate from past actions and originate from anticipatory actions for the future. For example, one could design a trial order that cycles through three stages, two random non-zero target forces followed by one zero target, so that the average past action is distinct from the average future actions. Even the formulation of the error-reducing tendency must have been an oversimplification if the aim was to closely understand what people perceive as a target. Error function could have a different form depending on the number of dots presented as a target, or could take into account how individual subjects subjectively defined the tasks.

There could be various biases in human motor control, and some of them could happen immediately without task-specific experiences while some of them may need learning of a task. Some of the biases could take a long time to change their properties, while others may rapidly adapt to each of the tasks. We assumed that subjects readily had an expectation of the center of the target when we modeled central tendency bias, but further research is needed to justify this in depth. We chose to model the central tendency bias this way because we had speculated that the bias

does not seem to rely on learning from each trial, because force tracking errors seemed to happen instantly when testing began, and because we do not observe clear changes over the course of the trial. However, we do not have strong evidence to show whether subjects make biases based on their experience of the trial or expectation of it, or based on the combination of them or even neither of them. It is conceivable that people may start making biases based on their prior expectations and refine the expectations as they have more experience with the task. It would be interesting to design experiments that give subjects a more different impression of the task from its actual composition, and to see which one is a better predictor of the behaviors.

One of the reasons that biases in force tracking tasks were not commonly recognized in biomechanics studies might be due to the specifics of the common experimental designs. In biomechanics literature, it is common to 1) measure force transients that start from rest, and 2) report the absolute value of the error, which omits the directionality of the error. Researchers sometimes describe that people are less accurate at producing bigger forces. Our findings suggest that this description might be highly context-dependent, and there could be a more general description of the phenomenon. Our error-and-bias model predicts that absolute error is minimized near the center of the tasks (figure 4.12A), rather than monotonically increasing with the force magnitude. Despite that overall root-mean-squared (RMS) errors in experimental results were shifted up compared to the model predictions (potentially due to human variabilities), our model captures the overall trend of error (figure 4.12B) that had minima near the center of the task.

Our results are still consistent with the previous studies, when we look at

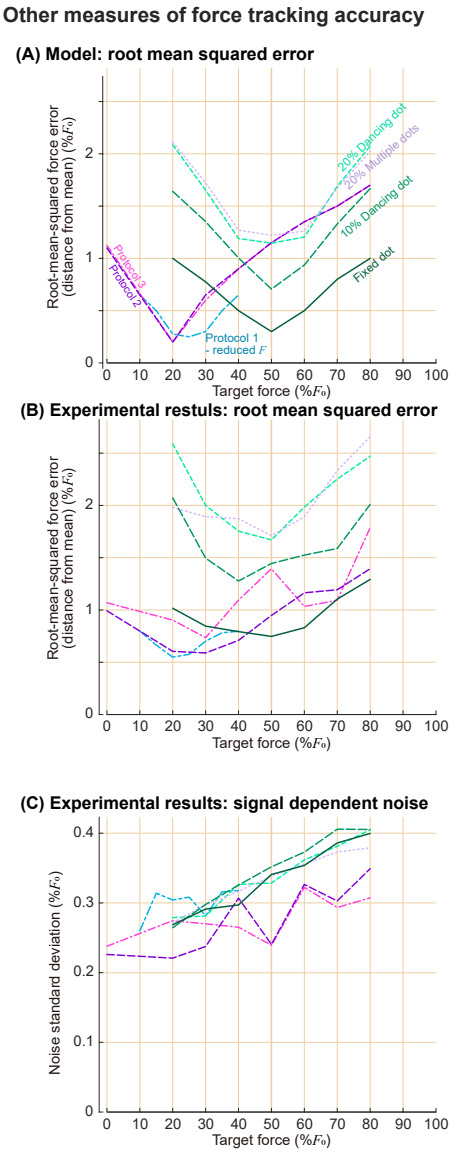


Figure 4.12: **Root-mean-squared error and signal-dependent noise during force tracking tasks.** For root-mean-squared (RMS) error, we use error defined as a distance between the mean of the target distributions and the average force applied during the last 0.5 seconds of the sub-trials. We show RMS error that (A) model predicted and (B) measured from experiments. Lines of different colors indicate different protocols and target types. The target force on the x-axis indicates the mode of the target distributions. (C) The standard deviation of the higher frequency component of the force, with respect to the target force. This higher frequency component of force is referred to as motor noise in some literature, and its dependency on the target force is an example of signal-dependent noise. Lines of different colors indicate different protocols and target types.

the non-zero sub-trials of our Protocols 2 and 3, which were always followed by zero force sub-trials. RMS errors indeed roughly increased with the force magnitude in these cases. Directionality of the error during these sub-trials was also consistent with previous studies: we predict and measure negative errors, and previous studies also usually measured negative force tracking errors (e.g., directly reported in Todorov (2002), could be inferred from figures in (Kudzia et al., 2022)). However, what had been usually not measured and reported in previous studies is that RMS force error during zero force sub-trials increases again (figure 4.12A), and that people tend to make a positive error for this range. The RMS error trend was even more dramatically different from the monotonic increase when we consider Protocol 1 results, where target forces were not reset to zero force.

This leaves us a question of whether we could truly eliminate order effects in scientific measurements. As we pointed out, even separating trials by resting periods and having a "fresh start" could give us a wrong impression of the phenomenon, because starting from zero is one of the special cases as well. It would be important to be 1) consistent and clear with what we measure, 2) recognize that what we observe might be a special case of a more general phenomenon, and 3) try to distinguish co-varying variables if possible. For example, force magnitude and force increment co-varies if tests always begin from zero, but they did not co-vary in our Protocol 1, and provided us with a more general view of the nature of force tracking errors. On the other hand, signal-dependent noise, which is defined as the standard deviation of force after removing a low-frequency component, had a closer match between trials and seemed to increase with force (figure 4.12C; consistent with Jones et al. (2002)). This quantity seems to be less

context-dependent than force error, and thus, has a higher chance of being explained by simpler physiological properties such as muscle characteristics or nervous system dynamics. However, what we measured could still be a partial description of a more general phenomenon, as it always is in science.

It was interesting to us that we did not observe a significant bias when people performed an almost fully visual task (figure 4.10), considering that many studies on recency bias and central tendency bias are measured from visual pattern recognition tasks. It is conceivable that human minds would have various biases without involving the muscular system. On the other hand, some biases may be caused by more passive and physical properties of the body without involving perceptions and judgments, and some biases might be caused by combinations of them. From studying the biases of force tracking tasks, we became curious if there is a chance that some of the perceptual biases could be attributed to motor control biases more than researchers commonly thought. For example, ocular motor control may have a similar bias as what we observed in this study that involved arm muscles, and that could result in a bias in visual sensation. There could be biases caused during measurement procedures as well, because subjects were often asked to indicate their perception of patterns using some physical device by manipulating it, which involves some degree of motor control.

Force bias does not seem to be a commonly recognized phenomenon in an isolated motor control setting, but we could relate it to a broader field of motor control. In a singing study, it was reported that people tend to compress the pitch shifts, and "bad singers" tend to make more such compression (Pfordresher and Brown, 2007). In speech studies, there is a window model suggesting that people make minimal shifts between ac-

ceptable windows of some variables (Keating et al., 1990). Moreover, when we consider the recency bias in broader terms that people tend to keep acting similarly, there are more such examples in biomechanics studies. For example, walk-to-run and run-to-walk speeds are reported to be different ("hysteresis effect in speed for the walk-run transition", Diedrich and Warren Jr (1995)), which is not simply explained by the idea that animals choose the most economic gait at a given speed. People change their behavioral mode between one-handed grasping and two-handed grasping depending on the size of the object, and it is reported that there is an order effect in such shifts (Frank et al., 2009). Some researchers attribute these biases to the "economy", that people save energy by reducing transitions, although this claim is usually difficult to be directly tested. We hope that an extension of our current study could give insights into these broader fields of behavioral studies.

To conclude, we examined which objective function best describes human force tracking errors. In many motor control studies, objective functions are modeled to include error and effort terms, typically in quadratic forms. However, we designed an experiment to test them and indeed found a different formulation. The exponent on the error we found was smaller than 2, and bias term(s) were needed instead of an effort term in order to capture the behavior that was consistent across participants. Our findings on biases suggest that biological motor control, even in a simple isometric force production task, can be highly context-dependent, and commonly hypothesized formulation might not be adequate to represent the phenomenon. As we continue to explore the intricacies of human force control, further research may offer valuable insights into our understanding of human move-

ment behaviors and underlying principles of the nervous system.

## 4.5 Methods

### Experimental procedure

Subjects ($N_{\text{subjects}} = 12$; 4 Female, 8 Male) participated in Protocol 1, and a subset of them participated in additional studies later. This human subject research was reviewed and approved by The Ohio State University's Institutional Review Board, and all subjects participated with written informed consent.

We measured elbow height from the ground and subtracted half of the subject's forearm length to set a platform height they pressed onto, which made the forearm angle about 30 degrees below the horizontal line. After setting the force platform, we measured the individualized force target range $F_0$ by asking the participants to apply a force that they could comfortably hold for 30 seconds. We encouraged participants to apply reasonably high force, and reduce it until it felt comfortable to hold. Real-time force feedback was given on the monitor, and we encouraged them to control the feedback bar location. After measuring the force range, we verified again that subjects could comfortably exert the force for 30 seconds. The process was repeated until we found the force that the subject was comfortable with producing for an extended amount of time.

After giving participants a verbal description of the tasks, we provided them with practice trials, which were shorter versions of the trials so that they could see the test procedure and try the tasks. We introduced different target

types in turn – fixed single dot, then single dancing dot, and then multiple dots. The target changed color between blue and red in each sub-trial, and all participants confirmed that the colors were significantly different for them. We instructed the participants that the target location changed every 4 seconds with the change of the target color, and asked them to apply force so that the force feedback bar points to the target. For vague targets, we told them that the dots are dancing around some fixed point and are not moving away as long as the color stays the same, and asked them to point where they perceive as a target from the overall impression of the dots. We explicitly asked them not to chase individual occurrences of the dots, but to perceive its center and place the bar there. Participants practiced each of the target types for at least 5 sub-trials, and we repeated the practice if subjects desired to do so or were unclear about the task.

Each trial was composed of 74 sub-trials. The first three trials were excluded from the analysis to make sure that subjects adapted to a different target type. The following 70 conditions covered all possible combinations of force level and distribution parameters in a random order, which is described in the following paragraph. After these 70 sub-trials that are used for analysis, the last sub-trial of each trial was 100%$F_0$ one, from which we checked that subjects were still capable of producing more than 80% of $F_0$. 4 seconds of 74 sub-trials took about 5 minutes.

We tested 20, 30, ..., 80% of $F_0$ in Protocol 1, and used distribution parameter $\alpha = -2, -1, -0.5, -0.1, -0, +0, +0.1, +0.5, +1, +2$ to generate vague targets, resulting in 7 force levels $\times$ 10 distribution parameters = 70 combinations. For the fixed single dot condition, we measured each force level 10 times to ensure the same number of sub-trials. In Protocol 1 - reduced $F$,

force levels we tested were 10, 15, ..., 40 %$F_0$. In Protocols 2 and 3, non-zero forces were 20, 30, ..., 80%$F_0$, and each force level was measured 5 times, again resulting in a total of 70 sub-trails including zero force periods. In Protocol 2 and 3 - reduced $F$ conditions, non-zero force levels were 20, 25, 30, ..., 50 %$F_0$. Protocol 3 had binary visual target locations, which were the same as the target for 0 force and 80%$F_0$ in Protocol 2.

We defined the distribution parameter $\alpha$ as follows. Positive non-zero distribution parameters correspond to a shape parameter of Pareto Distribution truncated between 0 and 5 (Zaninetti and Ferraro, 2008). The range was scaled to match 10% and 20%$F_0$. We generated distributions of negative non-zero $\alpha$ same as a positive $\alpha$, except that the whole distribution was flipped so that the tail of the distribution goes the opposite way. Two symmetric distributions were also used: truncated uniform distribution was referred to as $\alpha = -0$, and truncated normal distribution that had similar standard deviation as other Pareto distributions were referred to as $\alpha = +0$ in this study as special cases of skewed distributions.

Six of the subjects had force feedback that went down as they applied force, and six of the subjects had force feedback that went up as they applied force. We did so to see if there was a visual bias linked to a vertical directionality. We did not observe a notable difference between the subjects of each feedback directionality. Each time before the test started, we asked subjects to place their hands on the platform and relax their arm muscles, try not to exert active force onto the platform, and let the platform take the weight of the hands. This hand weight was set to zero force so that participants did not need to actively spend energy lifting up their hands to match low force requirements.

Protocols 1 and 4 involved testing vague targets. In Protocol 1 – dancing dot target condition, a dot appeared within 10% and 20%$F_0$ range, and in Protocol 1 and 4 – multiple dots conditions, 240 dots appeared within 20%$F_0$. We tested all target types in a random order two times. Other protocols were measured once per protocol. Subjects took about 2 minutes of rest between trials and occasionally took longer breaks as desired.

## Data collection and processing

Custom MATLAB software was used to show targets and force feedback on the screen. A force plate (Bertec Corporation, Ohio, USA) mounted on the ground was used to collect force data. Force plate data was collected through a motion capture interface (Nexus, Vicon, Oxford, UK) that was relayed to MATLAB software. Target and force feedback were updated at 60 Hz, which matched the monitor refresh rate. Force was collected at 8 times faster speed, which is 960 Hz. Multiple dots changed their horizontal positions in every frame. The target radius was about 0.7%$F_0$.

The mean value of force during the last 0.5 seconds of each sub-trial was defined as the steady-state force value, and this value minus the target force was defined as force error. We normalized force error by $F_0$. The mean value of force during the first 0.1 seconds of each sub-trials was defined as an initial force, and was used to calculate recency bias. To study signal-dependent noise, we obtained a fast component of the force change by subtracting a slow frequency response from a faster frequency response. Fifth-order Butterworth low pass filters with a cut-off frequency of 25Hz and 5Hz were applied to force data using zero-phase filtering in order to calculate

these slow and faster responses. Standard deviation of this fast component during the last 0.5 seconds was reported as a "noise" to investigate signal-dependent noise (figure 4.12).

## Protocol 4 - test using a computer mouse with negligible forces

Custom MATLAB software was used to conduct tests of Protocol 4. We kept the testing interface as similar as possible to other protocols, except that the vertical position of the horizontal bar that used to indicate the applied force was changed to indicate the vertical position of the mouse pointer on the screen. The cursor was hidden and subjects could only see the height of the horizontal bar as they moved the computer mouse.

We used a MATLAB callback function that responded to mouse position changes. Trials were similar to those of Protocol 1, in terms of test duration and conditions. We tested a fixed single dot and multiple dots using this interface. Unlike Protocol 1, multiple dots did not change their horizontal locations in Protocol 4, because we could not guarantee a constant refresh rate through the interface we employed. We recorded the time and position of the mouse pointer each time there was a change. Clicking was not required to perform the task.

## Predictions for additional protocols based on the bias terms.

We considered two types of biases in this paper. Predictions of the force tracking error based on central tendency bias and recency bias are as follows.

**Predictions based on central tendency bias.** We modeled a tendency to shift towards the "center" of the tasks, where “center” was defined as the mean of the target forces throughout the trial. The mean of the tasks in Protocol 1 was 50%$F_0$, and the mean of the tasks in Protocol 1-reduced $F$ was 25%$F_0$. Using this model, we expected that errors would in general cross 0 around these force levels in each of the protocols. In Protocol 2 and 3, since half of the sub-trials were at 0%, the mean of the targets was 25%$F_0$. We expected that zero force sub-trials would have positive errors, and non-zero force sub-trials would have more negative errors as the target force increased. We used the same center for Protocols 2 and 3 – reduced $F$, because subjects were unaware of the reduced force range.

**Predictions based on recency bias.** We modeled a tendency to shift towards the recent past action. In Protocol 1 and Protocol 1-reduced $F$, the prediction based on the recency bias model was that lower target forces would have positive errors, because their recent past force is higher than their current forces on average. Similarly, the prediction on higher forces was that they would have negative errors, and medium-range forces would have errors near zero. This distinction of low, medium, and high forces was all relative to the force range of each trial in this bias model. Similar to the central tendency bias model, we expect that errors would cross zero near 50% $F_0$ and 25% $F_0$ respectively for Protocol 1 - full range and reduced $F$ conditions.

In Protocols 2 and 3 where there were zero reset periods, we expected that zero force sub-trials would have positive errors because their

recent past forces were always higher than the current force. Similarly, we expected that non-zero sub-trials would have more negative error as the target force increased, because their recent past forces were always zero. Protocols 2 and 3 – reduced $F$ were expected to have similar error trends as their full $F$ range versions. The only difference could be on zero force sub-trials, because their average distance to the recent past target was smaller in reduced range protocols than in full-range protocols, thus resulting in a slightly smaller positive error on zero force sub-trials.

Both central tendency bias and recency bias models predict similar overall error trends because their expected values are similar to each other. Both models predict that neither error-target force relationship, nor visual error-visual location relationship will be consistent across different protocols, because bias is dependent on force and the context of the experiments. In addition, both bias models predict that there is a bias in the force domain, not in the visual domain; thus, we predicted that Protocol 4 will not have such bias because the task does not require maintenance force.

## Inverse optimization

We did grid search to perform inverse optimization to select hyperparameters of objective function models. We used a similar mathematical formulation to represent both central tendency bias and recency bias, which was:

$$F^* = \arg\min_F \sum_{j=1}^{N} \frac{\text{error}_j^p}{N} + b d_{\text{bias}}^{\beta},$$

where $F^*$ is the prediction of the force which minimizes the given objective function, $\text{error}_j$ is absolute distance between $j$-th dot and the force applied, summed over number of target dots $N$. $d_{\text{bias}}$ is absolute distance from the applied force to the bias center. It is the distance to the perceived average of the target forces for central tendency bias, and distance to the initial force at the beginning of the sub-trial for recency bias.

We searched for error exponents $p$ between 1.4 and 1.9 range by the increments of 0.1, bias weightings $b$ between 0.01 and 0.25 by the increments of 0.01, and bias exponent $\beta$ between 1 and 2 by the increments of 0.05. For each combination of these hyperparameters, we calculated the model prediction of each sub-trials. The model predicts the forces that minimize the given objective function. To avoid local minima issue and to improve the computational efficiency, we evaluated the objective function within $\pm 30\% F_0$ around the target by the increments of $0.05\% F_0$, and found the minimum value among them.

After calculating predictions for each sub-trial and each combination of hyperparameters, we selected the set of hyperparameters that produced a similar error-force relationship as the experimental results. Since error trend we aimed to model was in a relatively small magnitude compared to large inter-subject and intra-subject variabilities, we selected an objective function that captures the overall behavior. The objective functions that minimized mean RMS error between mean data and mean model prediction on each force condition for the entire protocols were:

- Error-and-central tendency bias model:

$$F^* = \arg\min_F \sum_{j=1}^{N} \frac{\text{error}_j^{1.7}}{N} + 0.09 d_{\text{ctr-bias}}^{1.55},$$

- Error-and-recency bias model:

$$F^* = \arg\min_F \sum_{j=1}^{N} \frac{\text{error}_j^{1.5}}{N} + 0.15 d_{\text{rec-bias}}^{1.3}.$$

After performing inverse optimization on the central tendency bias model and recency bias model separately, we confirmed that they indeed have a similar formulation and have a similar effect of the force error predictions. We performed an inverse optimization on a combined bias model while keeping some of the hyperparameters fixed based on these results. We chose to fix some parameters to avoid overfitting, because we have confirmed that two biases have similar effects on the overall results, and human data is already very noisy.

We scanned the error exponent $p$ between 1.4 and 1.9 by the increments of 0.1, while changing two bias weightings between 0.01 and 0.25 by the increments of 0.01. The bias exponent $\beta$ was fixed to the optimal value that was found earlier. The objective function that minimized RMS distance between mean data and mean model predictions on error-force relationships was:

- Error-and-combined bias model:

$$F^* = \arg\min_F \sum_{j=1}^{N} \frac{\text{error}^{1.6}}{N} + 0.05 d_{\text{ctr-bias}}^{1.55} + 0.07 d_{\text{rec-bias}}^{1.3}.$$

## 4.6 Appendix

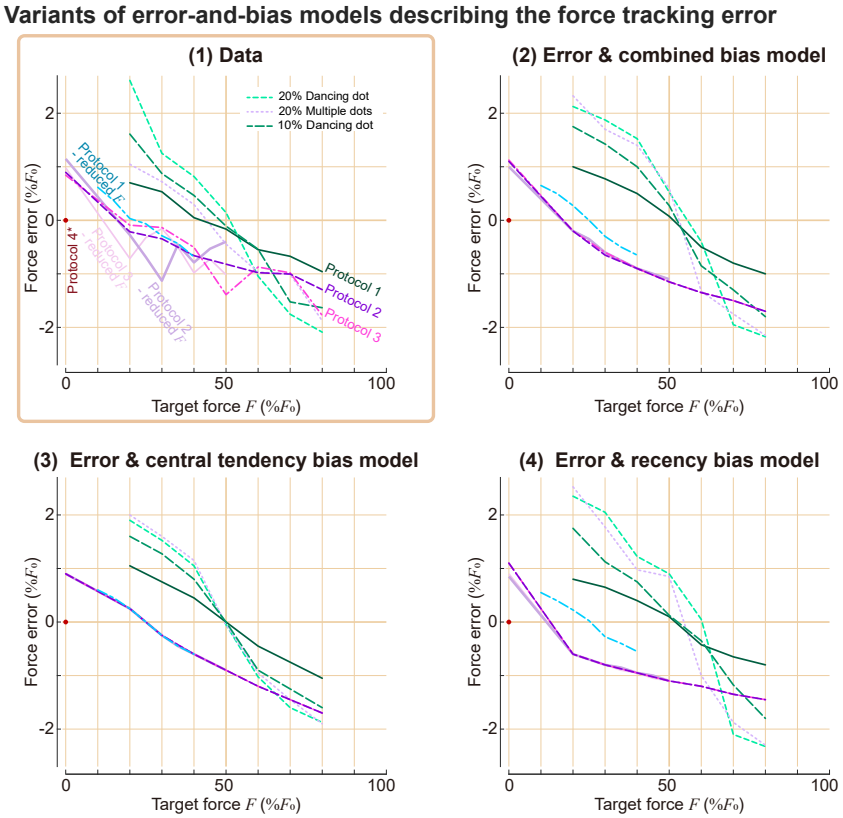


Figure 4.13: **Variants of error-and-bias models describing the force tracking error from various protocols.** (1) Experimental data from various protocols. Different lines indicate the median results of each protocol. (2)-(4) Models that best fit the overall experimental data, whose objective functions are weighted sums of the error terms and (2) both central tendency bias and recency bias terms, (3) central tendency bias term, and (4) recency bias term.

# Chapter 5

# Conclusion

흔들리지 않고 피는 꽃이 어디 있으랴.

No flower blooms without wavering.

---

도종환, *흔들리며 피는 꽃*

Poem by Jong-Hwan, Do.

## 5.1 Findings from the three studies

In the previous three chapters, each describing a distinct study, I investigated optimality with respect to the multiple objectives and trade-offs between them during motor control and pattern recognition under uncertainty. Optimization and inverse optimization analysis were used to study what principles may explain biological movement control.

The study presented in Chapter 2 was based on a complex model that represents a whole goal-directed movement. The control objectives that were considered in this study – root mean squared estimation error, mean time between falls, step length variability, and mechanical cost of transport

– were all represented in commonly used formulations. In contrast, the studies presented in Chapters 3 and 4 delved more deeply into the formulations of objective functions using simpler settings. Chapter 3 focused on the perception of visual targets, while Chapter 4 examined the isometric force production, which also involved the perception of visual targets. In Chapter 3, we found huge variability and systematic behavioral shifts associated with data sparsity, unlike widely adopted error models. In Chapter 4, we found that even a simple motor control task like isometric force production could not be fully explained by a commonly used objective function model that incorporates energy minimization. Our alternative model, incorporating recency bias and central tendency bias, suggests that biological motor control is highly context-dependent and may have more nuanced aspects than previously assumed.

In Chapter 2, I used a biped walking model simulation to demonstrate the effect of motor noise and sensor noise on the optimal locomotor control circuit. Integration of neural pattern generator and sensory measurements was optimized to have minimum state estimation error. Such optimization also resulted in optimal performance in terms of energy efficiency, variability reduction and fall prevention. Changes in the relative amount of motor noise and sensor noise shifted the optima systematically.

In Chapter 3, I designed a visual pattern recognition task to study how humans perceive noisy visual targets and performed inverse optimization on the measurement. Objective functions similar to what is commonly used in statistics and machine learning fields could capture general behaviors and systematic shifts in the behaviors. As the sparsity of the noisy information decreased, or as the amount of information increased, participants tended

to reduce small and prevalent errors at the cost of increased large and scarce errors. The inferred loss function describing human behavior also changed systematically with the data sparsity.

In Chapter 4, I extended the task in Chapter 3 and tested how human subjects performed force tracking tasks when the force target was presented with visual noise of varying degrees. Increased noise in the target induced higher force tracking errors in both over-exerting and under-exerting ways, depending on the force requirement. This force tracking error was not explained by optimization models that minimize error, efforts, or a combination of them. Rather, an objective function that balances error-reducing tendency and force bias tendency could explain the observation fairly well. This force bias tendency was modeled as a tendency to move towards the recent past action or towards the expected future action. This bias was not readily explained by a tendency to save energetic costs, nor by a perception bias.

## 5.2 Discussion

I showed that optimization and inverse optimization could be used to describe motor control under uncertainty. However, being able to express behaviors as an optimization problem does not mean that there is necessarily a neural circuit that evaluates and minimizes the objective function. Nonetheless, it still provides us useful insights into understanding biological motor control and ideas for future studies. Whether such optimization frameworks are useful for designing simulation models and robot algorithms depends on the context. For instance, robots may not need to make a similar

force tracking bias as humans do, especially when its benefit is unclear, but some robots may benefit from having a model of human biases when they are designed to collaborate with humans.

Optimality and suboptimality could sometimes be dependent on how closely we look at a phenomenon. Shifts in behaviors that I described in Chapters 3 and 4 could be negligible in some contexts, while they could result in a significant difference in other contexts. Walk-to-run and run-to-walk transition happens roughly at the speeds predicted by metabolic energy minimization, but the average transition speed is systematically slightly lower than what energy minimization would predict (Abe et al., 2019; Kung et al., 2018). There seems to be an order effect too – reducing speed from running and increasing speed from walking has close, but different transition speed (Diedrich and Warren Jr, 1995). If someone needs to accurately predict the transition speed, metabolic cost minimization is an incomplete descriptor of the phenomenon; however, it could be adequate for qualitatively capturing the general principle of locomotion across species. In a previous study where optimal step frequency for a given walking speed was altered through an exoskeleton that was responsive to step frequency, researchers found that their human participants chose to alter their walking accordingly only after being instructed to experience the condition (Selinger et al., 2015). Some people may regard it as an example that humans do prefer energetically optimal gait, but others may regard it as a counterexample of the energy minimization hypothesis.

Sometimes multiple objectives co-vary, so optimizing for one could nearly optimize for other measures too. Symmetric gait could be also energetically cheaper in healthy subjects (Ellis et al., 2013). Peak force could

be reduced while average force is reduced in a reasonable mode of gait. In Chapter 2, optimizing for minimum state estimation error also yielded optimal gait in terms of other performance measures. Gait adaptation on a split-belt treadmill, which operates at different belt speeds for each leg, was commonly explained by improving the symmetry (Reisman et al., 2007), but some researchers claim that this coincided with a path of minimizing metabolic cost up to some degree, and people further change their gaits to become less symmetrical but more energetically efficient (Sánchez et al., 2019) after they became symmetric. Sometimes it is not useful to distinguish what was the true cause of some phenomenon between co-varying objectives, but if needed, experiments should be designed so that normally co-varying quantities can be separated. In either case, to understand biological control objectives and behaviors, it would be important to be aware of a potential confusion between causality and correlation.

There also could be more general versions of some motor control models. For example, minimizing metabolic energy expenditure is a useful explanation of many biological movement behaviors, but stated without additional context and caveats, it contains an inherent dilemma because it is actually most energy-saving not to live at all. However, it could be a special case of a more general survival strategy: animals collect food while saving energy so that they can eat before they starve to die (Schoener, 1971; Krebs et al., 1974), and they can carry on with life. Some of seemingly unexplainable behavioral traits could even be byproducts of pursuing other more sensible objectives, or they may rise because an objective function has the problem of extrapolation outside of its normal working range. Force bias towards the recent past target or towards the expected target which I studied in Chapter

4 is plausible in some sense, when we consider that our mind often stays in the past or in the future. Reflection and anticipation might be useful tools for survival in a broad sense, but they often interfere with the execution of the current task and seem to be suboptimal at least in the short term. Similarly, somewhat analogously, addiction issues are believed to arise when addictive drugs "hijack" reward circuits in the brain, which is essential for the normal operation of humans and animals when it functions with life's normal rewards (Volkow and Wise, 2005; Kauer and Malenka, 2007; Elman et al., 2013).

The considerations mentioned above might be addressed in future studies. Investigating the direct causality between the behavioral changes and objective functions that describe the behavior would be an interesting future work. A more general model of motor control which could be applied to a broader field would be useful. However, since overly general models could be hard to falsify while also not useful at predicting or explaining things, it may be important to have a structured view of the scopes and limitations of each model.

# References


Giovanni Abbruzzese and Alfredo Berardelli. Sensorimotor integration in movement disorders. *Movement disorders*, 18(3):231–240, 2003.

Daijiro Abe, Yoshiyuki Fukuoka, and Masahiro Horiuchi. Why do we transition from walking to running? energy cost and lower leg muscle activity before and after gait transition under body weight support. *PeerJ*, 7:e8290, 2019.

Marko Ackermann and Antonie J Van den Bogert. Optimality principles for model-based prediction of human gait. *Journal of biomechanics*, 43(6): 1055–1060, 2010.

Franz Alexander. A contribution to the theory of play. *The Psychoanalytic Quarterly*, 27(2):175–193, 1958.

R McN Alexander. Optimization and gaits in the locomotion of vertebrates. *Physiological reviews*, 69(4):1199–1227, 1989.

R McN Alexander. Simple models of human movement. 1995.

R McNeill Alexander. *Optima for animals*. Princeton university press, 1996.

Hal R Arkes and Peter Ayton. The sunk cost and concorde effects: Are humans less rational than lower animals? *Psychological bulletin*, 125(5): 591, 1999.

Edgar Atzler and Robert Herbst. Arbeitsphysiologische studien: Iii. teil. *Pflüger's Archiv für die gesamte Physiologie des Menschen und der Tiere*, 215:291–328, 1927.

Sayantan Auddy, Sven Magg, and Stefan Wermter. Hierarchical control for bipedal locomotion using central pattern generators and neural networks. In *2019 Joint IEEE 9th International Conference on Development and Learning and Epigenetic Robotics (ICDL-EpiRob)*, pages 13–18. IEEE, 2019.

Adelchi Azzalini. A class of distributions which includes the normal ones. *Scandinavian journal of statistics*, pages 171–178, 1985.

Timothy D Barfoot. *State estimation for robotics*. Cambridge University Press, 2017.

Sheldon Baron and David L Kleinman. The human as an optimal controller and information processor. *IEEE Transactions on Man-Machine Systems*, 10(1):9–17, 1969.

Richard Bellman. The theory of dynamic programming. *Bulletin of the American Mathematical Society*, 60(6):503–515, 1954.

Bastien Berret, Enrico Chiovetto, Francesco Nori, and Thierry Pozzo. Evidence for composite cost functions in arm movement planning: an

inverse optimal control approach. *PLoS computational biology*, 7(10): e1002183, 2011.

John EA Bertram and Andy Ruina. Multiple walking speed–frequency relations are predicted by constrained optimization. *Journal of theoretical Biology*, 209(4):445–453, 2001.

Christopher M Bishop and Nasser M Nasrabadi. *Pattern recognition and machine learning*, volume 4. Springer, 2006.

Thomas Bliss, Tetsuya Iwasaki, and Hilary Bart-Smith. Central pattern generator control of a tensegrity swimmer. *IEEE/ASME Transactions on Mechatronics*, 18(2):586–597, 2012.

T Graham Brown. On the nature of the fundamental activity of the nervous centres; together with an analysis of the conditioning of rhythmic activity in progression, and a theory of the evolution of function in the nervous system. *The Journal of physiology*, 48(1):18, 1914.

Arthur E Bryson. Applied optimal control: Optimization. *Estimization and Control*, 2, 1975.

Katie Byl and Russ Tedrake. Metastable walking machines. *The International Journal of Robotics Research*, 28(8):1040–1064, 2009.

U Bässler. On the definition of central pattern generator and its sensory control. *Biological cybernetics*, 54(1):65–69, 1986.

Ulrich Bässler and Ansgar Büschges. Pattern generation for stick insect walking movements—multisensory control of a locomotor program. *Brain research reviews*, 27(1):65–88, 1998.

Ansgar Büschges. Sensory control and organization of neural networks mediating coordination of multisegmental organs for locomotion. *Journal of neurophysiology*, 93(3):1127–1135, 2005.

Terry Caelli, Ingo Rentschler, and W Scheidler. Visual pattern recognition in humans: I. evidence for adaptive filtering. *Biological Cybernetics*, 57(4-5): 233–240, 1987.

William S Cleveland, Persi Diaconis, and Robert McGill. Variables on scatterplots look more highly correlated when the scales are increased. *Science*, 216(4550):1138–1141, 1982.

Steve Collins, Andy Ruina, Russ Tedrake, and Martijn Wisse. Efficient bipedal robots based on passive-dynamic walkers. *Science*, 307(5712):1082–1085, 2005.

Michael Correll and Jeffrey Heer. Regression by eye: Estimating trends in bivariate visualizations. In *Proceedings of the 2017 CHI Conference on Human Factors in Computing Systems*, pages 1387–1396, 2017.

Julian Cristiano, Miguel Angel Garcia, and Domenec Puig. Deterministic phase resetting with predefined response time for cpg networks based on matsuoka's oscillator. *Robotics and Autonomous Systems*, 74:88–96, 2015.

Holk Cruse. The functional sense of central oscillations in walking. *Biological Cybernetics*, 86(4):271–280, 2002.

Monica A Daley, G Felix, and Andrew A Biewener. Running stability is enhanced by a proximo-distal gradient in joint neuromechanical control. *Journal of Experimental Biology*, 210(3):383–394, 2007.

Thi-Kien Dao, Tien-Szu Pan, and Jeng-Shyang Pan. A multi-objective optimal mobile robot path planning based on whale optimization algorithm. In *2016 IEEE 13th international conference on signal processing (ICSP)*, pages 337–342. IEEE, 2016.

Keith Davids, A Mark Williams, and John G Williams. *Visual perception and action in sport*. Routledge, 2005.

Friedl De Groote and Antoine Falisse. Perspective on musculoskeletal modelling and predictive simulations of human movement to assess the neuromechanics of gait. *Proceedings of the Royal Society B*, 288(1946): 20202432, 2021.

Friedl De Groote, Allison L Kinney, Anil V Rao, and Benjamin J Fregly. Evaluation of direct collocation optimal control problem formulations for solving the muscle redundancy problem. *Annals of biomedical engineering*, 44:2922–2936, 2016.

F Delcomyn. Reflexes and pattern generation, ch. 16. *Foundations of neurobiology*, pages 383–400, 1998.

Frederick J Diedrich and William H Warren Jr. Why change gaits? dynamics of the walk-run transition. *Journal of Experimental Psychology: Human Perception and Performance*, 21(1):183, 1995.

Michael Dimitriou and Benoni B Edin. Human muscle spindles act as forward sensory models. *Current Biology*, 20(19):1763–1767, 2010.

Winand H Dittrich. Action categories and the perception of biological motion. *Perception*, 22(1):15–22, 1993.

J Maxwell Donelan and Keir G Pearson. Contribution of sensory feedback to ongoing ankle extensor activity during the stance phase of walking. *Canadian journal of physiology and pharmacology*, 82(8-9):589–598, 2004.

J Maxwell Donelan, Rodger Kram, and Arthur D Kuo. Mechanical work for step-to-step transitions is a major determinant of the metabolic cost of human walking. *Journal of experimental biology*, 205(23):3717–3727, 2002.

Harris Drucker, Christopher J Burges, Linda Kaufman, Alex Smola, and Vladimir Vapnik. Support vector regression machines. *Advances in neural information processing systems*, 9, 1996.

Florin Dzeladini, Jesse Van Den Kieboom, and Auke Ijspeert. The contribution of a central pattern generator in a reflex-based neuromuscular model. *Frontiers in human neuroscience*, 8:371, 2014.

Herbert Elftman. Biomechanics of muscle: with particular application to studies of gait. *JBJS*, 48(2):363–377, 1966.

Albert Ellis. The biological basis of human irrationality. 1975.

Richard G Ellis, Kevin C Howard, and Rodger Kram. The metabolic and mechanical costs of step time asymmetry in walking. *Proceedings of the Royal Society B: Biological Sciences*, 280(1756):20122784, 2013.

Igor Elman, David Borsook, and Nora D Volkow. Pain and suicidality: insights from reward and addiction neuroscience. *Progress in neurobiology*, 109:1–27, 2013.

Jeremy L Emken, Raul Benitez, Athanasios Sideris, James E Bobrow, and David J Reinkensmeyer. Motor adaptation as a greedy optimization of error and effort. *Journal of neurophysiology*, 97(6):3997–4006, 2007.

Gen Endo, Jun Morimoto, Jun Nakanishi, and Gordon Cheng. An empirical exploration of a neural oscillator for biped locomotion control. In *IEEE International Conference on Robotics and Automation, 2004. Proceedings. ICRA'04. 2004*, volume 3, pages 3036–3042. IEEE, 2004.

AG Feldman and GN Orlovsky. Activity of interneurons mediating reciprocal 1a inhibition during locomotion. *Brain research*, 84(2):181–194, 1975.

Antonio Foncubierta Rodríguez and Henning Müller. Ground truth generation in medical imaging: a crowdsourcing-based iterative approach. In *Proceedings of the ACM multimedia 2012 workshop on Crowdsourcing for multimedia*, pages 9–14, 2012.

Till D Frank, Michael J Richardson, Stacy M Lopresti-Goodman, and Michael T Turvey. Order parameter dynamics of body-scaled hysteresis and mode transitions in grasping behavior. *Journal of biological physics*, 35:127–147, 2009.

Hartmut Geyer and Hugh Herr. A muscle-reflex model that encodes principles of legged mechanics produces human walking dynamics and muscle activities. *IEEE Transactions on neural systems and rehabilitation engineering*, 18(3):263–273, 2010.

Douglas J Gillan. Fitting regression lines to scatterplots: The role of perceptual heuristics. In *Proceedings of the Human Factors and Ergonomics*

*Society Annual Meeting*, volume 64, pages 1650–1654. SAGE Publications Sage CA: Los Angeles, CA, 2020.

Leon Glass and Rafael Pérez. Perception of random dot interference patterns. *Nature*, 246(5432):360–362, 1973.

Leon Glass and Eugene Switkes. Pattern recognition in humans: Correlations which cannot be perceived. *Perception*, 5(1):67–72, 1976.

James Gopsill, Mark Goudswaard, David Jones, and Ben Hicks. Capturing mathematical and human perceptions of shape and form through machine learning. *Proceedings of the Design Society*, 1:591–600, 2021.

Arnulf BA Graf, Felix A Wichmann, Heinrich H Bülthoff, and Bernhard Schölkopf. Classification of faces in man and machine. *Neural Computation*, 18(1):143–165, 2006.

Sten Grillner. Locomotion in vertebrates: central mechanisms and reflex interaction. *Physiological reviews*, 55(2):247–304, 1975.

Maki K Habib, Keigo Watanabe, and Kiyotaka Izumi. Biped locomotion using cpg with sensory interaction. In *2009 IEEE International Symposium on Industrial Electronics*, pages 1452–1457. IEEE, 2009.

John Burdon Sanderson Haldane. *What is life?* Lindsay drummond, 1949.

Jeffrey M Hausdorff, Dean A Rios, and Helen K Edelberg. Gait variability and fall risk in community-living older adults: a 1-year prospective study. *Archives of physical medicine and rehabilitation*, 82(8):1050–1056, 2001.

Nicolas Heess, Dhruva Tb, Srinivasan Sriram, Jay Lemmon, Josh Merel, Greg Wayne, Yuval Tassa, Tom Erez, Ziyu Wang, SM Eslami, et al. Emergence of locomotion behaviours in rich environments. *arXiv preprint arXiv:1707.02286*, 2017.

Norbert Henze. A probabilistic representation of the'skew-normal'distribution. *Scandinavian journal of statistics*, pages 271–275, 1986.

Brian L Hills. Vision, visibility, and perception in driving. *Perception*, 9(2): 183–216, 1980.

Neville Hogan and Dagmar Sternad. On rhythmic and discrete movements: reflections, definitions and implications for motor control. *Experimental brain research*, 181:13–30, 2007.

Harry Levi Hollingworth. The central tendency of judgment. *The Journal of Philosophy, Psychology and Scientific Methods*, 7(17):461–469, 1910.

Donald F Hoyt and C Richard Taylor. Gait and the energetics of locomotion in horses. *Nature*, 292(5820):239–240, 1981.

Eun Jung Hwang and Reza Shadmehr. Internal models of limb dynamics and the encoding of limb state. *Journal of neural engineering*, 2(3):S266, 2005.

Ainsley Iggo. Handbook of sensory physiology. volume ii: Somatosensory system, 1973.

Tetsuya Iwasaki and Min Zheng. Sensory feedback mechanism underlying entrainment of central pattern generator to mechanical resonance. *Biological cybernetics*, 94(4):245–261, 2006.

Jun Izawa, Tushar Rane, Opher Donchin, and Reza Shadmehr. Motor adaptation as a process of reoptimization. *Journal of Neuroscience*, 28(11): 2883–2891, 2008.

Rongyu Jin, Paolo Rocco, and Yunhai Geng. Cartesian trajectory planning of space robots using a multi-objective optimization. *Aerospace Science and Technology*, 108:106360, 2021.

Kelvin E Jones, Antonia F de C Hamilton, and Daniel M Wolpert. Sources of signal-dependent noise during isometric force production. *Journal of neurophysiology*, 88(3):1533–1544, 2002.

Daniel Kahneman. *Thinking, fast and slow*. Macmillan, 2011.

Daniel Kahneman, Olivier Sibony, and Cass R Sunstein. *Noise: A flaw in human judgment*. Little, Brown, 2021.

Thomas Kailath. *Linear systems*, volume 156. Prentice-Hall Englewood Cliffs, NJ, 1980.

Mrinal Kalakrishnan, Peter Pastor, Ludovic Righetti, and Stefan Schaal. Learning objective functions for manipulation. In *2013 IEEE International Conference on Robotics and Automation*, pages 1331–1336. IEEE, 2013.

Rudolf Emil Kalman et al. Contributions to the theory of optimal control. *Bol. soc. mat. mexicana*, 5(2):102–119, 1960.

Julie A Kauer and Robert C Malenka. Synaptic plasticity and addiction. *Nature reviews neuroscience*, 8(11):844–858, 2007.

Mitsuo Kawato. Internal models for motor control and trajectory planning. *Current opinion in neurobiology*, 9(6):718–727, 1999.

Patricia A Keating, John Kingston, and Mary E Beckman. The window model of coarticulation: articulatory evidence. *UCLA Working papers in Phonetics*, 69:3–29, 1990.

Daniel A Keim, Florian Mansmann, Jörn Schneidewind, and Hartmut Ziegler. Challenges in visual data analysis. In *Tenth International Conference on Information Visualisation (IV'06)*, pages 9–16. IEEE, 2006.

Hiroshi Kimura, Yasuhiro Fukuoka, and Avis H Cohen. Adaptive dynamic walking of a quadruped robot on natural ground based on biological concepts. *The International Journal of Robotics Research*, 26(5):475–490, 2007.

Shinichi Kimura, Masafumi Yano, and Hiroshi Shimizu. A self-organizing model of walking patterns of insects. *Biological Cybernetics*, 69:183–193, 1993.

David L Kleinman, S Baron, and WH Levison. An optimal control model of human response part i: Theory and validation. *Automatica*, 6(3):357–369, 1970.

Konrad P Körding and Daniel M Wolpert. Bayesian integration in sensorimotor learning. *Nature*, 427(6971):244–247, 2004a.

Konrad Paul Körding and Daniel M Wolpert. The loss function of sensorimotor learning. *Proceedings of the National Academy of Sciences*, 101(26): 9839–9842, 2004b.

John R Krebs, John C Ryan, and Eric L Charnov. Hunting by expectation or optimal foraging? a study of patch use by chickadees. *Animal behaviour*, 22:953–IN3, 1974.

Pawel Kudzia, Stephen N Robinovich, and J Maxwell Donelan. Characterizing the performance of human leg external force control. *Scientific Reports*, 12(1):4935, 2022.

Scott Kuindersma, Robin Deits, Maurice Fallon, Andrés Valenzuela, Hongkai Dai, Frank Permenter, Twan Koolen, Pat Marion, and Russ Tedrake. Optimization-based locomotion planning, estimation, and control design for the atlas humanoid robot. *Autonomous robots*, 40:429–455, 2016.

Stacey M Kung, Philip W Fink, Stephen J Legg, Ajmol Ali, and Sarah P Shultz. What factors determine the preferred gait transition speed in humans? a review of the triggering mechanisms. *Human movement science*, 57:1–12, 2018.

Arthur D Kuo. An optimal control model for analyzing human postural balance. *IEEE transactions on biomedical engineering*, 42(1):87–101, 1995.

Arthur D Kuo. A simple model of bipedal walking predicts the preferred speed–step length relationship. *J. Biomech. Eng.*, 123(3):264–269, 2001.

Arthur D Kuo. Energetics of actively powered locomotion using the simplest walking model. *J. Biomech. Eng.*, 124(1):113–120, 2002a.

Arthur D Kuo. The relative roles of feedforward and feedback in the control of rhythmic movements. *Motor control*, 6(2):129–145, 2002b.

Arthur D Kuo. An optimal state estimation model of sensory integration in human postural balance. *Journal of neural engineering*, 2(3):S235, 2005.

Arthur D Kuo, J Maxwell Donelan, and Andy Ruina. Energetic consequences of walking like an inverted pendulum: step-to-step transitions. *Exercise and sport sciences reviews*, 33(2):88–97, 2005.

Leng-Feng Lee and Brian R Umberger. Generating optimal control simulations of musculoskeletal movement using opensim and matlab. *PeerJ*, 4: e1638, 2016.

Stephan Lewandowsky and Ian Spence. The perception of statistical graphs. *Sociological Methods & Research*, 18(2-3):200–242, 1989.

Weiwei Li and Emanuel Todorov. Iterative linear quadratic regulator design for nonlinear biological movement systems. In *First International Conference on Informatics in Control, Automation and Robotics*, volume 2, pages 222–229. SciTePress, 2004.

C Karen Liu, Aaron Hertzmann, and Zoran Popović. Learning physics-based motion style with nonlinear inverse optimization. *ACM Transactions on Graphics (TOG)*, 24(3):1071–1081, 2005.

CJ Liu, Z Fan, K Seo, XB Tan, and ED Goodman. Synthesis of matsuoka-based neuron oscillator models in locomotion control of robots. In *2012 Third Global Congress on Intelligent Systems*, pages 342–347. IEEE, 2012.

Shuang Liu and Dong Sun. Minimizing energy consumption of wheeled mobile robots via optimal motion planning. *IEEE/ASME Transactions on Mechatronics*, 19(2):401–411, 2013.

Leroy L Long III and Manoj Srinivasan. Walking, running, and resting under time, distance, and average speed constraints: optimality of walk–run–rest mixtures. *Journal of The Royal Society Interface*, 10(81):20120980, 2013.

David G Luenberger. *Optimization by vector space methods*. John Wiley & Sons, 1997.

Rodolfo Margaria. Positive and negative work performances and their efficiencies in human locomotion. *Internationale Zeitschrift für angewandte Physiologie einschließlich Arbeitsphysiologie*, 25(4):339–351, 1968.

Hamed Masnadi-Shirazi and Nuno Vasconcelos. A view of margin losses as regularizers of probability estimates. *The Journal of Machine Learning Research*, 16(1):2751–2795, 2015.

Kiyotoshi Matsuoka. Mechanisms of frequency and pattern control in the neural rhythm generators. *Biological cybernetics*, 56(5-6):345–353, 1987.

Tad McGeer. Passive dynamic walking. *The international journal of robotics research*, 9(2):62–82, 1990.

Zan Mi, Jingzhou James Yang, and Karim Abdel-Malek. Optimization-based posture prediction for human upper body. *Robotica*, 27(4):607–620, 2009.

Changwei Miao, Guangzhu Chen, Chengliang Yan, and Yuanyuan Wu. Path planning optimization of indoor mobile robot based on adaptive ant colony algorithm. *Computers & Industrial Engineering*, 156:107230, 2021.

Jeanne Moore. Data visualization in support of executive decision making. *Interdisciplinary Journal of Information, Knowledge, and Management*, 12:125, 2017.

Jun Morimoto, Gen Endo, Jun Nakanishi, S Hyon, Gordon Cheng, Darrin Bentivegna, and Christopher G Atkeson. Modulation of simple sinusoidal patterns by a coupled oscillator model for biped walking. In *Proceedings 2006 IEEE International Conference on Robotics and Automation, 2006. ICRA 2006.*, pages 1579–1584. IEEE, 2006.

Frederick Mosteller, Andrew F Siegel, Edward Trapido, and Cleo Youtz. Eye fitting straight lines. *The American Statistician*, 35(3):150–152, 1981.

Thomas Nagel. The absurd. *The Journal of Philosophy*, 68(20):716–727, 1971.

John Nassour, Patrick Hénaff, Fethi Benouezdou, and Gordon Cheng. Multi-layered multi-pattern cpg for adaptive locomotion of humanoid robots. *Biological cybernetics*, 108:291–303, 2014.

Shawn M O'Connor and Arthur D Kuo. Direction-dependent control of balance during walking and standing. *Journal of neurophysiology*, 102(3): 1411–1419, 2009.

Shawn Michael O'Connor. *The relative roles of dynamics and control in bipedal locomotion.* PhD thesis, University of Michigan, 2009.

Dai Owaki and Akio Ishiguro. A quadruped robot exhibiting spontaneous gait transitions from walking to trotting to galloping. *Scientific reports*, 7 (1):277, 2017.

Shawn M O'Connor, Henry Z Xu, and Arthur D Kuo. Energetic cost of walking with increased step variability. *Gait posture*, 36(1):102–107, 2012.

Stephen E Palmer. Visual perception and world knowledge: Notes on a model of sensory-cognitive interaction. *Explorations in cognition*, pages 279–307, 1975.

Keir G Pearson. Proprioceptive regulation of locomotion. *Current opinion in neurobiology*, 5(6):786–791, 1995.

KG Pearson. Central pattern generation: a concept under scrutiny. In *Advances in physiological research*, pages 167–185. Springer, 1987.

Stefania Pellegrinelli, Stefano Borgia, Nicola Pedrocchi, Enrico Villagrossi, Giacomo Bianchi, and Lorenzo Molinari Tosatti. Minimization of the energy consumption in motion planning for single-robot tasks. *Procedia Cirp*, 29:354–359, 2015.

Xue Bin Peng, Glen Berseth, KangKang Yin, and Michiel Van De Panne. Deeploco: Dynamic locomotion skills using hierarchical deep reinforcement learning. *ACM Transactions on Graphics (TOG)*, 36(4):1–13, 2017.

Peter Q Pfordresher and Steven Brown. Poor-pitch singing in the absence of" tone deafness". *Music Perception*, 25(2):95–115, 2007.

Jan P Piek and Murray J Dyck. Sensory-motor deficits in children with developmental coordination disorder, attention deficit hyperactivity disorder and autistic disorder. *Human movement science*, 23(3-4):475–488, 2004.

JWS Pringle. The reflex mechanism of the insect leg. *Journal of Experimental Biology*, 17(1):8–17, 1940.

Uwe Proske and Simon C Gandevia. The proprioceptive senses: their roles in signaling body shape, body position and movement, and muscle force. *Physiological reviews*, 2012.

John R Rebula, Lauro V Ojeda, Peter G Adamczyk, and Arthur D Kuo. The stabilizing properties of foot yaw in human walking. *Journal of biomechanics*, 53:1–8, 2017.

Darcy S Reisman, Robert Wityk, Kenneth Silver, and Amy J Bastian. Locomotor adaptation on a split-belt treadmill can improve walking symmetry post-stroke. *Brain*, 130(7):1861–1872, 2007.

Fred Rieke, David Warland, Rob de Ruyter Van Steveninck, and William Bialek. *Spikes: exploring the neural code*. MIT press, 1999.

Ludovic Righetti and Auke Jan Ijspeert. Pattern generators with sensory feedback for the control of quadruped locomotion. In *2008 IEEE International Conference on Robotics and Automation*, pages 819–824. IEEE, 2008.

Dimitri Ryczko, András Simon, and Auke Jan Ijspeert. Walking with salamanders: from molecules to biorobotics. *Trends in neurosciences*, 43(11): 916–930, 2020.

Natalia Sánchez, Surabhi N Simha, J Maxwell Donelan, and James M Finley. Taking advantage of external mechanical work to reduce metabolic cost: the mechanics and energetics of split-belt treadmill walking. *The Journal of physiology*, 597(15):4053–4068, 2019.

Thomas W Schoener. Theory of feeding strategies. *Annual review of ecology and systematics*, 2(1):369–404, 1971.

Eileen C Schwab and Howard C Nusbaum. *Pattern recognition by humans and machines: speech perception*, volume 1. Academic Press, 2013.

Michael Sedlmair, Andrada Tatu, Tamara Munzner, and Melanie Tory. A taxonomy of visual cluster separation factors. In *Computer Graphics Forum*, volume 31, pages 1335–1344. Wiley Online Library, 2012.

Jessica C Selinger, Shawn M O'Connor, Jeremy D Wong, and J Maxwell Donelan. Humans can continuously optimize energetic cost during walking. *Current Biology*, 25(18):2452–2456, 2015.

Charles Scott Sherrington. Flexion-reflex of the limb, crossed extension-reflex, and reflex stepping and standing. *The Journal of physiology*, 40 (1-2):28, 1910.

John E Shore and Robert M Gray. Minimum cross-entropy pattern classification and cluster analysis. *IEEE Transactions on Pattern Analysis and Machine Intelligence*, (1):11–17, 1982.

Herbert A Simon. Dynamic programming under uncertainty with a quadratic criterion function. *Econometrica, Journal of the Econometric Society*, pages 74–81, 1956.

Mark W Spong. Passivity based control of the compass gait biped. *IFAC Proceedings Volumes*, 32(2):506–510, 1999.

Manoj Srinivasan. Optimal speeds for walking and running, and walking on a moving walkway. *Chaos: An Interdisciplinary Journal of Nonlinear Science*, 19(2), 2009.

Manoj Srinivasan. Fifteen observations on the structure of energy-minimizing gaits in many simple biped models. *Journal of The Royal Society Interface*, 8(54):74–98, 2011.

Manoj Srinivasan and Andy Ruina. Computer optimization of a minimal biped model discovers walking and running. *Nature*, 439(7072):72–75, 2006.

Hans Straka, John Simmers, and Boris P Chagnaud. A new perspective on predictive motor signaling. *Current Biology*, 28(5):R232–R243, 2018.

Albert Tarantola. *Inverse problem theory and methods for model parameter estimation*. SIAM, 2005.

Adam Taylor, Garrison W Cottrell, and William B Kristan Jr. A model of the leech segmental swim central pattern generator. *Neurocomputing*, 32: 573–584, 2000.

L Tesio, GS Roi, and F Möller. Pathological gaits: inefficiency is not a rule. *Clinical Biomechanics*, 6(1):47–50, 1991.

Emanuel Todorov. Cosine tuning minimizes motor errors. *Neural computation*, 14(6):1233–1260, 2002.

Emanuel Todorov. Stochastic optimal control and estimation methods adapted to the noise characteristics of the sensorimotor system. *Neural computation*, 17(5):1084–1108, 2005.

Emanuel Todorov and Michael I Jordan. Optimal feedback control as a theory of motor coordination. *Nature neuroscience*, 5(11):1226–1235, 2002.

Mats Trulsson. Mechanoreceptive afferents in the human sural nerve. *Experimental Brain Research*, 137:111–116, 2001.

Philipp Tschandl, Noel Codella, Bengü Nisa Akay, Giuseppe Argenziano, Ralph P Braun, Horacio Cabo, David Gutman, Allan Halpern, Brian Helba, Rainer Hofmann-Wellenhof, et al. Comparison of the accuracy of human readers versus machine-learning algorithms for pigmented skin lesion classification: an open, web-based, international, diagnostic study. *The lancet oncology*, 20(7):938–947, 2019.

Kazuo Tsuchiya, Shinya Aoi, and Katsuyoshi Tsujita. Locomotion control of a biped locomotion robot using nonlinear oscillators. In *Proceedings 2003 IEEE/RSJ International Conference on Intelligent Robots and Systems (IROS 2003)(Cat. No. 03CH37453)*, volume 2, pages 1745–1750. IEEE, 2003.

Yoji Uno, Mitsuo Kawato, and Rika Suzuki. Formation and control of optimal trajectory in human multijoint arm movement. *Biological cybernetics*, 61 (2):89–101, 1989.

Nora D Volkow and Roy A Wise. How can drug addiction help us understand obesity? *Nature neuroscience*, 8(5):555–560, 2005.

Ulrike Von Luxburg, Robert C Williamson, and Isabelle Guyon. Clustering: Science or art? In *Proceedings of ICML workshop on unsupervised and transfer learning*, pages 65–79. JMLR Workshop and Conference Proceedings, 2012.

Howard Wainer and David Thissen. On the robustness of a class of naive estimators. *Applied Psychological Measurement*, 3(4):543–551, 1979.

P Wallén and TL Williams. Fictive locomotion in the lamprey spinal cord in vitro compared with swimming in the intact and spinal animal. *The Journal of physiology*, 347(1):225–239, 1984.

Qi Wang, Yue Ma, Kun Zhao, and Yingjie Tian. A comprehensive survey of loss functions in machine learning. *Annals of Data Science*, 9(2):187–212, 2022.

Max Wertheimer. Laws of organization in perceptual forms. 1938.

Eric R Westervelt, Jessy W Grizzle, and Daniel E Koditschek. Hybrid zero dynamics of planar biped walkers. *IEEE transactions on automatic control*, 48(1):42–56, 2003.

Matthew M Williamson. Neural control of rhythmic arm movements. *Neural networks*, 11(7-8):1379–1394, 1998.

DM Wilson and RJ Wyman. Motor output patterns during random and rhythmic stimulation of locust thoracic ganglia. *Biophysical Journal*, 5(2): 121–143, 1965.

Donald M Wilson. The central nervous control of flight in a locust. *Journal of Experimental Biology*, 38(2):471–490, 1961.

David A Winter, Sandra J Olney, Jill Conrad, Scott C White, Sylvia Ounpuu, and James R Gage. Adaptability of motor patterns in pathological gait. In *Multiple muscle systems: biomechanics and movement organization*, pages 680–693. Springer, 1990.

Bang Wong. Color blindness. *nature methods*, 8(6):441, 2011.

David Wooden, Matthew Malchano, Kevin Blankespoor, Andrew Howardy, Alfred A Rizzi, and Marc Raibert. Autonomous navigation for bigdog. In *2010 IEEE international conference on robotics and automation*, pages 4736–4741. Ieee, 2010.

Paola Zamparo, Maria Pia Francescato, G De Luca, L Lovati, and PE di Prampera. The energy cost of level walking in patients with hemiplegia. *Scandinavian journal of medicine & science in sports*, 5(6):348–352, 1995.

Lorenzo Zaninetti and Mario Ferraro. On the truncated pareto distribution with applications. *Open Physics*, 6(1):1–6, 2008.

Juanjuan Zhang, Pieter Fiers, Kirby A Witte, Rachel W Jackson, Katherine L Poggensee, Christopher G Atkeson, and Steven H Collins. Human-in-the-loop optimization of exoskeleton assistance during walking. *Science*, 356 (6344):1280–1284, 2017.

# Appendix

## Copyright permissions

Signatures have been removed in accordance with the University of Calgary thesis guidelines.

Sept. 22, 2023

I write this memo as the Director of the Biomedical Engineering Graduate Program. This memo is to serve in lieu of the 'Letter of Permission' to use a previously published co-authored paper as Chapter 2 in Hansol Ryu's PhD dissertation. In discussion with Dr. Donna-Marie McCafferty, then Acting Dean Faculty of Graduate Studies, the position of FGS was that, even though Ms Ryu and her former supervisor could not achieve consensus on IP, the agreements submitted to FGS permitted her use of that previously published paper in her dissertation.

John EA Bertram
Professor - Cumming School of Medicine
Director - Biomedical Engineering Graduate Program

THE OHIO STATE UNIVERSITY

College of Engineering
Mechanical and Aerospace Engineering
Manoj Srinivasan / Associate Professor
srinivasan.88@osu.edu
Movement Lab

To Hansol Ryu: Sept 18, 2023

Through this letter, I am pleased to provide formal permission for inclusion in the PhD thesis of Hansol Ryu (University of Calgary) as chapters, the following two manuscripts I'm a co-author of:

- Chapter 3: What loss Functions do humans optimize when they perform regression and classification
- Chapter 4: Human force control may trade-off force error with central tendency and recency biases.

Please let me know if you have any questions at srinivasan.88@osu.edu

Sincerely,
Manoj Srinivasan

--
Professor Manoj Srinivasan
Mechanical and Aerospace Engineering . The Ohio State University
Associate Chair . Undergraduate Programs and Teaching
Email: srinivasan.88@osu.edu . Web: https://manojsrinivasan.org

Sincerely,

Professor Manoj Srinivasan, Associate Chair, Mechanical and Aerospace Engineering
Ph. +1 607 229 3627. Email: srinivasan.88@osu.edu, http://movement.osu.edu